TRANSCRIPTOMIC ALTERATIONS IN THE AGED BRAIN WITH AND WITHOUT DIETARY AND DIETARY-MIMETIC MANIPULATIONS

A DISSERTATION SUBMITTED TO

THE GRADUATE SCHOOL OF ENGINEERING AND SCIENCE

OF BILKENT UNIVERSITY

IN PARTIAL FULFILLMENT OF THE REQUIREMENTS FOR

THE DEGREE OF

DOCTOR OF PHILOSOPHY

IN

NEUROSCIENCE

By

Begün ERBABA

December, 2021

TRANSCRIPTOMIC ALTERATIONS IN THE AGED BRAIN WITH AND WITHOUT DIETARY AND DIETARY-MIMETIC MANIPULATIONS

By Begün Erbaba

December 2021

We certify that we have read this dissertation and that, in our opinion, it is fully adequate, in scope and in quality, as a dissertation for the degree of Doctor of Philosophy.

Michelle M. Adams (Advisor)

Özlen Konu Karakayalı

Erkan Kiriş

Mehmet Somel

H. Hulusi Kafalıgönül

Approved for the Graduate School of Engineering and Science:

Ezhan Karaşan

Director of the Graduate School

ABSTRACT

TRANSCRIPTOMIC ALTERATIONS IN THE AGED BRAIN WITH AND WITHOUT DIETARY AND DIETARY-MIMETIC MANIPULATIONS

Begün Erbaba

Ph.D. in Neuroscience

Advisor: Michelle M. Adams

December 2021

Aside from many genetic and environmental influences on the brain, aging itself is a significant risk factor for accelerated cognitive decline, making aging research crucial due to the increasing population age in our era. We aimed to discover gene expression differences in the aging zebrafish brain using three age groups in the first aim. We identified *gjc2* (*CX47*) and *alcamb* (*ALCAM*) cell adhesion genes showing consistent downregulation with age across all experiments. ALCAM is also known to be associated with neuroinflammation, which has been implicated to be lowered using anti-aging, non-genetic nutrient interventions. In the second aim, we applied 12 weeks of two opposing nutrient interventions, caloric restriction (CR) and overfeeding (OF) in aging zebrafish, in order to be able to propose a reliable therapeutic approach for reversing age-related neurobiological changes. We measured protein and expression level differences of selected genes related to proliferation to inflammation with these diets. The results showed that *sox2* gene expression was significantly upregulated following OF treatment than CR diet, and *myca* and *tp53* mRNA levels were significantly downregulated with advanced age. *Alcamb* and *tfdp1* expression levels were also marginally significantly lowered with CR compared to other groups. Meanwhile, we also conducted another transcriptomic approach using microarray to assess gene expression differences with CR compared to *Ad-libitum*

(AL) feeding. Thus, lastly, in the third part, we found that CR causes changes in cell cycle regulation among several other functional regulatory pathways in zebrafish brains. We identified the tfdp1 gene, which showed downregulation with CR, as a possible CR regulator. Then, to create a CR mimic, we performed morpholino oligo (MO) injections to zebrafish embryos and adult brains to knock down *tfdp1* gene expression levels. The injections were not successful in altering Tfdp1 protein levels in neither embryos and adults. However, 8ng *tfdp1*-MO injections in embryos significantly increased *myca* and *tp53* expression levels, which are among the downstream targets of *tfdp1*. Our examinations shed light on healthy brain aging and possibly propose new drug targets.

Keywords Zebrafish, Brain, Aging, Caloric Restriction.

ÖZET

DİYET VE DİYET-MİMETİĞİ MANİPÜLASYONLARIN GEN ANLATIMI AÇISINDAN YAŞLANAN BEYNE ETKİLERİ

Begün Erbaba

Nörobilimler, Doktora

Tez Danışmanı: Michelle M. Adams

Aralık 2021

Beyin üzerindeki birçok genetik ve çevresel etkinin yanı sıra, yaşlanmanın kendisi de bilişsel gerileme için önemli bir risk faktörüdür ve bu çağımızda sürekli artan nüfus yaşı ile birlikte yaşlanma araştırmalarını çok önemli bir hale getirmektedir. Bu tez çalışmasının birinci deneysel bölümünde üç farklı yaş grubunda yaşlanan zebra balığı beynindeki gen ekspresyon farklılıklarını keşfetmeyi amaçladık. Anlatımları tüm deneylerde yaşla birlikte tutarlı bir şekilde azalan *gjc2* (*CX47*) ve *alcamb* (*ALCAM*) hücre yapışma genlerini belirledik. *Alcamb*'nin ayrıca nöroinflamasyonla da ilişkili olduğu, nöroinflamasyonun da yaşlanma karşıtı besin müdahaleleri ile düşürüldüğü bilinmektedir. Buradan yola çıkarak, ikinci kısımda, yaşlanma sırasında nörobiyolojik değişiklikleri tersine çevirmek ve güvenilir bir terapötik yaklaşım önerebilmek adına yaşlanan zebra balığı üzerinde kalori kısıtlaması (CR) ve aşırı besleme (OF) olmak üzere 12 haftalık iki zıt besin müdahalesi uyguladık. Bu diyetlerle, proliferasyondan inflamasyona kadar yaşlanmayla ilişkilendirilmiş anahtar kavramlarla ilgili seçilmiş genlerin protein ve anlatım düzeyi farklılıklarını ölçtük. Sonuçlar bize, OF uygulamasının ardından CR diyetine kıyasla *sox2* gen ekspresyonlarının önemli ölçüde arttığını ve *myca* ve *tp53* mRNA düzeylerinin ileri yaşla birlikte önemli ölçüde azaldığını gösterdi. *alcamb* ve *tfdp1* anlatım seviyelerinin de diğer gruplara kıyasla CR ile marjinal anlamlı olarak azaldığı gözlemlendi. Bu sırada, *Ad-libitum* (AL) beslemesine kıyasla CR ile gen anlatım farklılıklarının değerlendirilmesi

amacıyla mikrodizi yöntemi kullanılarak başka bir transkriptomik yaklaşım da yürüttük. Bu doğrultuda, son olarak üçüncü bölümde, CR'in zebra balığı beyinlerindeki diğer birkaç fonksiyonel düzenleyici yol arasında hücre döngüsü düzenlemesinde değişikliklere neden olduğunu bulduk. Olası bir CR düzenleyicisi olarak CR ile anlatımı azalan gösteren *tfdp1* genini belirledik. Daha sonra, bir CR taklidi oluşturabilmek adına, *tfdp1* genini knockdown edebilmek için hem zebra balığı embriyosuna hem de yetişkinlere morfolino oligo (MO) enjeksiyonları yaptık. Enjeksiyonlar hem embriyo hem de yetişkinlerde Tfdp1 protein seviyelerini değiştirmeyi başaramadı. Fakat, embriyo 8ng *tfdp1*-MO enjeksiyonlarının, *tfdp1*'in anlatımlarını düzenlediği hedef genleri arasında yer alan *myca* ve *tp53* 'nin anlatım seviyelerini önemli ölçüde artırdığını gördük. İncelemelerimizin sağlıklı beyin yaşlanmasına ışık tutabileceğine ve yeni ilaç hedefleri önerebileceğini umuyoruz.

Anahtar kelimeler: Zebra Balığı, Beyin, Yaşlanma, Kalori Kısıtlaması.

Acknowledgment

Firstly, I would like to express my endless and deepest gratitude to Assoc. Prof. Dr. Michelle M. Adams, and Assoc. Prof. Dr. Ayca Arslan-Ergul for their guidance, advice, time, and efforts on me, making it possible for me to work on a topic of great interest to me. I am inspired by their knowledge, courage, strength, and most importantly their always smiling attitudes. I learned never to lose hope even in tough times and constantly push harder to move further from them. Secondly, I am grateful to my dear jury members for their efforts on me during my Ph.D. studies and their sincere kindness in accepting to take part in my thesis committee. Thirdly, I wish to express my sincere thanks to my family for their moral support at all times. Furthermore, I feel tremendously fortunate to have such a beautiful lab family in Ankara. I am thankful for their unworldly support and infectious joy. Lastly, I owe a special thanks to Zeliha Gozde Turan for sparing her precious time to help with the microarray analysis and statistics. This work was supported by The Scientific and Technological Research Council of Turkey with grant numbers 114S548, 214S236, and an EMBO Installation Grant to Michelle Adams.

Contents

List of Figures

indicates the relative gene expression levels. N = 3 for each group. *p < 0.05, ***p < 0.001. (Reprinted from Erbaba et al., 2020b)

Figure 5 Relative expression levels of selected genes in human normal and Alzheimer's RNA samples (Biochain). (A) RT-PCR results are shown regarding several aging and developmental markers. (B) Cell adhesion genes were measured for assessment on expression levels via RT-PCR. Y-axis indicates the relative gene expression levels. *p < 0.05, **p < 0.01, ***p < 0.001. (Reprinted from Erbaba et al., 2020b)

Figure 6 Clustering of the selected genes is demonstrated with Aging, Dementia, and TBI (Traumatic Brain Injury) data. Brain regions of frontal white matter, hippocampus, parietal cortex, and temporal cortex were included in the study. Each brain region is grouped into patients with or without dementia and then further organized in increasing age from 78 to 100+. The red color demonstrates the highest expression, and blue indicates the lowest expression. Genes are shown in rows. Aging, Dementia and TBI Study. 2016 Allen Institute for Brain Science. Allen Human Brain Atlas is available from human.brainmap.org. (Reprinted from Erbaba et al., 2020b)

Figure 7 (A) An illustration demonstrating the interactions of cell adhesion molecules in the junctions, and (B) a summary table of gene expression levels of the genes of interest in different experimental set-ups. In the table, blue circles indicate a decreased expression during aging, and the red colored circles mean an increased expression with age. The one yellow circle indicates the expression remains the same. Stars in the middle of the circles refer to the significance. Adapted from Kegg pathway no: hsa04514, except cx47 interactions, which was adapted from Kim et al. (2013). APC: antigen-presenting cell, Astro: astrocyte, Axon: axon of a neuron, endothelial: endothelial cell, Myelin: myelin-producing oligodendrocyte, Olig: oligodendrocyte, Post: postsynaptic neuron, Pre:

presynaptic neuron, Schwann: Schwann cell, T cell: T lymphocytes. (Reprinted from Erbaba et al., 2020b)

Figure 8 Average (A) weight, (B) length, and (C) Body Mass Index (BMI) data across feeding groups are shown. All values are significantly increasing with age ($p < 0.001$), and there are significant main effects of treatment for all three data points ($p < 0.001$). Overall, all CR groups showed significantly lower body weight ($p < 0.001$), length ($p < 0.001$), and BMI ($p < 0.001$) than both their AL and OF counterparts.

Figure 9 (A) Representative Western blot images for Dcamkl1, HuC, Gfap:GFP, Pcna, Tfdp1, L-plastin, and β-Tubulin protein levels from the different feeding groups. Protein levels of (B) Dcamkl1, (C) HuC, (D) Gfap, (E) Pcna, (F) Tfdp1, and (G) L-plastin across different feeding regimens and age. Whole-brain lysates from six animals per feeding group were used for Western blotting experiments. No protein levels changed significantly with respect to age or diet. AL: Ad-libitum, OF: overfed, CR: Caloric restriction

Figure 10 Expression levels of proteins of interest clustering in an age- and the treatment-specific manner in the principal component analysis. Data is visualized in 2-dimensions using the principal component 1 (PC1), principal component 2 (PC2), and principal component 3 (PC3). The factor of age arranges data shown in scatterplots on A, B, and C. (A) On the PC1 axis, in which Lplastin, HuC, and Gfap are the leading contributors, the young CR group clusters higher than the OF group. (B) On the PC3 axis, where Tfdp1 is the negative and Dcamkl1 is the leading positive contributor, the young CR group scores higher values than the young AL and OF groups. (C) On the PC2 axis, in which Pcna is the leading positive contributor and, Gfap and HuC are the leading negative contributors, the young OF group has higher values than the young AL and CR groups. Groups are denoted

by different colors, as shown from the legends. AL: Ad libitum-feeding, OF: overfeeding, CR: Caloric restriction feeding.

Figure 11 mRNA level comparisons of selected genes analyzed by RT-PCR; (A) *tfdp1*, (B) *e2f5*, (C) *sox2*, (D) *myca*, (E) *tp53*, (F) *alcamb*, (G) *rest*, (H) *il1b*, (I) *tnfa*, (J) *lcp1*. All data were normalized and log fold change values were calculated using the delta delta Ct method. A main effect of treatment was found for *sox2* ($p = 0.02$), and a marginally significant main effect of treatment was found for *alcamb* mRNA levels ($p=0.09$). A main effect of age was detected for *tp53* ($p = 0.001$), *myca* ($p = 0.02$), and *lcp1* ($p = 0.01$) expression levels. *actin* and *rpl13a* genes were used as reference genes. Four animals per age and dietary group were included for a total of 24 animals used in the RT-PCR experiments.

Figure 12 Expression levels of genes of interest cluster in an age- and treatment-specific manner in the principal component analysis. Data is visualized in 2-dimensions using the principal component 1 (PC1), principal component 2 (PC2), and principal component 3 (PC3). The factor of age arranges data shown in scatterplots on a, b, and c. (A) On the PC1 axis, in which *rest*, *tfdp1*, *lcp1*, *sox2*, *tp53*, *myca*, *tnfa*, and *il1b* are the leading positive contributors, the young OF group clusters higher than the young AL group. Young OF and CR groups cluster at higher values of the PC1 axis than the old OF and CR groups, respectively. (B) On the PC3 axis, to which *sox2* contributed positively and Rest negatively, CR samples cluster at lower values than OF animals. (C) On the PC2 axis, where *il1b* and *e2f5* are the strongest positive contributors, and *myca* is the negative contributor, the young CR group clusters closer to the lower margin than young OF and AL groups. The old CR group samples cluster on higher values of the PC2 axis compared to the young CR group animals. Groups are denoted by different colors, as shown from the legends. AL: Ad libitum-feeding, OF: overfeeding, CR: Caloric restriction feeding.

Figure 13 Embryo injections were performed at 1-4 cell stage of embryos as shown

Figure 14 Embryo MO injections comprised of approximately 200 embryos injected per group for each subgroup. NC: Negative Control Morpholino injected group. NI: Non-injected group.

Figure 15 Left image shows a zebrafish brain (right image taken in our fish facility). Right images show fluorescent tracking dye CMTP-X (red) delivered with the morpholino solution given with the injection solution to track its diffusion during CVMI optimized in our facility. Three different zebrafish brains are shown. Images were taken under diluted anesthetic solution, 30 minutes after injection. Injection sites on are shown with yellow arrows.

Figure 16 A histogram of the p-value distribution of the probe sets obtained from the *t*-test was plotted. Probe sets accumulate around $p < 0.001$.

Figure 17 Looking at the most profound functional categories among 526 differentially expressed genes (DEG) on microarray, three KEGG pathways were extracted via DAVID Functional Annotation Tool. Figure shows the DEGs associated with these pathways.

Figure 18 Microarray results for selected 23 DEGs are shown. Plots were obtained using Graphpad software.

Figure 19 RT-PCR results for selected 23 DEGs with additional durations of CR are shown. Plots were obtained using Graphpad software.

Figure 20 A) Representative western blot image of zebrafish whole-brain Tfdp1 protein levels comparing young and old adult fish. B) Tfdp1 protein level differences with respect to age. Tfdp1 protein levels in old fish brains are significantly higher than in young fish brains ($p < 0.001$). Whole brain lysates from four animals per age group were used for

Western blot experiments. Band intensities were quantified on ImageJ software. For each well firstly within gel normalization then tubulin normalization were performed.

Figure 21 A) Representative western blot membrane bands of a set of 8ng embryo injections (3dpi) are shown measuring Lplastin, Tubulin, Tfdp1, and Pcna protein levels. *tfdp1*-MO: 8ng *tfdp1* morpholino injected ~20 pooled embryos; NC-MO: 8ng Negative Control morpholino injected ~20 pooled embryos; NI: non-injected ~20 pooled embryos. B) No significant change was observed at the embryo protein levels of Tfdp1, Pcna, or Lplastin following 8ng *tfdp1*-MO injection (3dpi).

Figure 22 Tfdp1 downstream gene expression levels following 2ng MO injections on embryos. No significant effect of treatment was observed. In terms of duration after injections, duration was a significant main effect on *ccna2* expression levels ($p = 0.024$). (N=5 for each group, N=30 in total).

Figure 23 Tfdp1 downstream gene expression levels following 4ng MO injections on embryos. No significant effect of treatment was observed. In terms of duration after injections, there was a significant main effect of duration on *ccne1* ($p < 0.001$), *cdk1* ($p = 0.026$), *rrm1* ($p=0.028$), and *tp53* ($p = 0.031$) expression levels. (N=5 for each group, N=30 in total).

Figure 24 Tfdp1 downstream gene expression levels following 8ng MO injections on a different set of embryos than western blot experiments. A significant main effect of treatment was observed for *myca* expression levels ($p=0.029$) between *tfdp1*-MO and NC-MO injected groups ($p = 0.016$), and for *tp53* expression levels ($p=0.01$) between *tfdp1*-MO and NI groups (0.011). In terms of duration after injections, there was no significant difference between 3dpi and 5dpi groups on the Tfdp1 downstream gene expression levels. (N=5 for each group, N=30 in total).

Figure 25 A) A representative western blot is shown for Tfdp1 protein levels after *tfdp1* Vivo-MO injection. Blotting was performed against Tfdp1 and Tubulin antibodies. NC stands for negative control group; heads were incised and anesthesia were performed as done for treatment groups, but no injection solution was given. B) *tfdp1* Vivo-MO Time curve. No statistical difference were found on Tfdp1 protein levels between NC or any time point after *tfdp1*-Vivo-MO injection. N=16 (N=2 for each group).

Figure 26 Tfdp1 downstream gene expression levels on adult fish brains following Vivo MO injections. No significant change was detected. *tfdp1*-MO: 500uM *tfdp1* Vivo MO injected adult fish brains' gene expression levels, NC-Vivo-MO: 500 uM NC-Vivo-MO injected brains, NI: Non Injected brains. N=9.

Figure 27 Zebrafish embryos 5dpf are shown. Left three embryos are with normal swim bladders (thought to be heterozygous or wild type), while the on left is with a deflated swim bladder (thought to be homozygous). Red arrows show regions where swim bladders are found. Image was taken in Bilkent University Zebrafish Facility.

Figure 28 Pooled samples (10-30 embryos per sample) first trial - all cut. PCR reaction was set using 250ng DNA. RE digestion was performed using 1ug PCR product for 20min on 37ºC. 2% agarose, 25ul pcr product, 48ul RE digested sample used.

Figure 29 Pooled samples (10-30 embryos per sample) second trial - all cut. PCR reaction was set using 250ng DNA. RE digestion was performed using 1,2ug PCR product at 37ºC overnight. 2% agarose, 10ul pcr product, and 45ul RE digested samples used

Figure 30 Individual samples first trial - all cut. PCR reaction was set using 250ng DNA. RE digestion was performed using 3ug PCR product for 30min on 37ºC. 2% agarose, 40ul sample used

Supplementary Figure 1 The interaction of the proteins of interest with each other and with some age-related proteins in Chapter 2. We used the Cytoscape software. (Reprinted from Erbaba et al., 2020b)

List of Tables

Supplementary Table 2 Chapter 2 primer list for zebrafish samples

CHAPTER 1

INTRODUCTION

1.1.Aging

Aging is an inevitable biological process and a very complex state that induces numerous alterations in the human body, such as dysregulation of nutrient sensing, stem cell exhaustion, epigenetic alterations, genomic instability, loss of protein homeostasis, and altered intercellular communication (Jones, 2014; López-Otín, 2013). The aging-related alterations could lead to an increased risk for neurodegeneration and associated cognitive impairments, including gradual declines in conceptual reasoning, memory, and processing speed (Harada et al., 2013). Various factors influencing the aging process have been highlighted in the literature, from molecules to cellular components and pathways. Complement system genes were discovered as biomarkers for aging (Bae et al., 2018). Similarly, immune system genes are upregulated in the hippocampus during aging (Ianov et al., 2017). Another study examined the roles of micro RNAs (miRNAs) in aging. For example, a specific miRNA, miR-34, was observed to be effective in preventing neurodegeneration (Kennerdell et al., 2018). Another factor affecting aging is post-

transcriptional regulation. Throughout aging, increases in RNA editing are a conserved trait in primates (Li et al., 2013). It has been shown that intron retention plays a different role in regulating biological functions at different stages of aging (Adusumalli et al., 2019). Similarly, splicing patterns were investigated during aging. Although most splicing is limited to developmental stages, some persist during aging (Mazin et al., 2013). Last but not least, autophagy-lysosomal-related pathways were prominent in the dorsolateral prefrontal cortex in AD (Raj et al., 2018).

To overcome the impairments mentioned above that occur with advanced age, it is therefore crucial to identify new potential therapeutic targets for neurodegenerative interventions. Identifying the genetic pathways that change during the aging process will enable us to understand the mechanisms related to brain aging. Neurodegenerative disease risk increases with aging, and these diseases place a significant burden on patients and caregivers. In order to interpret the diseased states, we must first have a comprehensive understanding of the healthy aging brain. As transcriptional profile changes were observed to occur throughout life and with advancing age, having a minor effect on individual genes but being more widespread throughout the transcriptome level (Somel, 2006; Kedlian, 2019), in the second chapter of this thesis, we first followed RNA sequencing to understand healthy brain aging. RNA sequencing is a method that provides a comprehensive study of the molecular and cellular aspects of the brain. It is widely used in many different approaches for humans and animals. RNA sequencing data from aging human brains is available to anyone through the Aging, Dementia and Traumatic Brain Injury (TBI) Study (http://aging.brain-map.org). The human brain regions were sequenced from donors aged 78-100+ years with defined dementia or TBI status in that study.

1.2. Zebrafish

All the experiments performed in this thesis were conducted on the zebrafish (*Danio rerio*) model organism. Its genome resembles the human genome, and 71% of its genes have been estimated to have human orthologs (Howe, 2013). We used this model organism because it has become an essential and appropriate gerontological model to study human-associated diseases as well as aging (Arslan-Ergul et al. 2013; Kishi, 2009; Gerhard, 2007; Lieschke 2007). The animals live up to 3 to 5 years on average and show gradual aging like humans (Kishi, 2003; Kishi, 2004). Although widely used in biological research, most experiments have been performed on larval or young zebrafish (less than six months old). However, it is possible to study zebrafish at older ages (more than 24 months). During normal brain aging in zebrafish, cognitive decline occurs, and this process is similar to that described in humans and likely under the influence of both genetic and environmental factors (Yu, 2006). The zebrafish nervous system is comparable with humans, having fore-, mid-, hind-brain structures. They also have an integrated nervous system and show higher behavioral capabilities such as memory and social behavior (Lieschke, 2007). However, most importantly, they show greater proliferative potential than mammals (Zupanc, 2005; Grandel, 2006). Neurogenesis in the zebrafish brain continues throughout life, and they are capable of repairing damages on the optic tectum and preserving vision even in advanced age (Kızıl, 2018). This regenerative potential earned its significance when previous research studies documented the decline in neuronal generation and turn-over rates arising with age in rats, mice, and humans (Encinas, 2011; Kuhn, 1996; Knoth, 2010; Luo, 2006; Lugert, 2010; Maslov, 2004; Sanai, 2011; Rao, 2006). In older fish, the number of regenerating axons and the outgrowth are reduced compared to younger animals (Van Houcke et al., 2017).

1.3. About this thesis

Overall, this thesis comprises three main experimental chapters after the first introductory chapter. The second chapter examined the gene expression changes on the zebrafish brains of three age groups; young adult, adult, and old age. The first part of the study aimed to investigate the transcriptomic alterations in aging zebrafish brains using neural cell populations and compare them with human brain samples. For this purpose, we extracted cells from young-adult (3 months), adult (5.5-8.5 months), and old (26-31 months) zebrafish brains, then performed RNA sequencing. We obtained a list of genes whose expressions were altered significantly with age following data analysis. After testing our gene list in whole zebrafish brains, human brain samples, and Allen Brain Atlas data, we found that cell adhesion molecules, more specifically *ALCAM* (*Alcamb* in zebrafish) and *GJC2* (*Cx47* in zebrafish), are critical during brain aging.

The findings we reached in the second chapter encouraged us to intervene/overcome the brain aging process; thus, we applied non-genetic nutrient interventions on aging fish in the third chapter. We examined the effects of two opposite feeding regimens, CR and OF, on the young and aged fish brains. We analyzed the effects of two dietary interventions on markers of cell proliferation, inflammation, cytoskeletal regulation, and cell adhesion in the aging zebrafish brain. In order to quantify the differences between the effects of diets on the brains of young and old animals, we applied a 12-week long diet of either ad libitum (AL)-feeding, OF, or CR similar to our previous studies (Arslan-Ergul et al. 2016; Celebi-Birand et al. 2020; Karoglu-Eravsar et al. 2021). The differences in brain protein and mRNA levels were compared for selected markers related to cell proliferation (Pcna, *sox2*), cell cycle regulation (*tfdp1*, *e2f5*, *myca*, *tp53*), neuronal/glial identity (HuC, Gfap), neuronal migration/cytoskeletal regulation (Dcamkl1, L-plastin), and inflammation (*il1b*, *tnfa*). In addition, we added *alcamb* in order to determine its relationship to stem cell engraftment potential (Jeanneet, 2013) since we previously suggested it to be involved in

brain aging (Erbaba et al. 2020b). *rest* was also added for its strong correlations towards increased longevity and neuronal protection by repressing genes involved in oxidative stress, neuronal death, and β-amyloid toxicity (Hwang, 2018). In this study, *myca*, *tp53*, and *lcp1* expression levels were significantly decreased with advancing age, and OF significantly elevated *sox2* expression levels in zebrafish brains. Finally, we showed with multivariate analyses that the OF diet groups clustered at higher values for proliferation and inflammation-related protein and gene expression levels, while CR diet groups clustered at lower values. These data suggest that OF is correlated with increases in cell proliferation and inflammation, while CR induces the opposite effects. The results from this study identify alternative therapeutic approaches and targets for reversing neurobiological changes during brain aging.

Since in the third chapter, we reached a conceptual conclusion with CR related to its possible contributions on metabolism to slow it down with more controlled cell proliferation and promoting quiescence, the affected mechanisms can be thought to be passing from the cell cycle regulations. Therefore, in the fourth chapter, we aimed to discover the transcriptional alterations with CR by utilizing the microarray technique. Identifying 526 differentially expressed genes (DEG) with CR on advanced aged brains, we determined the functional annotations of those DEGs. Then we tried to validate a selection of 23 genes via RT-PCR after. Among those 23 genes, we further chose the *tfdp1* gene to proceed with since also in the second chapter, by multivariate analyses, we inferred the effect of CR on cell cycle regulations. As we tested with another cohort of zebrafish brains, Tfdp1 protein levels significantly increased with advancing age. This outcome intrigued our attention to whether this could be a candidate gene to pursue a CR mimicking approach by simulating its downregulating expression pattern on zebrafish embryos and adult animals by using specifically designed morpholino oligos (MO). MO has previously

been suggested and used to knock down a gene transiently, *tfdp1* in our case. Then, we tested the MO on both zebrafish embryos and adult animals and analyzed the Tfdp1 downstream gene expressions in all. Though we reached no significant differences with the adult injections and embryo injections with 2ng and 4ng doses, results showed that 8ng *tfdp1*-MO embryo injections caused upregulations in *myca* and *tp53* expression levels.

To sum up, with this thesis, the neurobiology of first aging, then caloric restriction, lastly, the effects of a potential CR mimicking attempt on a cell cycle-related gene *tfdp1* were investigated. Conducting our experiments, we ultimately aimed to intervene brain aging with non-invasive dietary interventions in search of a reliable therapeutic approach for reversing/alleviating neurobiological changes during brain aging, besides being able to propose new drug targets for neurodegenerative diseases.

CHAPTER 2

TRANSCRIPTOMIC ALTERATIONS DURING BRAIN AGING IN ZEBRAFISH USING RNA SEQUENCING

2.1. Introduction

The brain shows transcriptional profile changes throughout life. Identifying the genetic pathways that change during the aging process will enable us to understand the mechanisms related to brain aging. It is crucial to determine how similar neurodegenerative processes such as Alzheimer's (AD) or Parkinson's disease are to healthy brain aging, and to find a treatment or prevention strategy for them. These diseases place a significant burden on patients and caregivers. However, in order to interpret the diseased state we must first have a comprehensive understanding of the healthy aging brain. To date, human lifespan has been extended, and the same should be possible for the duration of human health. One of the methods that provides a comprehensive study of the molecular and cellular aspects of the brain is RNA sequencing. It is widely used in many different approaches for humans and animals. RNA sequencing data from aging human brains is available to anyone through the Aging, Dementia and Traumatic Brain Injury

(TBI) Study (http://aging.brain-map.org). In that study, The human brain regions were sequenced from donors aged 78-100+ years with defined dementia or TBI status.

Various factors influencing the aging process have been highlighted in the literature, from molecules to cellular components and pathways. To begin with, complement system genes were discovered as biomarkers for aging (Bae et al., 2018). Similarly, immune system genes have been found to be upregulated in the hippocampus during aging (Ianov et al., 2017). In another study, the roles of micro RNAs (miRNAs) in aging were examined. A specific miRNA, for example miR-34, was observed to be effective in preventing neurodegeneration (Kennerdell et al., 2018). Another factor affecting aging is post-transcriptional regulation. Increases in RNA editing throughout aging is a conserved trait in primates (Li et al., 2013). It has been shown that intron retention plays a different role in the regulation of biological functions at different stages of aging (Adusumalli et al., 2019). Similarly, splicing patterns were investigated during aging. Although most splicing is limited to developmental stages, some still persist during aging (Mazin et al., 2013). Last but not least, autophagy-lysosomal related pathways were prominent in the dorsolateral prefrontal cortex in AD (Raj et al., 2018). To overcome the aforementioned impairments that occur with advanced age, it is therefore crucial to trace the identification of new potential therapeutic targets for AD interventions. Another such improvement is the restoration of neural stem cell (NSC) proliferative ability through interleukin-4 restoring plasticity inhibited by AD (Papadimitriou et al., 2018).

There is also interindividual variability in gene expression, and heterogeneity increases with age. A recent study found that middle-aged women and Alzheimer's patients have more similar patterns in the prefrontal cortex than younger women (Sanfilippo et al., 2019). As suggested by Kedlian et al. (2019), this variation of gene expression that occurs

with advanced age is not limited to a specific pathway, but instead is distributed across various biological pathways.

A previous study examining existing databases to find a common pathway contributing to AD pointed out that the cell adhesion molecule pathway is the only consistent pathway (Liu et al., 2012). In addition, cell adhesion molecules, as a gene ontology (GO) biological process category, were found among the categories that were significantly enriched in genes that demonstrating consistent upregulation during postnatal development and downregulation in aging (Dönertaş et al., 2017). Similarly, genes with roles in cell membrane, regulation of neurogenesis, and long-term potentiation, as well as genes related to cell adhesion, have been shown to be downregulated with age in the rat hippocampus (Pereira et al., 2017). Similarly, Frahm et al. (2017) found that focal adhesion genes are downregulated with age. Another study analyzing 2 whole-genome AD transcriptome data and 4 brain expression genome-wide association study datasets showed that cis regulatory single-nucleotide polymorphisms are enriched in the cell adhesion molecules pathway (Bao et al., 2015).

The aim of this study is to investigate the gene expression differences in aging zebrafish brain using neural cell populations and comparing them with human brain samples. For thi purpose, we extracted cells from young-adult (3 months), adult (5.5-8.5 months) and old (26-31 months) zebrafish brains, then performed RNA sequencing. Following data analysis, we obtained a list of genes whose expressions were alteredsignificantly with age. After testing our gene list in whole zebrafish brains, human brain samples, and Allen Brain Atlas data, we found that cell adhesion molecules, more specifically ALCAM (Alcamb in zebrafish) and GJC2 (Cx47in zebrafish)), are critical during brain aging.

2.2. Experimental

2.2.1. Cell extraction from the whole brain

The cell extraction and tissue culture procedure from zebrafish brains was specially adapted from the Kızıl laboratory thanks to Christos Papadimitriou and Dr. Çağan Kızıl. Miltenyi Biotec Neural Tissue Dissociation Kit (130-092-628) was used for cell extraction from zebrafish brains. Briefly, the fish were washed in 70% ethanol, and brain dissection was performed as previously described (Arslan-Ergul et al., 2016), except that in Dulbecco's phosphate-buffered saline (DPBS), 1% penicillin-streptomycin, 1% anti-anti solution (all from Gibco). Up to 5 brains per reaction, individual brains were collected in isolation medium containing 4 mL of Leibowitz (L) 15 medium and 1% 40 µL pen strep. The enzyme mixture was prepared as 25 µL of papain enzyme in 1,950 µL enzyme buffer, added to the brain in an isolation medium, and incubated in this solution at 28 ^{o}C for 25 minutes. Then, enzyme mix 2 (5 µL enzyme A and 10 µL buffer Y) was added to the brain tissue mixture and similarly incubated in this solution at 28 ^{o}C for 25 minutes. After the triturated glass pipettes were washed successively with DPBS, then 70% ethanol, then again with DPBS, the brain tissue mixture was passed through these pipettes 20 times for homogenization. Lysates were then passed through 70 µm filters for single-cell dissociation and washed with wash buffer (L15 medium supplemented with 5% fetal bovine serum (FBS), 1% pen-strep and 1% anti-anti solution). Finally, the lysates were centrifuged, the pellet dissolved in wash buffer, and then centrifuged again. The final pellet was dissolved in culture medium (L15 supplemented with 5% FBS, 1% pen-strep, 20 ng/mL epidermal growth factor and 20 ng/mL basic fibroblast growth factor). Finally, the cells were incubated at 28 ^{o}C in a CO_2-free incubator. The medium was refreshed in half every two days. Cells were plated in CellBIND (Corning) flasks.

2.2.2. Animals

AB strain wild-type zebrafish were used in this part of the experiments. Animals were fed dry food twice daily and artemia three times a week. Fish were kept in standard conditions. Bilkent University Animal Ethics Committee approved the methods used in this study with the decisions of 2014/18 and 2016/1.

2.2.3. RNA Isolation

According to the manufacturer's instructions, total RNAs were isolated from scraped cell cultures using Qiagen's RNeasy Mini Kit. The isolation protocol was followed by DNase treatment using Thermo Fisher Scientific's Ambion TURBO DNA-free Kit. Human RNA samples were obtained from Biochain (USA). Healthy RNA samples (R1234035-P) were stated to be collected from 5 donors aged 21, 24, 26, 26, and 66 years old. Alzheimer's RNA sample (R1236035Alz-50) was stated to be obtained from an 87-year-old Alzheimer's patient. As commercially indicated, all human samples were collected from males.

2.2.4. RNA Sequencing

RNA samples were sent to TÜBİTAK MAM Gebze Laboratories for the RNA sequencing experiments, where the Illumina HiSeq 2500 was used. Briefly, RNA libraries were prepared according to the manufacturer's protocol using the TruSeq Stranded Total RNA Library Prep Human/Mouse/Rat (ILLUMINA), which also supports zebrafish. The first step in library preparation was the removal of cytoplasmic ribosomal RNA using biotinylated, target-specific oligos coupled with Ribo-Zero ribosomal RNA extraction beads. After this depletion, the RNA was fragmented into small fragments using divalent cations under high temperatures. The cleaved RNA fragments were transcribed into first-strand complementary cDNA using reverse transcriptase and random primers, followed by second-strand cDNA synthesis using DNA polymerase I and RNase H. Double-stranded

cDNA was A-tailed, and barcoding indices were added via ligation enzyme. All samples were single-indexed. The products were then purified and enriched by PCR to create the final cDNA library.

Data analysis was done by our group members and Novogene Ltd (China). Briefly, raw FASTQ files were cleared from adapters, Q20, Q30, and GC contents were calculated. High-quality clean data was used in downstream analyses. The reference genome and transcriptome index was constructed using Bowtie v2.2.3, and paired-end clean reads were aligned using TopHat v2.0.12. The transcript's fragments per kilobase (FPKM) were calculated after read counts mapped to each gene via HTSeq v0.6.1. Differential expression analysis was performed with the DESeq R package (1.18.0). Genes with an adjusted p-value of < 0.05 (Benjamini and Hochberg approach) were assigned as differentially expressed. GO enrichment analysis was performed by the GOSeq R package (Ashburner et al., 2000; Young et al., 2010) with a corrected p-value of < 0.05. Pathway and process enrichment analysis was performed in Metascape (Zhou et al., 2019). All raw and processed data has been uploaded to the Gene Expression Omnibus and can be accessed from the GSE133436 registry.

2.2.5. Real-timePCR

To synthesize cDNA, we used Roche Transcriptor HiFi cDNA Synthesis Kit. We used Roche FastStart Essential DNA Green Master on a LightCycler 480 machine and SensiFAST SYBR Mix on a Mic PCR from Biomolecular Systems for RT-PCR experiments. The primers used are given in Supplementary Table 1-2.

2.2.6. Statistics

All statistics and graphs were performed in Prism 8 for macOS, version 8.1.1. For experiments on zebrafish brain cells, there were 3 samples: old, adult, and young-adult. Therefore, we applied two-way analysis of variance, followed by the Tukey's multiple comparison test. A p value less than 0.05 was considered significant. For whole zebrafish brains and Alzheimer's samples, there were 2 groups, as 7- and 17-month-old fish, and healthy and Alzheimer's samples. Accordingly, we applied the 2-tailed t-test. Again, $p < 0.05$ was considered significant for all tests.

2.3. Results

2.3.1. Gene expression profiling reveals distinct grouping

This study aimed to obtain cell suspensions from zebrafish brains of different ages. By combining young-adult (3 months old), adult (5.5-8.5 months), and aged (26-31 months) zebrafish cohorts as shown in Table 1, we obtained a progenitor-enriched cell culture. Then we followed RNA sequencing from the total RNAs of these samples (Figure 1A). The progenitor status of these samples was confirmed by RT-PCR measuring *nestin, sox2, neun, s100b,* and *tmem119* (Figure 1B). We used *nestin* for proliferating precursors (Mahler and Driever, 2007), *sox2* for progenitor cells, *s100beta* for glial cells (März et al., 2010), *tmem119* for microglia (Satoh et al., 2016), and *neun* (*rbfox3b*) to mark post-mitotic neurons (Won et al., 2016). There was a significantly higher expression of *nestin* ($p = 0.0160$) and *neun* ($p = 0.0103$) in the young-adult group than in the old group. For *sox2* and *tmem119*, the young-adult group had higher expression than the adult and old groups (*sox2*: $p = 0.085$, $p = 0.0003$; *tmem119*: $p = 0.0231$, $p = 0.0005$). The expression levels of *s100beta* increased numerically during aging, albeit slightly. Thus, the two markers of progenitor cells, *nestin,* and *sox2* were highly expressed in young adults but showed lower expression in older groups, though still retaining the expression of those. Neurons, glia,

and microglia were also represented in our cell culture. The young-adult group had more neurons and microglia, while the older group was slightly enriched in glia. We observed a gradual change during aging for all markers. Therefore, our cell culture represents brain cells and progenitors for all age groups.

Table 1 Sample characteristics. (Reprinted from Erbaba et al., 2020b)

Sample	Age	Pool
Old1	26–28 months old	5 brains
Old2	30–31 months old	5 brains
Old3	30–31 months old	5 brains
Adult1	8.5 months old	5 brains
Adult2	5.5 months old	5 brains
Adult3	5.5 months old	5 brains
Young-adult1	3 months old	10 brains
Young-adult2	3 months old	10 brains
Young-adult3	3 months old	10 brains

After quality controls, bioinformatics analysis was performed to identify differentially expressed genes shown in a Venn diagram (Figure 2A). Here we compared young adults to adults, and adults to older groups. We omitted the young-adult to old comparison since we wanted to focus on genes that change consistently and continuously during aging. Therefore, we only analyzed genes that are differentially expressed between adult and young-adult groups and the old and adult groups. However, we performed a young-adult-old comparison and plotted a 3-component Venn diagram in addition to plotting volcano plots to distinguish differentially expressed genes between groups. Thirty-seven genes were differentially expressed between the olds and adults, and 153 genes were different in expressions between adults and young adults. Of these, 14 genes were common to both lists. A total of 176 genes were found to differ significantly in either comparison. We mapped a cluster from these 176 genes (Figure 2B). After looking at the hierarchical clustering of genes and samples, adult and old were found closer together, while the young-adult profile formed a separate group. We also sought to determine whether there

are groups of genes that were prominently expressed at developmental stages. Principal component analysis was performed for all data, and groups were distinctly separated as expected. This confirms that the stages of adulthood differ from each other in gene expression.

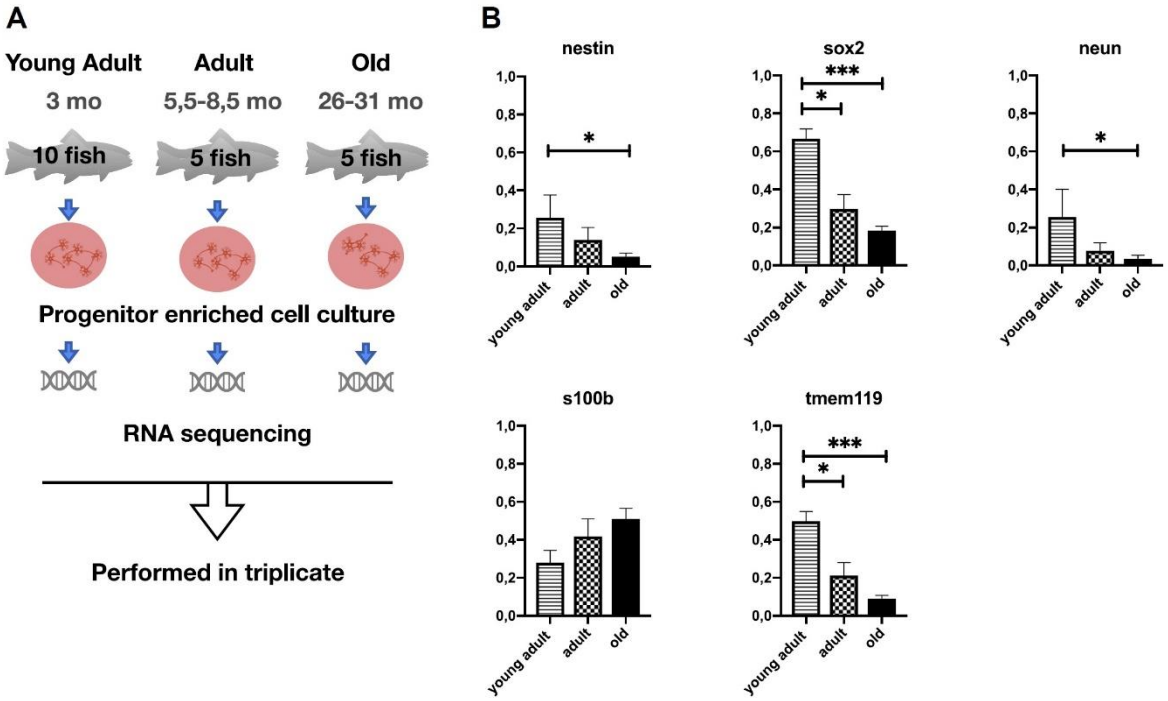

Figure 1 (A) Experimental scheme for isolation and characterization of cells obtained from zebrafish brains. Young-adult (3 groups, 10 fish in each group), adult (3 groups, 5 fish in each group), and old (3 groups, 5 fish in each group) fish were used to isolate cells from whole brains. Total RNAs were isolated following 5-7 days of cell culture. (B) Cells were characterized by progenitor cell markers by RT-PCR. Y-axis is the relative gene expression levels. N = 3 for each group. *$p < 0.05$, ***$p < 0.01$. (Reprinted from Erbaba et al., 2020b)

GO terms described gene annotations in relation to the cellular component, molecular function, and biological processes of genes. The GO enrichment table shows the number of differentially expressed genes associated with the indicated GO terms. By running our 176 genes in the GO analysis, we observed that several GO terms were associated with our genes (Figure 2C). Similarly, we performed Metascape analysis on the same gene set (Figure 2D). Highly enriched terms included cell adhesion, biological adhesion, movement, axon guidance, and neuron development from biological processes; membrane from the cellular compartment; and protein binding from receptor binding, cell adhesion molecule binding, and molecular function. Cell adhesion and biological adhesion terms were found to be statistically significant. Thus, the cell adhesion explanation from GO analysis stands out as a fundamental pathway that changes throughout aging.

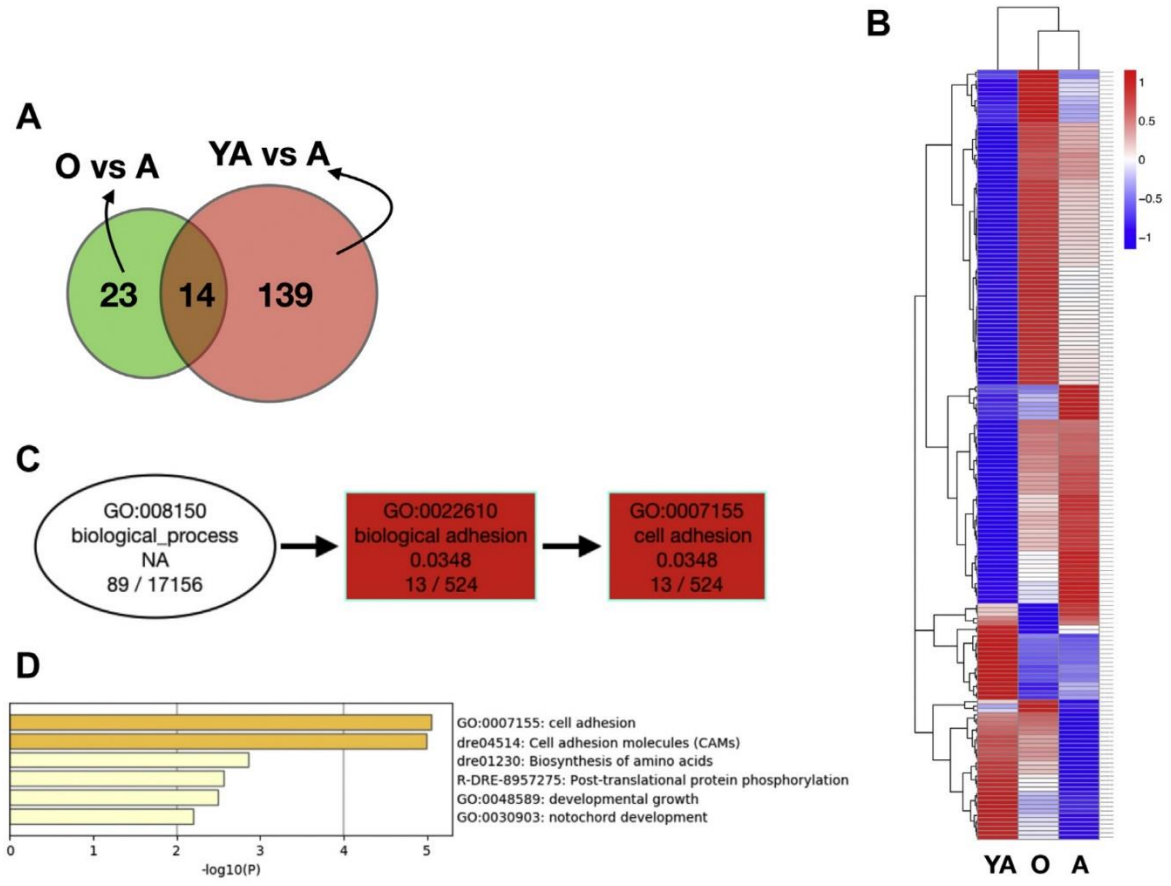

Figure 2 Description of the differentially expressed genes (DEG) is shown. (A) A Venn diagram for the DEGs in young-adult versus adult, and adult versus old groups. (B) A heat map of the DEGs is shown. Blue color demonstrates low expression, red indicates high, and white represents middle-level expression. Experiment groups are in columns, and genes are in rows. It is an unsupervised clustering, and subclusters are shown by diagrams on the left and top of the map. (C) Directed acyclic graph diagram of the most significant GO term descriptions of the DEGs. GO terms are given. In the biological process description, 89 genes were found from our list. Within this group, 13 genes are present in the biological adhesion and cell adhesion descriptions ($p = 0.0348$). (D) Metascape pathway and process analysis of the 176 DEGs. (Reprinted from Erbaba et al., 2020b)

2.3.2. Functional classification reveals two classes of cell adhesion molecules

We aimed to find human orthologs from 176 significantly differentiated genes. To this end, we first ran the gene conversion tool of the database for annotation, visualization, and integrated discovery (DAVID) (Huang et al., 2009a) to transform the gene IDs.134 genes were assigned with an Entrez Gene ID. From this list, two comparison lists were created with fold changes from old to adult, and from adult to young adult. There we aimed to find the significant changes through aging. From the list of statistically significant differentially expressed genes (DEG), we manually selected genes meeting three criteria decided as follows: (1) either <0.5 or >2 fold change, (2) changed in the same direction in both lists of comparisons, and (3) had a gene name, meaning that the transcript was annotated. The final list had 39 genes. We performed a functional classification in DAVID from selected genes. This tool helps reduce large lists to functional groups so that a subset of genes of interest can be further investigated (Huang et al., 2009b). There, we identified two gene groups as given in Table 2.

All of these genes, except *cldnk*, had human orthologs. Although there were two groups, they all had a standard definition: cell adhesion. Therefore, in both this analysis and the previous GO analysis, we found that cell adhesion is an important class of genes, and therefore we decided to focus on these genes.

2.3.3. Relative expression levels of cell adhesion molecules in progenitor cell culture and whole zebrafish brains

Table 2 DAVID gene functional classification result. (Reprinted from Erbaba et al., 2020b)

Ensemble gene ID	Gene name in zebrafish	Gene name in human
Gene group 1		
30634	Neural adhesion molecule L1.2 (*nadl1.2*)	L1 cell adhesion molecule (*L1CAM*)
100141490	Neurofascin homolog (chicken) a (*nfasca*)	Neurofascin (*NFASC*)
474346	Myelin associated glycoprotein (*mag*)	Myelin associated glycoprotein (*MAG*)
100142639	T-cell immunoglobulin and mucin domain containing 4 (*timd4*)	T-cell immunoglobulin and mucin domain containing 4 (*TIMD4*)
323919	Activated leukocyte cell adhesion molecule b (*alcamb*)	Activated leukocyte cell adhesion molecule (*ALCAM*)
Gene group 2		
445070	Claudin k (*cldnk*)	–
447835	Connexin 47.1 (*cx47.1*)	Gap junction protein gamma 2 (*GJC2*)
100142639	T-cell immunoglobulin and mucin domain containing 4 (*timd4*)	T-cell immunoglobulin and mucin domain containing 4 (*TIMD4*)
550431	Claudin 19 (*cldn19*)	Claudin 19 (*CLDN19*)

Because RNA-seq can be noisy, we asked if the results could be replicated in RT-PCR. Different RNA samples were taken from different fish cohort sets from the same age groups for validation. RT-PCR experiments were performed after RNA isolation. The RT-PCR results for the genes given in Table 2 were as expected. The fold changes for *alcam*, *cldn19*, *nadl1.2*, and *mag* were in the same direction. Fold changes for the *nfasca*, *timd4* (p=0.04, between old and young-adult), and *cx47* genes were in a different direction from the RNA sequencing results (Figure 3).

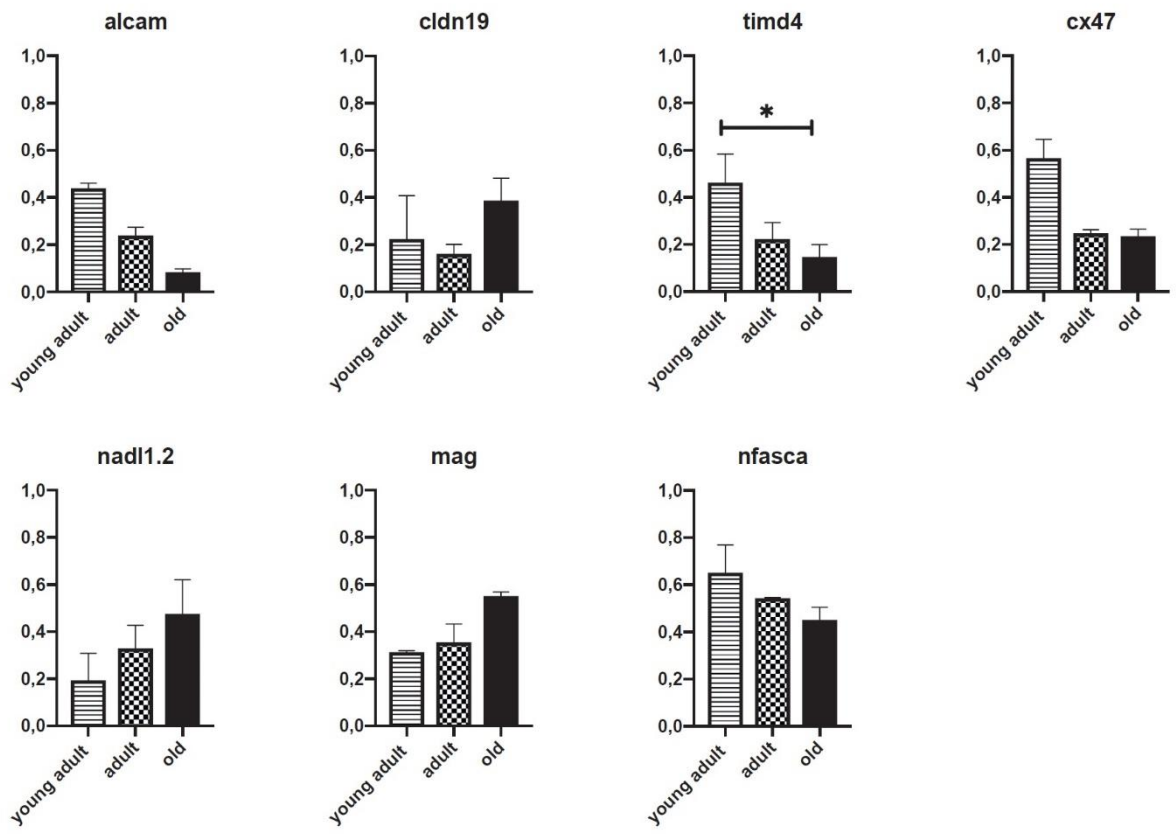

Figure 3 RT-PCR validation of the RNA sequencing results. Cells were tested for cell adhesion gene expressions. RNAs were obtained from the cultured cells on days 5-7. Y-axis shows the relative gene expression levels. N = 3 for each group. *$p < 0.05$. (Reprinted from Erbaba et al., 2020b)

Results so far have been from progenitor cell culture from pooled zebrafish brains. We also wanted to test the expression of these genes in individual whole brains by RT-PCR to detect the expression difference or similarity between the progenitor rich cell culture and whole brain samples. For this purpose, 7-month-old and 17-month-old fish were used. Gene expressions changed significantly between 7-month and 17-month samples for all genes except *nfasca* (Figure 4). Expression levels of *alcam* ($p = 0.0011$), *cldn19* ($p < 0.0001$), *timd4* ($p = 0.0003$), *cx47* ($p < 0.0001$), *nadl1* ($p < 0.0001$) and *mag* ($p < 0.0001$) decreased while *nfasca* increased with age.

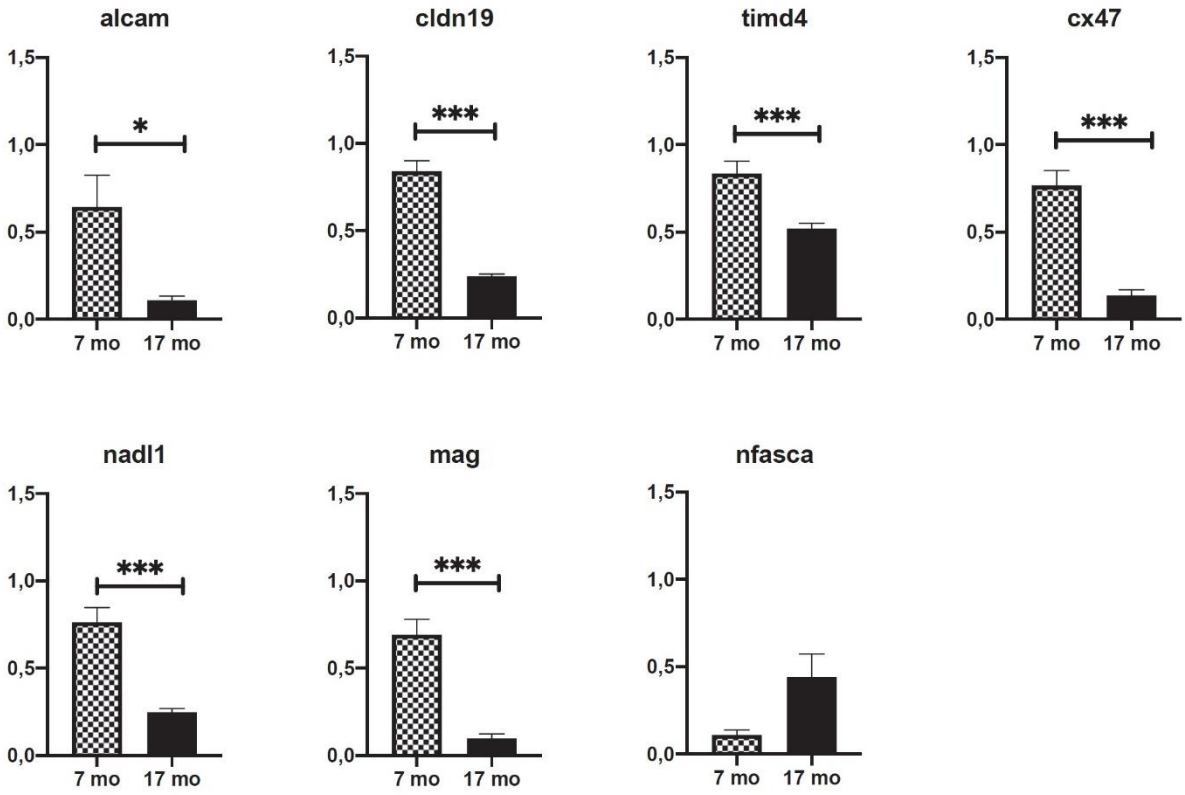

Figure 4 Relative expression levels of the cell adhesion genes measured by RT-PCR in whole zebrafish brains. Whole brains of 7 and 17 months old fish were used. Y axis indicates the relative gene expression levels. N = 3 for each group. *p < 0.05, ***p < 0.001. (Reprinted from Erbaba et al., 2020b)

There was differential expression of cell adhesion genes in different zebrafish samples up to this point. Next, we decided to check the expression patterns of these genes now in the human brain samples.

2.3.4. Analysis of the selected genes in healthy and Alzheimer human brain samples

Therefore, as a next step, the expression levels of the selected genes were analyzed in human samples. For this, we ordered human brain RNA samples from Biochain. It was stated by the company that one RNA sample was extracted and pooled from 5 young human male brains, and the other RNA was stated to be collected from the brain of an 87-

year-old Alzheimer's patient. We wanted to test the samples for known markers of aging and development first. The human telomerase complex has an RNA component called TR and an enzyme component called TERT. Expressions of both *TR* and *TERT* genes are greatly reduced during adulthood; however, they remain at detectable levels (Spilsbury et al., 2015; Ishaq et al., 2016). Consistent with this, we observed a weak but detectable level of *TERT* in our Alzheimer's sample RNA (Figure 5A) ($p = 0.0297$). Likewise, *TR* expression was missing in the Alzheimer's sample ($p = 0.0013$). For undifferentiated stem cells, POU Class 5 Homeobox 1 (*POU5F1*/*OCT4*) and Nanog homeobox (*NANOG*) gene expressions are known to be critical for cell proliferation while Tubulin beta 3 class III (*TUBB3*/*TUJ1*) gene is known to be primarily expressed in neurons. We ran RT-PCR for these three genes for healthy and Alzheimer's samples and found that all three were significantly reduced in Alzheimer's samples (Figure 5A). Expressions for *DNMT1* ($p = 0.012$), *OCT4* ($p = 0.0344$), *NANOG* ($p = 0.06$) and *TUJ1* ($p = 0.001$) were lower in the Alzheimer's sample than in the healthy sample. We then analyzed the cell adhesion-related genes we selected from the RNA sequencing data. We found that each of these genes was downregulated in Alzheimer's samples, except for *TIMD4*, which had similar levels in both samples. The reductions in the expression levels of *ALCAM* ($p < 0.0001$), *CLDN19* ($p = 0.008$), *L1CAM* ($p < 0.0001$), *MAG* ($p = 0.0006$) and *NFASC* ($p = 0.0002$) were statistically significant in the Alzheimer's sample (Figure 5B).

To examine the interaction of these proteins with each other and with some age-related proteins, we used the Cytoscape software (Supplementary Figure 1). Findings indicated that *L1CAM* and *ALCAM* were found to interact with each other, and *MAG* and *GJC2* established a separate interaction together. Moreover, *ALCAM* was also found to interact directly with *NANOG*, *OCT4*, and *SOX2;* and indirectly with *TERT* and *DNMT1*.

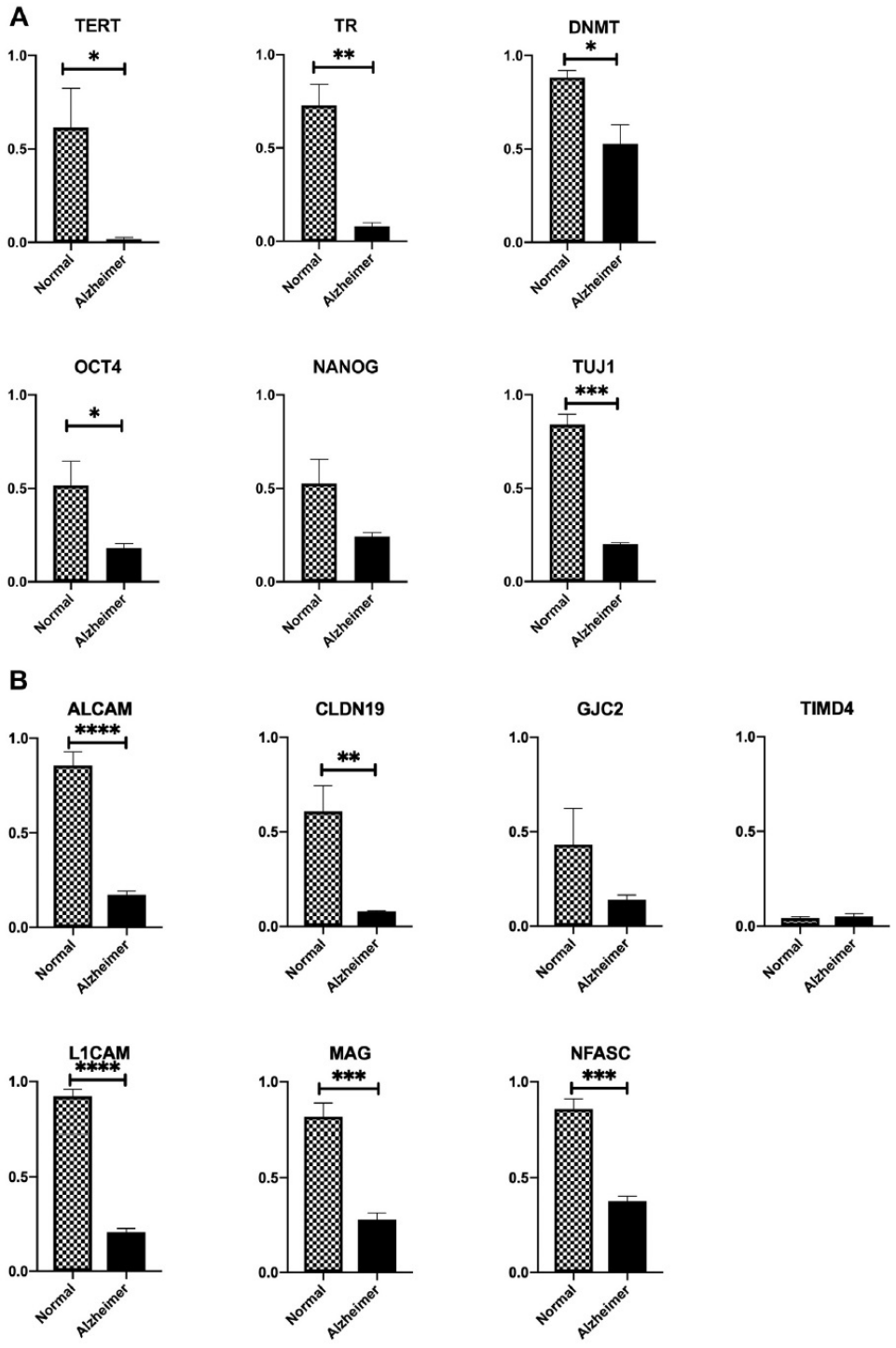

Figure 5 Relative expression levels of selected genes in human normal and Alzheimer's RNA samples (Biochain). (A) RT-PCR results are shown regarding several aging and developmental markers. (B) Cell adhesion genes were measured for assessment on

expression levels via RT-PCR. Y-axis indicates the relative gene expression levels. *p < 0.05, **p < 0.01, ***p < 0.001. (Reprinted from Erbaba et al., 2020b)

2.3.5. Expression data of the selected genes in the Allen Brain Atlas dataset

Finally, we studied the expression profile of selected genes in the available RNA sequencing data. We analyzed the distribution of selected genes from the "Aging, Dementia and TBI" database from the Allen Brain Atlas study. First of all, we performed cluster analysis according to increasing age. We did not observe any groupings here (data not shown). We hypothesized that the lack of grouping in the data was due to that the youngest person included in this database was 78 years old. So our analysis was actually a cluster analysis of the old versus the very old. However, interestingly, we noticed a remarkable grouping when we grouped the genes we selected according to brain regions. We selected genes highly expressed in the frontal white matter, a brain region particularly important in aging. As seen in Figure 6, the *NFASC*, *ALCAM*, *DLG1*, and *MAG* genes in the aged human brain were highly expressed in frontal white matter compared to other brain regions studied here. Also, the *L1CAM* gene was highly expressed in the parietal and temporal cortex compared to the hippocampus and frontal white matter. While we could not extract age differences from these data, the gene expression patterns in the old brain seem to differ notably between brain regions.

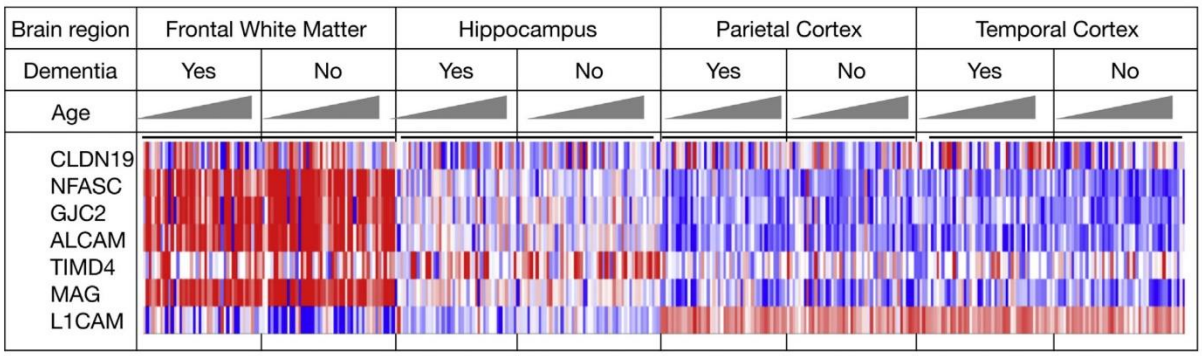

Figure 6 Clustering of the selected genes is demonstrated with Aging, Dementia, and TBI (Traumatic Brain Injury) data. Brain regions of frontal white matter, hippocampus, parietal cortex, and temporal cortex were included in the study. Each brain region is grouped into patients with or without dementia and then further organized in increasing age from 78 to 100+. The red color demonstrates the highest expression, and blue indicates the lowest expression. Genes are shown in rows. Aging, Dementia and TBI Study. 2016 Allen Institute for Brain Science. Allen Human Brain Atlas is available from human.brainmap.org. (Reprinted from Erbaba et al., 2020b)

Our results are aggregated with a visual representation (Figure 7). Figure 7A shows the positions of cell adhesion proteins and possible interactions, while Figure 7B summarizes our findings in this study in a tabular view. In the figure, ALCAM proteins are presented on the membranes of antigen-presenting cells that match CD6 proteins found on T cells (Figure 7A, label 1), L1CAM has been shown to form homodimers through pre- and post-synaptic neurons (Figure 7A, label 2), CLDN (CLDN19 and CLDN16) has been shown to form junctions in endothelial cells (Figure 7A, label 3), MAG is represented in myelin-producing Schwann cells, NFASC is found in myelin-producing cells that interact with the CNTN1 protein in axons (Figure 7A, label 4), and lastly GJC2 (CX47) is drawn attached to oligodendrocytes to form either homodimer in oligodendrocytes or heterodimer with a CX43 protein present in an astrocyte (Figure 7A, label 5). Our results showed that *ALCAM* and *GJC2* decreased consistently with age in all our analyses, with *CLDN19*, *L1CAM*, *MAG*, and *NFASC* forming a pattern of expression that decreased in 2 of 4 experiments and increased in others.

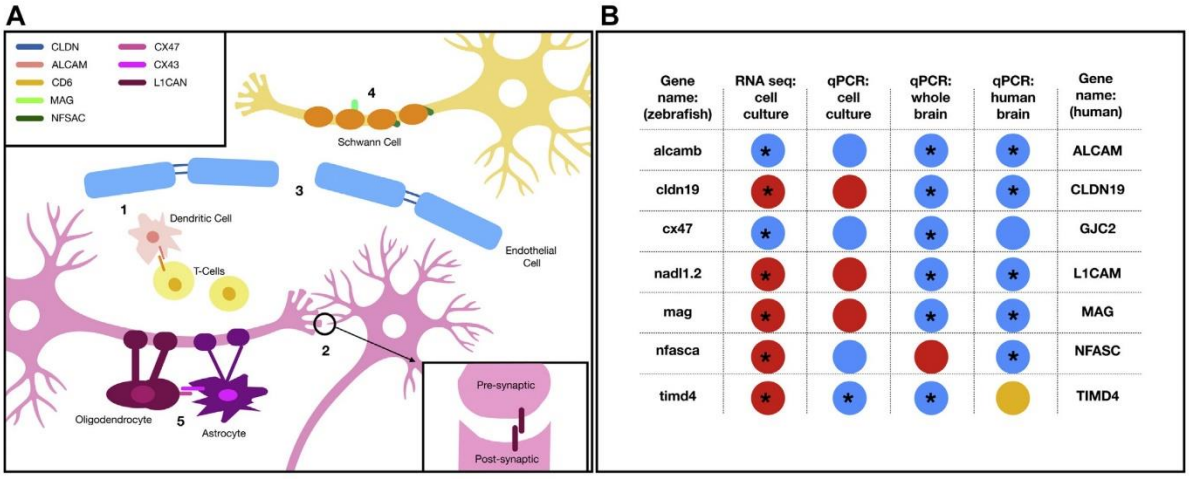

Figure 7 (A) An illustration demonstrates the interactions of cell adhesion molecules in the junctions, and (B) a summary table of gene expression levels of the genes of interest in different experimental set-ups. In the table, blue circles indicate a decreased expression during aging, and the red colored circles mean an increased expression with age. The one yellow circle indicates the expression remains the same. Stars in the middle of the circles refer to the significance. Adapted from Kegg pathway no: hsa04514, except cx47 interactions, which was adapted from Kim et al. (2013). APC: antigen-presenting cell, Astro: astrocyte, Axon: axon of a neuron, endothelial: endothelial cell, Myelin: myelin-producing oligodendrocyte, Olig: oligodendrocyte, Post: postsynaptic neuron, Pre: presynaptic neuron, Schwann: Schwann cell, T cell: T lymphocytes. (Reprinted from Erbaba et al., 2020b)

2.4. Conclusion

Here in this second chapter, age-related gene expression level differences of a group of cell adhesion molecules were studied. We tested the genes in progenitor-enriched cells derived from zebrafish brain via RNA sequencing and RT-PCR and in whole zebrafish brain and commercially available human brain samples via RT-PCR. We identified several cell adhesion protein genes with altered expression in aging. These are, *ALCAM*, *GJC2*,

L1CAM, CLDN19, MAG, NFASC, and *TIMD4*. Briefly, in this chapter, our results suggested that especially the cell adhesion molecules that we included in this study play a critical role in aging. Among all mentioned genes, the pattern of decreasing expression of *alcamb*/*ALCAM* and *cx47*/*GJC2* with age was remarkably consistent across all our data. Between these genes, since *ALCAM* has also been associated with neuroinflammation previously, we wondered whether it could also respond to nutrient interventions with aging in the brain. Therefore in the next chapter, along with other markers for different concepts to better understand alterations in the brain following nutrient interventions, we checked *alcamb* expression levels with respect to diet and age.

2.5. Discussion

In this second chapter of the thesis, the age-related gene expression level differences of a group of cell adhesion molecules were studied. We tested the genes in progenitor-enriched cells derived from zebrafish brain via RNA sequencing and RT-PCR, as well as in whole zebrafish brain and commercially available human brain samples via RT-PCR. Our results showed that especially the cell adhesion molecules that we included in this study play a critical role in aging. Among all mentioned genes, the pattern of decreasing expression of *alcamb*/*ALCAM* and *cx47*/*GJC2* with age was remarkably consistent across all our data; this highlights a possible target for age-related neurodegenerative diseases, which opens doors for new therapeutic strategies and drug targets age-related deterioration. Although some of these genes have been well studied and some have not been studied, there are not enough studies in the literature investigating their roles in aging or responses to therapeutic options targeting these genes. This makes our study an interesting one that allows us to observe their functional role with age. In this chapter, we identified several cell adhesion protein genes with altered expression in aging. Below we have briefly summarized the

literature on the most comprehensive: *ALCAM*, *GJC2*, *L1CAM*, *CLDN19*, *MAG*, *NFASC*, and *TIMD4*.

The active leukocyte cell adhesion molecule (ALCAM / CD166) is a member of the type I transmembrane immunoglobulin superfamily of cell adhesion molecules, and shares 93% similarity between human and mouse orthologs (Bowen et al., 1997). Its name stands because it is mainly expressed on the surface of active leukocytes (Bowen et al., 1995), participates in leukocyte migration through blood-brain barrier (BBB) tight junctions, and roles in modulation of synaptic transmission (Cayrol et al., 2008; Curis et al., 2016; Lécuyer et al., 2017; Park et al., 2017). It acts on leukocytes by attracting and collecting leukocytes to the site of inflammation (Shahaduzzaman et al., 2015). According to Cayrol et al. (2008) noted that blocking ALCAM reduces neuroinflammation by promoting leukocyte recruitment into the central nervous system. In addition to leukocytes, *ALCAM* is widely expressed in a variety of cells, including neurons, epithelial cells, fibroblasts, lymphoid cells, myeloid cells, and is also an accepted cell surface marker of mesenchymal and hematopoietic progenitor cells (Yasen, 2013; Shahaduzzaman et al., 2015). It was observed that migration and adhesion increased in synovial fluid-derived mesenchymal stem cells with *ALCAM* upregulation (Kim et al. 2017). And similarly, Alcam-null (*Alcam*-/-) mouse model hematopoietic stem cells were shown to be associated with reduced long-term grafting potential after transplantation and had no effect on cell cycle distribution regardless of age (Jeannet et al., 2014). The study also claimed that Alcam expression increased several fold in aged murine hematopoietic stem cells compared to younger ones. With regard to cancer, antibody neutralization of ALCAM (antibody-blocking antibodies that block specific tumor-expressing ligands) reduced tumor seeding in the brain, in keeping with the fact that natural ligands to cell adhesion molecules were shown to be highly expressed in metastatic tumor cells (Soto et al., 2014). In these aspects, increased

ALCAM expression levels appear to be associated with cancerous and inflammatory phenotypes in some cell types, while somewhat associated with stem cell ability, making fine-tuning of cells important for proper functioning. Given the research literature gap for *ALCAM* age-related changes in the brain, testing for gene expression change with age is thought to make important contributions to our understanding of age-related increased susceptibility to neurodegenerative diseases, in addition to its known roles. Metastasis and trafficking through the BBB. In addition, it is possible to consider a relationship between *ALCAM* gene expression and AD, since it has known effects on neuroinflammation.

The *GJC2* gene is expressed in oligodendrocytes and the protein is crucial for gap junction communication (Georgiou et al., 2017). A mutation in *GJC2* leading to loss of the connexin 47 protein has been implicated in hypomyelinating leukodystrophy-2 disease (Pelizaeus-Merzbacher-like disease), resulting in hypomyelination in its severe forms (Al-Yahyaee et al., 2013), and in hereditary spastic paraplegia (Abrams, 2019). Therefore, mutations in the GJC2 gene have serious consequences. Still, to our knowledge, there are no studies investigating how GJC2 is affected in the brain through aging and AD progression. We think that the gene, which has a function in myelination, may have a vital role in both aging and AD.

The immunoglobulin-like cell adhesion molecule (L1CAM / CD171), has a dual function in cells. One function is a static cell adhesion molecule and the other is a motility-promoting molecule that has functions during neural development and metastasis (Kiefel et al. al., 2012). Similarly, the integrin family of receptors and cell adhesion proteins provide cell-to-cell and cell-to-extracellular communication, as well as being known to be associated with cancer incidence and metastasis. The ability of L1CAM to bind to integrins has been suggested to be associated with its promoter and proinvasive effects in cancer

cells (Burgett et al., 2016; Nieberler, 2017). In another study, a zebrafish knockout model (*L1CAM* zebrafish ortholog; Table 2) of nadl1.2 was noted with problems in axonal growth as well as myelination abnormalities (Linneberg et al., 2019). In addition, Shi et al. (2016), tau proteins are clearly present in *L1CAM* expressing exosomes in human plasma, where toxic tau aggregates are transported from cell to cell, contributing to the formation of tauopathies according to one hypothesis. Talking about its relationship with aging, it is stated that L1CAM is enriched on the surface of senescent fibroblasts and helps their migration (Mrazkova et al., 2018).

CLDN19, another cell adhesion molecule, encodes a tight junction protein (Perdomo-Ramirez et al., 2019). It forms a permeable channel for magnesium and calcium ions together with CLDN16 (Giménez-Mascarell et al., 2018). CLDN19 mutations have been shown to impair retinal neurogenesis (Wang et al., 2019), leading to hypomagnesemia, hypercalciuria, and ocular abnormalities (Perdomo-Ramirez et al., 2019; Vall-Palomar et al., 2018). Therefore, it is intriguing whether this gene has a role in neurogenesis through aging. Expression of *CLDN19* in endothelial cells forming a magnesium channel suggests that it plays a role in senescence by upregulating BBB trafficking.

MAG is a type I transmembrane glycoprotein expressed in myelinating oligodendrocytes and Schwann cells (Pronker et al., 2016). As in the case of GJC2, it is involved in myelin maintenance and the survival of oligodendrocytes (Quarles, 2007). Mutations in this gene cause the same Pelizaeus-Merzbacher-like disease as *GJC2* gene mutations, which have malformed bulb structures and thin myelin sheaths of affected axons (Lossos et al., 2015). Similarly, MAG-deficient mice have defects in myelin formation and maintenance, and possibly axonal function (Bartsch et al, 1996; Kamil et al, 2019).

Besides the aforementioned, neurofascin cell adhesion proteins are located at the node of Ranvier, forming the nodal macromolecular complex containing voltage-gated sodium channels (Zhang et al., 2015). Along with N1CAM, they also have roles in maintaining the node and myelinated axon function (Ebel et al., 2014; Taylor et al., 2017) as well as providing a permissive environment for neurite extension (Volkmer et al., 1996).). Consistently, therefore, antibodies against neurofascin isoforms result in inflammatory demyelinating neuropathy and multifocal motor neuropathy (Delmont et al, 2017; Devaux et al, 2016; Notturno et al, 2014). Last but not least, another cell adhesion protein, TIMD4, is a type I membrane protein known to regulate the TH1 and TH2 cell response (Yano et al., 2017). It contains an arginine-glycine-aspartate tripeptide (RGD domain) indicating a role in cell adhesion.

Still, the second chapter of the study had several weaknesses. First, we were unable to find a commercially available healthy brain sample collected from an elderly human individual. Therefore, although we wanted to compare the healthy elderly person sample with the elderly Alzheimer's sample and the healthy elderly person with the young elderly sample, we could not perform these tests due to ethical limitations. Second, in Allen Brain Atlas, the ages are advanced again, from 78 to 100+. In other words, we could only work with the old age group in these data. Nevertheless, we tried to draw meaningful conclusions by combining data from different sources. Third, the reasons for the inconsistent results between the experiments for the genes except *alcamb* and *cx47* are thought due to the following reasons. I) Reference genes used in the RT-PCR experiments were different for different organisms (zebrafish/human) due to the nature of the housekeeping genes selected. II) Human and zebrafish have different regenerative capacities, which could be affecting the downstream results such as intrinsic compensation mechanisms responding to the age related molecular alterations in the brain. III) Cell culturing and tissue based

methods differ to an extend due the nature of the techniques; the reagents used, the in vivo and in vitro differences, and maybe unintended selection of a portion of cell types with the adjusted cell culture media/conditions.

The third chapter provided evidence that gene expression levels of a group of cell adhesion molecules alter with aging and AD. Among the mentioned genes, the pattern of decreasing expression of alcamb and cx47 with age was consistent across all the data, therefore were the ones having potential to further investigate. Blocking ALCAM has previously been stated to reduce neuroinflammation, and increased *ALCAM* expression levels appeared to be associated with cancerous and inflammatory phenotypes in some cell types (Shahaduzzaman, 2015; Cayrol, 2008). These are why we wanted to examine it also in response to nutrient interventions to aging in the brain, because CR and OF were also implicated to alter inflammation and protect or facilitate cancer phenotypes by previous studies. That is why, in the next (third) chapter, along with other markers for different concepts to better understand alterations in the brain following nutrient interventions, we checked alcamb expression levels with respect to diet and age.

CHAPTER 3

EFFECTS OF DIFFERENT FEEDING REGIMENS ON YOUNG AND OLD ZEBRAFISH BRAIN

3.1. Introduction

3.1.1. Two opposing short-term dietary regimens: Caloric restriction vs. Overfeeding

Accumulating evidence suggests that nutrient intake is a double-edged sword, with CR extending life and health span, guarding against the detrimental effects of aging, and conversely, excess nutrient uptake leading to worsened age-related symptoms. To begin with the first, CR is a dietary intervention that is reached by applying a 30-40% reduction in overall calorie intake without causing malnutrition with a reduced diet for a certain period. Effects of CR on increased life- and healthspan have been studied and shown in diverse species such as budding yeast, flies, spiders, worms, fish, and monkeys (Al-Regaiey, 2016; Weithoff, 2007; Pani, 2015). It affects cell protective responses in nearly all organs, including the brain (Pani, 2015). CR has previously been shown to decrease apoptosis, facilitate stem cell renewal, reduce DNA damage, exert antioxidant and anti-inflammatory properties, protect against tissue structure and function deterioration, modify insulin sensitivity, autophagy, and neuroendocrine function. It maintains stem cell function

that normally declines with age. Most importantly, in this context, CR increases resistance to age-related neurodegenerative diseases and increases learning and motor performance, thereby slowing down aging (Csiszar et al. 2009; Park and Lee 2011; Arslan-Ergul et al. 2016; Cavallucci et al. 2016a; Mojaverrostami et al. 2020, Arslan-Ergul, 2013; Cerletti, 2012; Si, 2014; Hao, 2016; Mohammadi, 2014; Ellis, 2013; Testa, 2014). It is also suggested to promote anticancer response and chemotherapeutic drugs in cancer treatment (Meynet, 2014). The overall effectiveness of CR on lifespan depends not only on the amount of calories and dietary composition but also on the length and time of initiation of the diet. Several scientific reports on the effect of initiation and duration of CR have been provided, and it is stated that CR applied in the first or second half of life was more effective than application during both halves (Feldman, 2013). A study presented on rotifer species demonstrated that increases in length of CR application up to more prolonged than the median life span of the animal extends the life span by decreasing the lifetime reproduction (Weithoff, 2007).

Secondly, the other edge of the nutrition sword is an increased caloric intake, or OF. The effects of increased caloric intake on the brain are systemic inflammation, induction of synaptic stripping by microglia, gliosis that is the brain's injury response, impairments of hippocampal plasticity, disrupted connectivity, blood-brain barrier damage, and cognitive dysfunction (Miller and Spencer 2014; Tucsek et al. 2014; de Git and Adan 2015; Dorfman and Thaler 2015; Hao et al. 2016; Guillemot-Legris and Muccioli 2017). Excess and chronic OF eventually lead to the development of obesity. Many studies claim that obesity pathogenesis is associated with harmful side effects on the brain such as hypothalamic inflammation (as well as affecting other brain structures such as hippocampus, cortex, brainstem, or amygdala), gliosis (brain's injury response), induction of synaptic stripping by microglia, disrupted connectivity, blood-brain barrier damage, impairment of

hippocampal plasticity, and cognitive dysfunction. It has also been associated with the aging-like symptoms of systemic inflammation (de Git, 2015; Dorfman, 2015; Miller, 2014; Guillemot-Legris, 2017; Hao, 2016; Tucsek, 2013). A study showed that impairment in the hippocampal function that occurred due to obesity was correlated with microglial activation, which puts its effects as neuroinflammation (Hao, 2016). Furthermore, increased body weight and metabolic disorders were associated with the generation of excessive ROS and oxidative free radicals. These harmful byproducts then cause alterations in cell cycle regulation and cell signaling (Rani et al., 2016). To sum up, excess caloric intake has the opposite effects of CR-mediated protective mechanisms. However, exactly which key pathways/proteins/genes are responding to nutrient uptake status remains to be elucidated. Therefore, in the third chapter of the thesis, we were mainly concerned with the translational and transcriptional alterations in the brain related to several aging-related concepts. Below, those concepts related to brain aging are covered, which are progenitor cell proliferation, inflammation, and cell cycle regulation.

3.1.2. Relation of diets to age related concepts

3.1.2.1. Neurogenesis

In this chapter, we focused on short-term dietary regimens in order to examine their effects on several aging-related concepts in the brain. The first of these concepts that we encountered concerning brain aging is neurogenesis. Neurogenesis, by meaning, is generating new neurons from neuronal precursors, and it continues during adult life (Eriksson, 1998). Though, adult neurogenesis occurs with a decreased pace compared to the developmental periods and is restricted to some discrete areas of the mammalian brain; i.e., subventricular zone (SVZ) of the lateral ventricle, the dentate gyrus of the hippocampus, and rostral migratory stream to the olfactory bulb, which are the regions

responsible for the control of neural stem cell (NSC) self-renewal and differentiation (Taupin, 2006; Ming, 2011; Apple, 2017). Alterations in adult neurogenesis have been linked to neurological diseases, brain injury, stress, and aging (Bergmann, 2015; Apple, 2017; Lee, 2000; Kempermann, 2015). Decreased progenitor cell proliferation and neuronal differentiation during aging contribute to reduced plasticity and aging-associated cognitive impairment (Apple, 2017). The literature reviewing insights for intervening NSC aging encourages CR and physical exercise as protective therapies for healthy brain aging along with the improved insulin sensitivity and glucose tolerance, enhanced anti-inflammatory properties, decreased disease markers, and increased neuronal plasticity (Apple, 2017; Lee, 2002; Pani, 2015; Kempermann, 2015; Van Praag, 1999; Van Praag, 2014; Cherif, 2016). In this study, we are concerned with the first of these therapies, ie. CR. The effects of long and short-term CR has been claimed to promote stem or progenitor cell proliferation in the hippocampus of aging and adult mice and adult rats (Park, 2013; Hornsby, 2016). Another article also claims a rise in neurogenesis with CR, suggesting the following statement. The findings demonstrating increment in neurogenesis results from the decreasing death rate of newly produced cells rather than increasing cellular proliferation (Lee, 2000). Mechanisms on how CR exerts its protective effects on neurogenesis serve an intriguing curiosity to the researchers. One proposed mechanism is through the fine-tuning of NSCs to be involved in activity states of quiescence or proliferation. The mechanism is such that lower nutrient intake or enhanced energy expenditure favors NSC quiescence, while anabolic growth signals and elevated calorie intake will cause excessive NSC proliferation and eventually deplete the stem cell reserve (Cavallucci, 2016). This mechanism seems somehow in accordance with the well-known “Live fast, die young” belief. Therefore neurogenic cell fate decisions play an essential role during aging for stem cell reserve maintenance.

3.1.2.2. Neuroinflammation

The second concept that captured our attention in relation to aging is inflammation. It has long been noted in the clinical literature that the aging and nutritional status of the organism independently have a direct relationship with metabolic inflammation (Mattson and Arumugam 2018). Studies show that aging is highly associated with increased levels of reactive oxygen species (ROS), accumulation of proinflammatory cytokines, reduction in autophagy, and microglial activation (exhibiting the M1 phenotype, rather than M2), along with increased prominence of memory impairments and neuroinflammation related disease phenotypes such as Alzheimer's (AD), Parkinson's, Huntington's, and prion diseases, as well as in amyotrophic lateral sclerosis, frontotemporal dementia, and chronic traumatic encephalopathy (Si, 2014; Ward, 2015; Hickman, 2018). In fact, microglial sensitization has become a hallmark for the increased neuroinflammatory response in the normal aging brain and therefore is thought to contribute to the neurodegenerative disease progression (Barrientos, 2015; Ward, 2015; Hickman, 2018). This is even though the primary role of microglia is to protect the brain in response to a specific stimulus or neuroinflammation, it also has the potential to harm or kill the neurons. There is also a close relationship between diet and inflammation as it was previously shown to promote antioxidative and anti-inflammatory effects (Si, 2014; Santos, 2018; Tucsek, 2014; Caracciolo, 2014; Mohammadi, 2014; Speakman, 2011; Csiszar, 2009). Thus, as a therapeutic approach aiming to decrease inflammation in the brain via reducing cytokine and ROS levels, promoting autophagy, and correcting the imbalance between microglial phenotypes (from an M1 to M2) (Ward, 2015), CR is suggested to be used as an intervention.

3.1.2.3. Cell Cycle Maintenance

As the third concept, cell cycle regulation has been implicated as being susceptible to the effects of aging. Indeed, cellular senescence, the state in which cells enter a permanent cell cycle arrest and lose the ability to divide and grow, is known to be associated with phenotypes in conjunction with age-related pathologies (Campisi and Robert 2014). The consequences of this will be affecting the downstream pathways related to cell renewal and repair. Although senescence may prevent cancerous development in mammals (He and Sharpless 2017), it also restricts cell proliferation and cell renewal. Cell cycle progression can be promoted or inhibited by different targets affecting overall proliferation. Disturbances in cell cycle regulation were previously associated with neurodegenerative diseases (Copani et al., 2007; Ting et al., 2014; van Leeuwen and Hoozemans, 2015). The differentiated mature neurons, which normally stay on phase G0 cell cycle arrest, can exit the arrest and re-enter the cell cycle due to external or internal factors. This process will result in de-differentiation of neurons and, according to a hypothesis, will lead to apoptosis, raise the phosphorylation of tau proteins, and promote AD progression (Ueberham, 2005).

Besides aging, CR was also implicated in cell cycle regulation in that it inhibits cell proliferation on bone marrow, mice thymus, spleen, and kidney tissues (Lu, 1993) as well as being proposed so via analysis of human transcriptome datasets on different tissues due to its being energetically expensive (Seim, 2016). Seim et al. (2016) found that cell cycle maintenance-related factors such as CDK regulators were negatively correlated with cell turnover rates according to their analysis of 21 somatic cell transcriptome data, including the brain. This indicates support for CR to suppress cell cycle progression for promoting the cells to spend more time on genomic stability, which decreases the cancer risk. The gene expression profile of long-lived neurons was associated with reduced protein metabolism, similar to that observed with CR mediated profiles (Stout 2013; Mayer, 2006).

It is proposed that the decrease in cell proliferation via CR increases the time cells spend on the G0/G1 phase of the cell cycle. Thus, the damaged cells would have more time to repair their DNAs before entering the S phase (Charnly, 1985; Lu, 1993). Mercken et al. (2013) also mention a metabolic shift on skeletal muscle cells under CR from proliferation to repair and maintenance. On the other hand, increments in cell proliferation were associated with decreased time spent for DNA repair, adding to the risk for unrepaired DNA synthesis (Charnly, 1985), eventually increasing DNA damage and driving cancer incidence (Tudek, 2010). This suggests an excellent protective mechanism achieved by CR against both cancer and aging, acknowledging the relationship between DNA damage build-up and aging (Warner, 1989; Gensler, 1981; Tudek, 2010; Nicolai, 2015). Along these lines, the gains with CR on life- and health-span seem to be strongly correlated with cell cycle maintenance; therefore, research investigating the cell cycle regulators with CR is essential to understand better the CR mediated lifespan extension. By so, it is prospective to be able to propose new therapeutic solutions to both aging and neurodegenerative diseases for the ultimate goal of healthy brain aging. In search of new targets, we attempted to study the *transcription factor dimerization partner 1* (*tfdp1*) gene implicated with its critical roles during cell cycle regulation, whose expression was found to be significantly downregulated following CR and upregulated with age in the fourth chapter of this thesis.

In the current chapter, we examined the effects of two dietary interventions on markers of cell proliferation, and inflammation in the aging zebrafish brain. We used this model organism because it has become an important and appropriate gerontological model (Arslan-Ergul et al. 2013). In order to quantify the differences between the effects of overfeeding (OF) and CR on the brains of young and old animals, we applied a 12-week long diet of either ad libitum (AL)-feeding, OF, or CR similar to our previous studies

(Arslan-Ergul et al. 2016a; Celebi-Birand et al. 2020; Karoglu-Eravsar et al. 2021). The differences in brain protein and/or mRNA levels were compared for selected markers related to cell proliferation (Pcna, Sox2), cell cycle regulation (Tfdp1, E2f5, Myca, Tp53), neuronal/glial identity (HuC, Gfap), neuronal migration/cytoskeletal regulation (Dcamkl1, L-plastin), and inflammation (Il1b, Tnfa). In addition, we added Alcamb in order to determine its relationship to stem cell engraftment potential (Jeanneet, 2013) since we previously suggested it to be involved in brain aging (Erbaba et al. 2020b), and Rest for its strong correlations towards increased longevity and neuronal protection by repressing genes involved in oxidative stress, neuronal death and β-amyloid toxicity (Hwang, 2018). In this study, m*yca*, *tp53*, and *lcp1* expression levels were significantly decreased with advancing age and OF significantly elevated Sox2 expression levels in the brains of zebrafish. Finally, we showed with multivariate analyses that the OF diet groups clustered at higher values for proliferation and inflammation-related protein and gene expression levels, while CR diet groups clustered at lower values. These data suggest that OF is correlated with increases in cell proliferation and inflammation, while CR induced opposite effects. The results from this study identify alternative therapeutic approaches and targets for reversing neurobiological changes during brain aging.

3.2. Experimental

3.2.1. Animals

A total of 60 TgBAC(Gfap-GFP)zf167 zebrafish were included in this study, with 30 young (5-month) and 30 aged (25-month) animals. Both male and female animals were included in the current experiments. All fish were kept in a controlled recirculating housing system designed by ZebTec (Tecniplast, Italy) with 14-hour light and 10-hour dark cycle at 28°C system water. For both ages, fish from an 8.5-liter tank were equally divided into

three 3.5-liter tanks and assigned randomly to one of the following feeding groups: *Ad libitum* (AL: regular feeding), OF, and CR. Six animals per treatment and age group (overall N=36) were assigned to Western blot experiments, and four animals per group (overall N=24) to the RT-PCR experiments.

Fish were fed according to a feeding schedule based on previously published studies from our group (Arslan-Ergul et al. 2016; Celebi-Birand et al. 2020; Karoglu-Eravsar et al. 2021). All dry flakes of food (TetraMin Flakes) were weighed and prepared as either 100 mg or 300 mg weekly (Table 3). The nutrient composition of the commercial dry flakes consisted of the following: crude protein equal to 46%, crude oils and fats 11%, crude fiber 3%, and moisture content 6%. Freshly-hatched artemia was prepared and given to the fish as indicated in Table 1. Fish were habituated to the tanks for a week prior to dietary interventions. Then the feeding protocol was applied for 12 weeks. The duration of the feeding intervention was chosen considering the previous reports that at least 8-weeks of feeding applications are necessary to affect cognitive and molecular phenotypes (Arslan-Ergul et al. 2016; Meguro et al. 2019; Celebi-Birand et al. 2020; Karoglu-Eravsar et al. 2021). At the end of the 12 weeks, fish were euthanized in ice-cold tank system water, which was indicated by a cessation of movements that occurred for 10 min. Both the weights and lengths of the young and aged fish were measured. Following these measurements, the heads were decapitated from the body and snap-frozen in liquid nitrogen to be stored at -80°C for molecular analyses. The animal protocol for this study was approved by the Bilkent University Local Animal Ethics Committee (HADYEK) with the approval date and number: Oct 10, 2019, no: 2019/37.

	MONDAY	TUESDAY	WEDNESDAY	THURSDAY	FRIDAY	SATURDAY	SUNDAY
AL	100mg Dry Food	100mg Dry Food	100mg Dry Food	100mg Dry Food	100mg Dry Food	100mg Dry Food	100mg Dry Food
	100mg Dry Food	100mg Dry Food	100mg Dry Food	100mg Dry Food	100mg Dry Food	100mg Dry Food	100mg Dry Food
	1x Artemia		1x Artemia		1x Artemia		
CR	100mg Dry Food		100mg Dry Food		100mg Dry Food		100mg Dry Food
			1x Artemia				
OF	300mg Dry Food	300mg Dry Food	300mg Dry Food	300mg Dry Food	300mg Dry Food	300mg Dry Food	300mg Dry Food
	2x Artemia	2x Artemia	2x Artemia	2x Artemia	2x Artemia	2x Artemia	2x Artemia
	300mg Dry Food	300mg Dry Food	300mg Dry Food	300mg Dry Food	300mg Dry Food	300mg Dry Food	300mg Dry Food
	2x Artemia	2x Artemia	2x Artemia	2x Artemia	2x Artemia	2x Artemia	2x Artemia

Table 3. Weekly feeding schedule applied to fish for 12 weeks

In order to obtain a sex balance, at the beginning of the feeding schedule, both male and female fish were tried to be included in each tank equally by eye. However, the dissections at the end of the feeding schedule revealed a sex imbalance between the treatment or age groups. Therefore, to maintain an equal sex ratio between treatment and age groups, we used only females for all the treatment and age groups in western blot experiments. In RT-PCR experiments, on the other hand, we could equalize the sexes between groups by using three male and one female fish per group.

3.2.2. Protein and RNA Isolation

For the Western blot experiments, individual whole brains were dissected from snap-frozen heads stored at -80oC, and proteins were extracted according to a previously-described protocol from our group (Karoglu et al. 2017). Briefly, brain tissues were first homogenized with a 30-gauge syringe in 300 µl of RIPA lysis buffer containing 50 mM Tris (pH 8.0), 150 mM NaCl, 0.1% SDS, 1% NP40, with protease inhibitor (Roche,

Mannheim, Germany, 5892970001), and then homogenates were centrifuged after 30 min incubation on ice. Finally, total protein concentrations were quantified using the Bradford Assay (Bradford Reagent, B6916, Sigma, St. Louis, MO, USA) with respect to known concentrations of bovine serum albumin (BSA) (Sigma, St. Louis, MO, USA).

For the real-time polymerase chain reaction (RT-PCR) experiments, whole brains were dissected in cold dPBS under the stereo microscope (Zeiss Stemi 1000, Germany) from the snap-frozen heads stored at -80oC. Total RNAs were isolated by homogenizing the tissues with a 30-gauge sterile syringe using Thermo Fisher Scientific's TRIzol Reagent (Waltham, MA, USA) according to manufacturer's instructions. The isolation protocols were followed by DNase treatment with an Ambion TURBO DNA-free Kit from Thermo Fisher Scientific following the manufacturer's instructions (Waltham, MA, USA). The concentrations of the isolated RNA samples were measured via a NanoDrop 2000 (ThermoScientific, Waltham, MA, USA), and the conversion of RNA to cDNA was performed using iScript cDNA Synthesis Kit (Biorad, Hercules, CA, USA).

3.2.3. Western Blotting

For both young and old groups, 40 µg of protein was loaded into SDS-PAGE gels to have comparable bands. Following gel separation, proteins were transferred onto the PVDF membrane. TBS-T with 5% milk powder was used as the blocking agent in all the procedures. The primary antibody concentrations were decided assay-dependent based on the manufacturer's instructions. For the Anti-Dp1 (ab208945, Abcam, UK), Anti-L-Plastin (ab210099, Abcam, UK), Anti-Pcna (ab29, Abcam, UK), Anti-GFP (ab6556, Abcam, UK), and Anti-HuC (ab78467, Abcam, UK) antibodies, concentrations of 1:1000 were used. For the Anti-Tubulin (CST-2146S, USA) and Anti-Dcamkl1 (ab109029, Abcam, UK) antibodies, concentrations of 1:5000 were used. For the secondary antibody, a 1:5000

dilution of the Anti-rabbit HRP linked antibody (CST-7074S, USA) was used for Anti-Dp1, Anti-L-Plastin, Anti-Dcamkl1, Anti-GFP, Anti-HuC, and Anti-tubulin antibodies, while a 1:5000 dilution of the Anti-mouse HRP linked antibody (ab97023, Abcam, UK) were utilized for the Anti-Pcna. Six brains were run as a cohort from each of the three feeding groups, including young and old animals. In order to minimize any potential systematic differences due to gel variation in the Western blotting experiments, the samples were loaded in alternating order. Lastly, chemiluminescent detection was performed using Thermo Scientific SuperSignal West Femto Maximum Sensitivity Substrate (Thermo Fisher Scientific, Rockford, IL, USA: 34095) on ChemiDoc MP Imaging System (BioRad, Hercules, CA, USA). Band intensities were quantified by a blind analysis using ImageJ software (NIH, Bethesda, MD, USA). Following band intensity quantifications, normalizations were performed within gel and against housekeeping protein (β-tubulin) as described previously (Karoglu et al., 2017).

3.2.4. Real-time Polymerase Chain Reaction (RT-PCR)

In this study, RT-PCR was used to screen for expression differences in the selected genes on the brains of animals given a 12-week OF or CR diet compared to AL-feeding. The primer sequences are provided in Table 4. For the RT-PCR experiments, LifeScience's LightCycler® 480 SYBR Green I Master kit (Roche, Germany) was used with the LightCycler® 480 machine (Roche, Basel, Switzerland). The protocol was completed with two µl of cDNA in a 20 µl reaction volume. Each sample had three technical replicates, which were run on different plates. The measurements were performed by normalizing Ct values to the geometric mean of two reference genes that included beta-actin1 and the 60S ribosomal protein, L13 (rpl13a).

Purpose	Name	Forward Sequence (5'→3')	Reverse Sequence (5'→3')
Cell cycle regulation	*tfdp1*	CAGGCTTTGACTGTTGGAAAA	GGCCTCTGAGGTGTGCTAAT
Cell cycle suppression	*tp53*	CGCGGATTTGCTTTGTGGAT	CGTTTTGCGCCATTGCTTTG
Cell cycle activation	*e2f5*	AGCGGAGACACTCTTCTAGC	TTGACCATTGTGGCCCATTT
Cell adhesion behavior [previously associated with stem cell maintenance (Erbaba et al. 2020b)]	*alcamb*	ACGGTGCAGTGGATTACCAA	TCACGTCCTCAACAAGCGAC
Cellular stemness	*sox2*	GACCATTCATCGACGAAGCC	CCTCCGGGGTCTGTATTTGT
Neuroprotection	*rest*	GCGTACACCACCATCAGTCA	GAATGGACGCTCACCAGTGT
Inflammation	*il1b*	GATCCGCTTGCAATGAGCTAC	TCAGGGCGATGATGACGTTC
Inflammation [previously associated with overall inflammation in zebrafish (Kyritsis et al. 2012)]	*lcp1*	GCCTTCACTAAAGTCGATGTGG	CGAAGGTGATCTTCCCGTCC
Cell growth/cell cycle regulation (Schmidt 1999)	*myca*	AACGGCATTCGTTAAACACA	ATCCTCATCGTCGTTGTCG
Inflammation	*tnfaF*	AGGAGAGTTGCCTTTACCGC	GTGAGTCTCAGCACACTTCCA
Reference gene	*actb1*	GCCTGACGGACAGGTCAT	ACCGCAAGATTCCATACCC
Reference gene	*rpl13a*	ATGAACACCAACCCTTCCCG	ACCATGCGCTTTCTCTTGTC

Table 4. Primers used for RT-PCR experiments.

3.2.5. Statistical Analysis

All statistical analyses were performed using IBM's SPSS statistical software (IBM, Armonk, NY, USA). Normality and homogeneity of variance assumptions were tested with Kolmogorov-Smirnov and Levene's tests, respectively. Whenever the assumptions were met, multifactorial analysis of variance (ANOVA) test with factors of age having two levels (young/aged), and feeding groups having three levels (AL/OF/CR) followed by Bonferroni posthoc tests in order to adjust for multiple comparisons. For the cases where the assumptions of normality or homogeneity of variance were violated, a non-parametric Kruskal Wallis test followed by Mann Whitney U tests for pairwise comparisons with Bonferroni corrected p-values were used. In order to investigate the relationships between the protein amounts and transcriptional differences among the selected markers, we formed

correlation matrices separately for both protein and gene expression datasets using a Spearman correlation coefficient test. Further investigation of the protein and gene expression levels in the whole fish brains was performed using principal component analysis (PCA) to determine the changes in each protein/gene expression relative to the other. Three principal components were extracted separately from each of the complete datasets of protein and gene expression levels regarding the band intensity measurements and Ct values, respectively. For component extraction, the eigenvalues were set above the 1.0 level. Significance levels in all analyses were set at $p < 0.05$ unless corrected as in the Mann Whitney U pairwise comparisons. Graphs of the data were made with Graphpad 8 software (San Diego, CA, USA). The PCA plots were generated using SPSS software.

3.3. Results

3.3.1. Fish weights, lengths, and body mass index (BMI) values were altered by age and dietary feeding regimens

Various dietary feeding regimens were given to the two age groups, a young (5-month-old) and an old (25-month-old) set of animals. In all cases, they were given a diet that was either AL, OF, or CR treatment for 12 weeks according to the schedule shown in Table 1. The weights (g) and lengths (cm) of the young and aged fish were quantified at the end of the 12-week diet application, as well as the BMI (g/cm2) values, which were calculated by dividing body weights by the square of the lengths. The dietary schedules stated in Table 1 induced significant BMI differences among the groups (Figure 8c). For all weight, length, and BMI data, there were both main effects of age (weight $U = 700$, $z = -5.899$, $p < 0.001$; length $U = 984$, $z = -4.115$, $p < 0.001$; BMI $U = 585.5$, $z = -6.128$, $p < 0.001$), and diet treatment (weight $H(2) = 33.772$, $p < 0.001$; length $H(2) = 35.592$, $p < 0.001$; BMI $H(2) = 29.382$, $p < 0.001$) (Figure 8A-C). Overall, the CR animals had significantly lower weight,

length, and BMI values than the AL ($p < 0.001$ for all) and OF groups ($p < 0.001$ for all). There was also a significant difference between AL and OF groups for the length data ($p = 0.046$). However, there were no significant increases in the OF fish levels compared to the AL in weight ($p > 0.05$), and BMI data ($p > 0.05$), although there were numerical increases in OF group for all three data points compared to AL and CR groups.

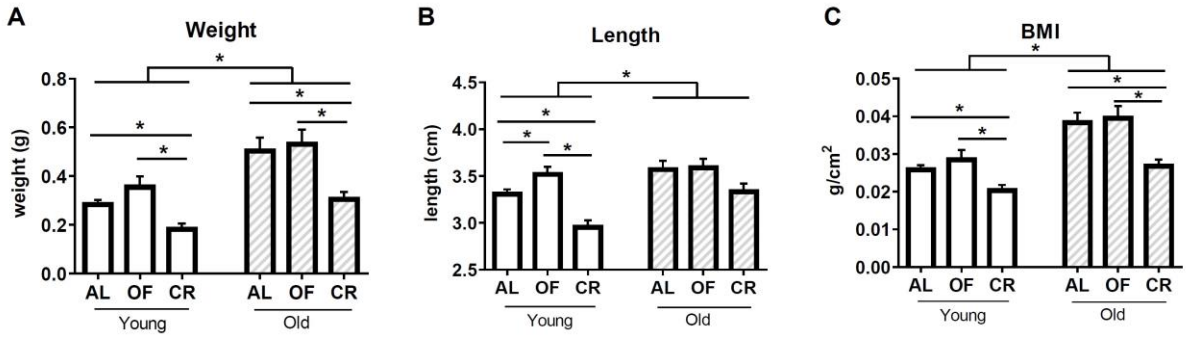

Figure 8 Average (A) weight, (B) length, and (C) Body Mass Index (BMI) data across feeding groups are shown. All values are significantly increasing with age ($p < 0.001$), and there are significant main effects of treatment for all three data points ($p < 0.001$). Overall, all CR groups showed significantly lower body weight ($p < 0.001$), length ($p < 0.001$), and BMI ($p < 0.001$) than both their AL and OF counterparts.

3.3.2. Selected protein levels related to cellular proliferation, cell cycle regulation, cellular differentiation and migration, and inflammation in the young and old brain were stable across the dietary groups

The brains from the different feeding groups were tested for possible age- and diet-related alterations in the amounts of target proteins related to cell proliferation, cell cycle regulation, neuronal/glial identity, neuronal migration/cytoskeletal regulation, and inflammation. The proteins included those in conjunction with cytoskeletal rearrangement Doublecortin like kinase (Dclk) 1 (Dcamkl1), cellular characterization of neural (ELAV-like neuron-specific RNA binding protein 3: HuC), and glial origin (Glial fibrillary acid

protein: Gfap), proliferation (proliferating cell nuclear antigen: Pcna), and cell cycle regulation (transcription factor Dp1: Tfdp1), as well as inflammation/cytoskeletal regulation (L-plastin) (Figure 9a). Representative protein bands from the brains of young and old animals treated with the various dietary interventions are shown together in Figure 9a.

Initially, Dcamkl1, a microtubule-polymerizing protein, was examined to determine whether there were any effects of age or dietary manipulation related to microtubule organization or neuronal migration (Vreugdenhil et al. 2007). The results showed that there was no main effect of treatment ($F(2, 30) = 1.923$, $p = 0.164$) or age ($F(1, 30) = 0.179$, $p = 0.675$) on the protein levels (Figure 9b). However, the Dcamkl1 protein levels showed a marginally significant effect of the interaction between treatment and age ($F(2, 30) = 2.847$, $p = 0.074$). Dcamkl1 protein levels are slightly elevated by a CR diet at a young age but not at old age. These data suggest that any effects of the diet depend on the animal's age when the treatment is given.

To infer the effects of diet on the amount of cells of either neuronal or glial origin, HuC and Gfap protein levels were measured across all of the feeding groups, respectively. For HuC protein levels, no observable change was detected in the brain with either any of the feeding interventions ($H(2) = 0.597$, $p = 0.742$) or with age ($U = 120$, $z = -0.542$, $p = 0.588$) (Figure 9c). Gfap levels in the brains of the young and old animals were measured to gain insight into the nature of the glial response. For this purpose, an anti-GFP antibody was used to measure GFAP levels. It has been previously shown that in this transgenic line, the fusion of the Gfap-GFP protein very closely mimics endogenous Gfap (Lam et al. 2009), and we wanted to use a commercially-available antibody that would work in the Western blot analyses. In the current study, our results demonstrated no main effect of age

($F(1, 30) = 0.038$, $p = 0.848$) nor showed any interaction ($F(2, 30) = 0.740$, $p = 0.489$) on Gfap levels. However, we did find a marginally significant main effect of treatment on Gfap levels ($F(2, 30) = 3.221$, $p = 0.059$). Overall, CR feeding appeared to increase Gfap protein levels in the brains compared to AL and OF treatments (Figure 9d).

In order to examine whether age or diet affects total cell proliferation, the protein levels of Pcna were measured. This antibody marks the actively dividing cells (Zhang and Jiao 2015). In our experiments, the Pcna protein levels were found to not be statistically different with respect to diet or age (treatment: $F(2, 30) = 0.758$, $p = 0.477$; age: $F(1, 30) = 0.076$, $p = 0.785$; interaction: $F(2, 30) = 1.759$, $p = 0.190$)) (Figure 9e). Thus, total cell proliferation is stable across the groups and not affected by diet or age.

Among many cell cycle regulatory genes, we were specifically interested in the effects of dietary interventions and age on *tfdp1*. The reasons for this are the following. The first is because, as a transcription factor, it has key roles during the cell cycle. Secondly, in a preliminary microarray study from our group *tfdp1* was significantly downregulated in aged animal brains following a short-term CR (unpublished data). A comparison in the brain protein level differences of Tfdp1 showed that there was no effect of age or interaction (age: $F(1, 30) = 0.027$, $p = 0.871$; interaction: $F(2, 30) = 0.163$, $p = 0.850$). However, there was a marginally significant main effect of treatment on Tfdp1 protein levels ($F(2, 30) = 2.807$, $p = 0.076$) (Figure 9f). This likely suggests that a CR diet in both young and old animals decreases the Tfdp1 protein levels compared to the AL-fed subjects and could alter cell cycle progression.

The last protein marker of interest measured in the brains was L-plastin, which is involved in regulations of the cytoskeleton. The results demonstrated no significant change in L-plastin protein levels in the brain with any of the short-term feeding interventions ($H(2) =$

0.263, p = 0.877) or with age (U = 125, z = -1.171, p = 0.242) (Figure 9g). The stability of L-plastin levels suggests that neither diet nor age causes a drastic and direct influence on cytoskeletal regulations.

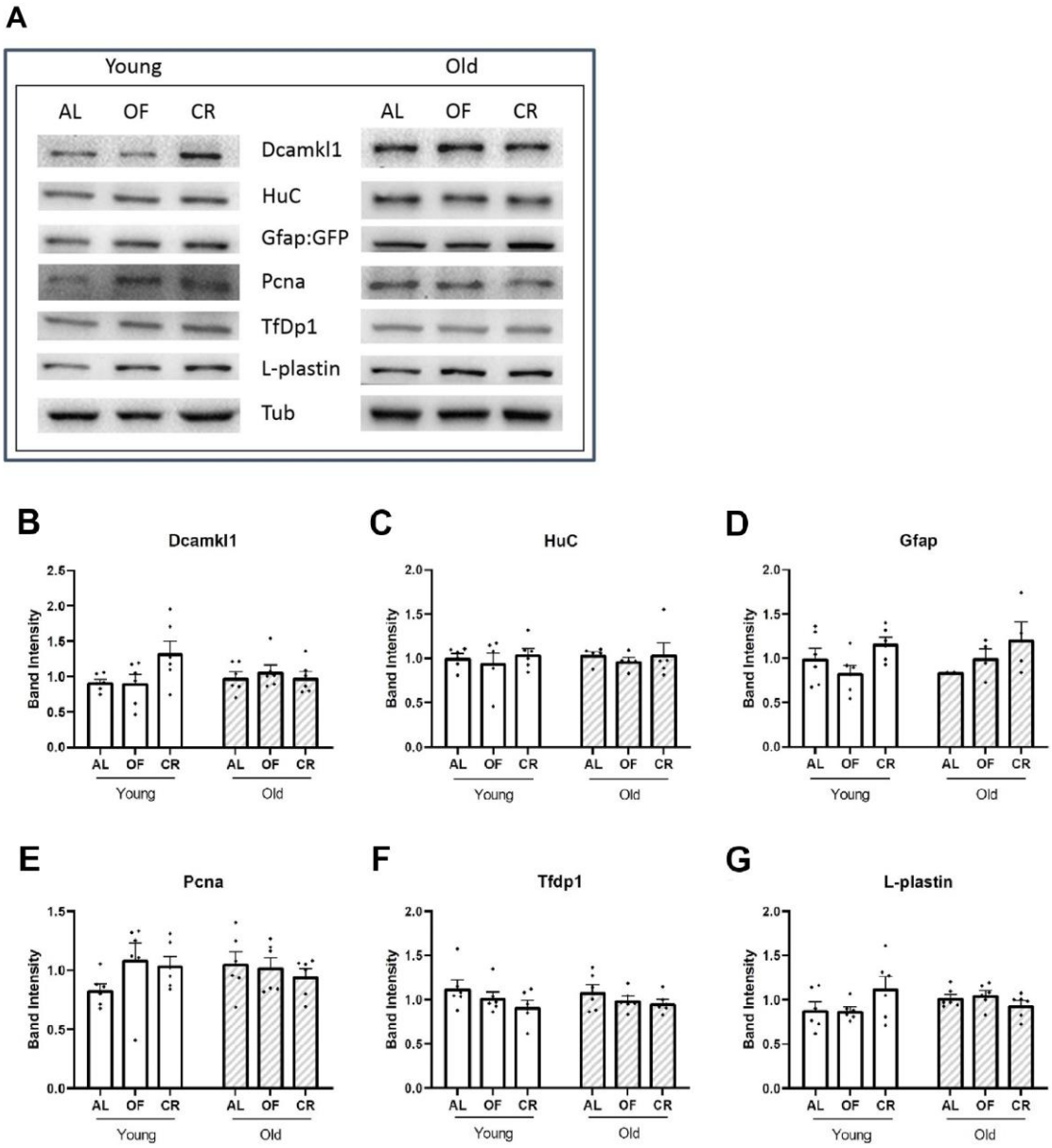

Figure 9 (A) Representative Western blot images for Dcamkl1, HuC, Gfap:GFP, Pcna, Tfdp1, L-plastin, and β-Tubulin protein levels from the different feeding groups. Protein levels of (B) Dcamkl1, (C) HuC, (D) Gfap, (E) Pcna, (F) Tfdp1, and (G) L-plastin across different feeding regimens and age. Whole-brain lysates from six animals per feeding

group were used for Western blotting experiments. No protein levels changed significantly with respect to age or diet. AL: Ad-libitum, OF: overfed, CR: Caloric restriction

3.3.3. Multivariate analysis of proteins of interest demonstrates differential clustering patterns with respect to diet showing upregulation in cell proliferation with an OF regimen and downregulation in proliferation and potential induction in neuronal plasticity with CR

Principal component analysis (PCA) was performed to explore the pattern of alterations in the levels of each protein compared to each of the others. Analysis was performed for the complete dataset of proteins of interest regarding the Western blot band intensities. The analysis extracted three main components, accounting for 70.1% of the variance in the protein expression data. The percentage of explained variance of each component and component loading scores equal to or greater than 0.5 are provided in Table 5. Visualization of the data in two dimensions is shown in Figure 10.

The first principal component (PC1) of the protein data was driven positively by L-plastin, a cytoskeletal regulator; HuC, a neuronal marker; and Gfap, a marker for astroglial reactivity (Anderson et al. 2014) (Table 5). For the PC1, the young CR samples partially clustered at higher values than the young OF group. This suggests a positive correlation between CR and cytoskeletal regulations concerning migration and attachment of neuronal and glial cells (Figure 10a). The second principal component (PC2) of the data was mainly driven positively by Pcna, a marker for the actively dividing cells, and negatively by Gfap and HuC. For the PC2, the young OF group scored higher values than the young AL animals (Figure 10c). The clustering of these markers indicates an upregulation in proliferation events and a downregulation in astroglial activity with an OF regimen compared to AL. Finally, the third principal component (PC3) was influenced negatively

by Tfdp1 and positively by Dcamkl1. Tfdp1 is a cell cycle promoting transcription factor associated with cell proliferation, and Dcamkl1 is a protein functioning in axonal wiring and neuronal migration (Vreugdenhil et al., 2007). Regarding the clusters of the young group, CR treated young samples had higher PC3 values than young AL and OF treated animal brains. This suggests decreased cell proliferation and promotion of neuronal rewiring/plasticity with the CR diet. Simple correlational analyses were also performed on the selected protein levels, which showed significant positive correlations between L-plastin and Dcamkl1 ($p = 0.033$), as well as between L-plastin and Tfdp1 ($p = 0.016$) (Table 6). Taken together, these indicate possible downregulation of cellular proliferation events and upregulations of cytoskeletal regulation/neuronal migration with CR treatment, whereas, with an OF regimen, there is upregulation in proliferation events and downregulation in astroglial activity.

Table 5		***% of Variance Explained***	***Component Loading Scores (>0.5)***		
Principal Component (Protein data)	***PC1***	28.82	L-Plastin (0.713)	HuC (0.685)	Gfap (0.554)
	PC2	22.77	Gfap (-0.654)	Pcna (0.519)	HuC (-0.517)
	PC3	18.52	Tfdp1 (-0.774)	Dcamkl1 (0.671)	
	Total	70.1			

Table 5. Each component of the PCA analysis of the protein datasets and the percentage of the explained variance is shown, as well as the factors having highest loading scores for

each component. The results demonstrated that 28.82% of the variance was explained by principal component 1 (PC1), 22.77% by PC2, and 18.52% by PC3. Only the factors with the loading scores of 0.5 and above are presented.

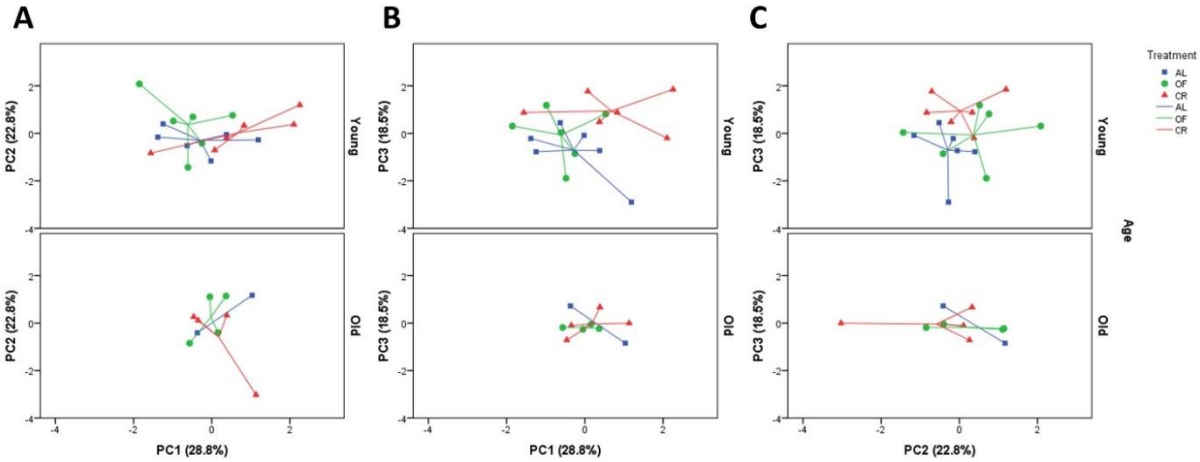

Figure 10 Expression levels of proteins of interest clustering in an age- and the treatment-specific manner in the principal component analysis. Data is visualized in 2-dimensions using the principal component 1 (PC1), principal component 2 (PC2), and principal component 3 (PC3). The factor of age arranges data shown in scatterplots on A, B, and C. (A) On the PC1 axis, in which Lplastin, HuC, and Gfap are the leading contributors, the young CR group clusters higher than the OF group. (B) On the PC3 axis, where Tfdp1 is the negative and Dcamkl1 is the leading positive contributor, the young CR group scores higher values than the young AL and OF groups. (C) On the PC2 axis, in which Pcna is the leading positive contributor and, Gfap and HuC are the leading negative contributors, the young OF group has higher values than the young AL and CR groups. Groups are denoted by different colors, as shown from the legends. AL: Ad libitum-feeding, OF: overfeeding, CR: Caloric restriction feeding.

3.3.4. Significant positive correlations were found among proteins having roles in cell cycle and cytoskeletal regulations in the zebrafish brains

In order to examine the potential relationships between the levels of the proteins of interest, a correlation matrix was constructed, shown in Table 6. Significant positive correlations were found between L-plastin and Dcamkl1 (p = 0.033), and L-plastin and Tfdp1 (p = 0.016), which was expected considering the common roles of these two proteins on cytoskeletal regulations.

		Dcamkl1	HuC	Gfap	Pcna	Tfdp1	L-plastin
Dcamkl1	Correlation Coefficient	*1.000*					
	Sig. (2-tailed)						
HuC	Correlation Coefficient	.166	*1.000*				
	Sig. (2-tailed)	.355					
Gfap	Correlation Coefficient	-.015	.245	*1.000*			
	Sig. (2-tailed)	.941	.209				
Pcna	Correlation Coefficient	.051	.105	-.122	*1.000*		
	Sig. (2-tailed)	.766	.561	.538			
Tfdp1	Correlation Coefficient	-.174	.240	-.111	.146	*1.000*	
	Sig. (2-tailed)	.309	.178	.574	.394		
L-plastin	Correlation Coefficient	.356*	.231	.086	.251	.400*	*1.000*
	Sig. (2-tailed)	.033	.196	.662	.139	.016	
***. Correlation is significant at the 0.05 level (2-tailed).**							

Table 6 Spearman correlation matrix of proteins of interest in whole zebrafish brain (N = 36). The significance levels of the correlation coefficients are given in the matrix. The squares with significant correlations are highlighted with gray.

3.3.5. CR significantly lowers *sox2* gene expression levels compared to OF, while *lcp1*, *myca*, and *tp53* were significantly downregulated by age

RT-PCR analysis measured the mRNA levels of certain target genes of interest. In the current study, ten genes were examined, and those were related to promoting cell cycle (*tfdp1*, *e2f5*, *myca*), cellular senescence (*tp53*), progenitor state (*sox2*), cell adhesion which

is implicated for roles of stem cell engraftment (*alcamb*), cytoskeletal plasticity/immunity (*lcp1*), inflammation (*tnfa*, *il1b*), and neuroprotection (*rest*).

Initially, we tested two cell cycle markers to see whether transcription levels change with respect to diet or age: *tfdp1*, and e2f5 (unpublished data). The mRNA levels of *tfdp1* did not show statistically significant change neither with age ($F(1, 24) = 0.506$, $p = 0.486$) nor with diet ($F(2, 24) = 0.774$, $p = 0.476$) (Figure 11a). In the case of *e2f5*, the binding partner of *tfdp1*, again no main effects of dietary treatment ($H(2) = 2.855$, $p = 0.24$) or age ($U = 61$, $z = -0.635$, $p = 0.551$) were found to be statistically significant (Figure 11b).

In terms of cell proliferation markers, we examined *sox2*, a marker for neural stem/progenitor cells, across multiple organisms (Mercurio et al., 2019). In our data, we found no effect of age ($F(1,24) = 1.225$, $p = 0.283$). However, there was a main effect of treatment on *sox2* expression levels in the zebrafish brain ($F(2, 24) = 4.866$, $p = 0.02$) (Figure 11c). A Bonferroni posthoc test revealed that in the CR group, *sox2* mRNA levels were significantly lower compared to OF treatment groups ($p = 0.018$), suggesting a downregulation in cell proliferation by CR. We also measured Myc protein (Myca in zebrafish), a proto-oncogene that stimulates proliferation (Uribesalgo et al., 2012). *myca* brain mRNA levels were significantly decreased with age ($F(1, 24) = 6.456$, $p = 0.02$), although there was no significant alterations in *myca* expression levels by diet ($F(2,24) = 0.974$, $p = 0.397$). This effect of age was driven by the CR group, such that in young CR fish, *myca* expression levels were significantly higher than those observed in aged CR animals ($p = 0.006$) (Figure 11d). These data indicate that both age and diet can have selective effects on stem cell markers.

Next, the mRNA levels of the negative proliferation regulator/tumor suppressor, *tp53*, were examined in the context of diet and aging (Perry and Levine 1993). *tp53* gene expression

levels were significantly lower in the old group than the young animals (U =16, z = -3.233, p =0.001) (Figure 11e). Although, there was no main effect of treatment on the *tp53* mRNA levels (H(2) = 1.235, p = 0.539). Thus, these data also support the premise that both age and diet can have selective effects on proliferation.

ALCAM is a cell adhesion molecule with various roles, but in the brain, it mostly regulates leukocyte transmigration through the BBB to the CNS, and therefore it is related to neuroinflammation (Swart 2002; Cayrol et al. 2008; Thelen et al. 2012; Jeannet et al. 2013; Shahaduzzaman et al. 2015; Kim et al. 2017; Lécuyer et al. 2017; Erbaba et al. 2020b). Our results showed no effect of age in terms of the *Alcamb* expression levels (U = 68, z = -0.231, p = 0.843), although results demonstrated a marginally significant main effect of dietary treatment on *Alcamb* transcription levels (H(2) = 4.82, p = 0.09) (Figure 11f). *Alcamb* mRNA levels of the CR group appear to follow a decreasing trend in both ages compared to AL and OF groups. Therefore, this would be consistent with CR lowering the brain towards an increased inflammatory response irrespective of age.

The RE1-silencing transcription factor (Rest) has been implicated in promoting longevity and neuronal survival during healthy brain aging, and therefore, is considered neuroprotective (McGann et al. 2021). In the current study, no significant changes in *rest* mRNA levels were found for the main effect of age (F(1,24) = 1.406 , p = 0.251) or diet treatment (F(2, 24) = 0.021, p = 0.979) (Figure 11g). This suggests that our dietary interventions did not significantly promote or reduce any neuroprotective potential of this marker.

In order to make diet-regulated connections to specific inflammatory pathways, we measured *il1b*, *tnfa* and *lcp1* expression levels (Lopez-Castejon and Brough 2011; Kyritsis et al. 2012; Hayashi et al. 2013). No main effects of dietary treatment or age were observed

for *il1b* (age: U = 70, z = -0.115, p = 0.932; treatment: H(2) = 1.625, p = 0.444) (Figure 11h) and *tnfa* (age: U = 53, z = -1.097, p = 0.291; treatment: H(2) = 3.155, p = 0.206) (Figure 11i). A significant main effect of age was found on showing a significant decline in older subjects (F(1, 24) = 8.269, p = 0.01) (Figure 11j). Our data did not show significant alterations in *lcp1* expression levels regarding our short-term diets (F(2, 24) = 0.587, p = 0.566), Taken together these data suggest that aging affects the inflammatory process in a pathway-specific manner.

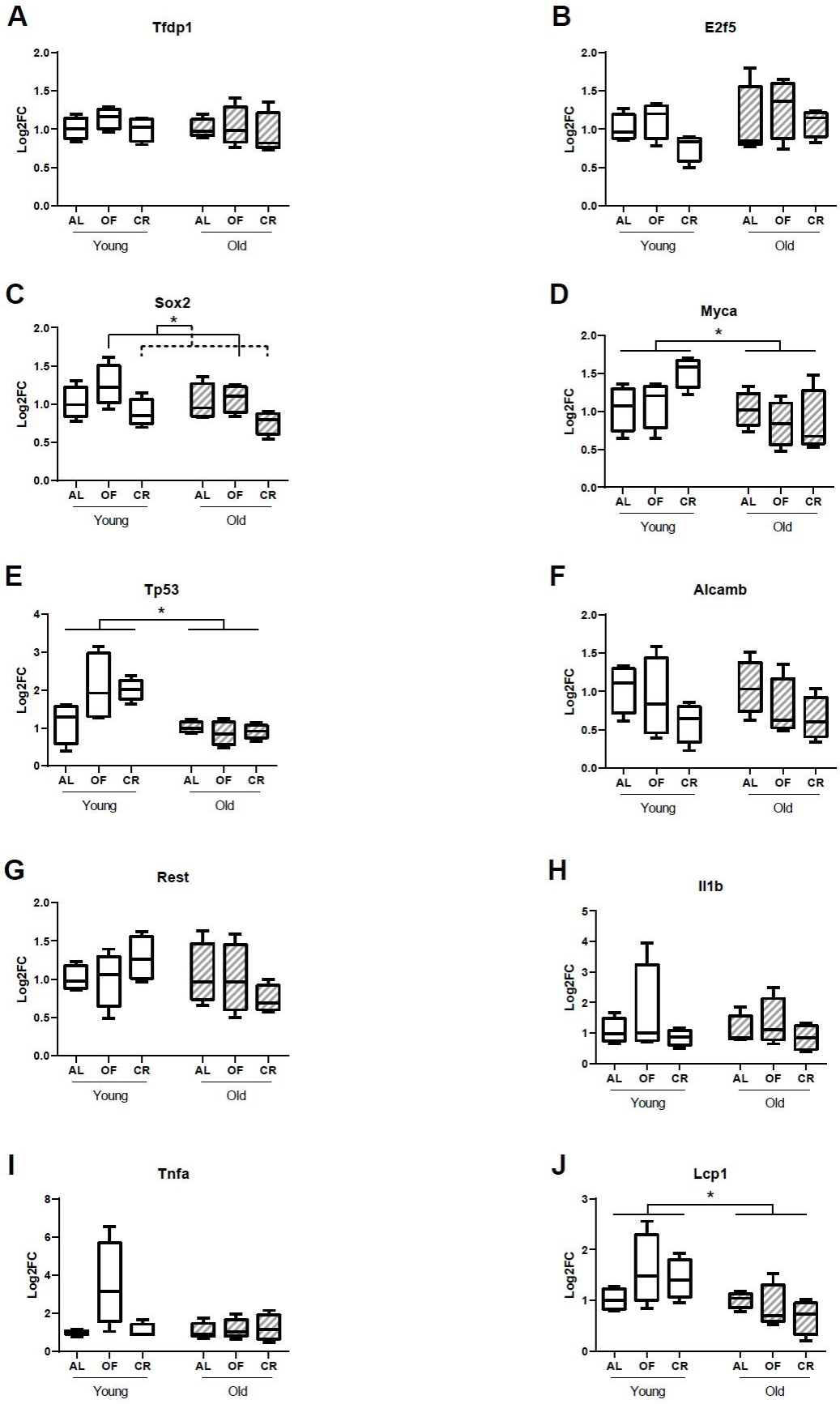
A
Tfdp1
B
E2f5
C
Sox2
D
Myca
E
Tp53
F
Alcamb
G
Rest
H
Il1b
I
Tnfa
J
Lcp1
Log2FC
AL
OF
CR
Young
Old
*

Figure 11 mRNA level comparisons of selected genes analyzed by RT-PCR; (A) Tfdp1, (B) E2f5, (C) Sox2, (D) Myca, (E) Tp53, (F) Alcamb, (G) Rest, (H) Il1b, (I) Tnfa, (J) Lcp1. All data were normalized, and log fold change values were calculated using the delta-delta Ct method. A main effect of treatment was found for *sox2* ($p = 0.02$), and a marginally significant main effect of treatment was found for *alcamb* mRNA levels ($p=0.09$). A main effect of age was detected for *tp53* ($p = 0.001$), *myca* ($p = 0.02$), and *lcp1* ($p = 0.01$) expression levels. *actin* and *rpl13a* genes were used as reference genes. Four animals per age and the dietary group were included for a total of 24 animals used in the RT-PCR experiments.

3.3.6. Multivariate analysis demonstrated diet-dependent clustering patterns with respect to the genes of interest, illustrating increases in proliferation and inflammation with an OF diet and decreases in proliferation and inflammation with CR

In order to explore the variation of expression levels of each gene with respect to one another, PCA was applied to the entire gene expression dataset. An analysis of the Ct values was run for the complete dataset of genes. Three main components were extracted from the analysis, accounting for 65.26% of the variance in the expression data. The percent of explained variance of each component and component loading scores equal to or greater than 0.5 are provided in Table 7. Visualization of the data in two dimensions is shown in Figure 12. As was observed in the protein data, the PCA for gene expression data did not explain much of the variance in the aged groups. So in the young group brains, the effect of diet was more prominent. PC1 of the gene expression data was driven by *rest*, *tfdp1*, *lcp1*, *sox2*, *tp53*, *myca*, *tnfa*, and *il1b* (Table 7). Therefore, PC1 reflects a large-scale pattern composed of suppression of neuronal excitation with *rest*, proliferation stimulation

with *tfdp1*, *sox2*, and *myca*, increase in inflammatory status with *tnfa*, and *il1b*, induction of growth arrest/repair mechanisms with *tp53*, and cytoskeletal rearrangements with *lcp1* expressions. The young OF animals scored higher for the PC1 component than the young AL group (Figure 12a). This is consistent with an OF-induced increase in proliferation and inflammation, as well as having impacts on cytoskeletal regulation and suppression of excessive neuronal excitation mechanisms. An age-dependent decrease in the PC1 scores of OF animals was observed in Figure 12a. The PC2 was mainly influenced positively by *il1b*, *e2f5*, *alcamb*, and *tnfa* and negatively by *myca*. Among those, *il1b*, *alcamb*, and *tnfa* alter inflammatory outcomes, while *e2f* and *myca* are proliferation-related genes. The young CR group samples clustered at lower PC2 values than the young AL and OF groups. This reflects a decrease in inflammation and proliferation with CR compared to the AL- and OF-treated subjects. PC3 was impacted positively by *sox2* and negatively by Rest. Although there does not seem to be a distinct grouping of samples for PC3, the CR samples cluster at lower values than OF animals (Fig. 5b). This likely confirms the possibility of OF increasing cell proliferation, as was seen with PC1. The data from the multivariate analyses were supported by correlational analyses (Table 8).

Table 7		**% of Variance Explained**	**Component Loading Scores (>0.5)**							
Principal Component (Expression data)	**PC1**	29.70	*rest* (0.687)	*tfdp1* (0.674)	*lcp1* (0.611)	*sox2* (0.601)	*tp53* (0.579)	*myca* (0.572)	*tnfa* (0.565)	*il1b* (0.545)
	PC2	22.86	*il1b* (0.718)	*myca* (-0.658)	*e2f5* (0.651)	*alcamb* (0.583)	*tnfa* (0.537)			
	PC3	12.70	*sox2* (0.608)	*rest* (-0.560)						
	Total	65.26								

Table 7. Percentage of explained variances and factors having the highest loading scores for each component in the gene expression level dataset PCA. The results demonstrated that 29.7% of the variance was explained by principal component 1 (PC1), 22.86% by PC2, and 12.7% by PC3. Only the factors with loading scores of 0.5 and above are presented. AL: Ad libitum-feeding, OF: overfeeding, CR: Caloric restriction feeding.

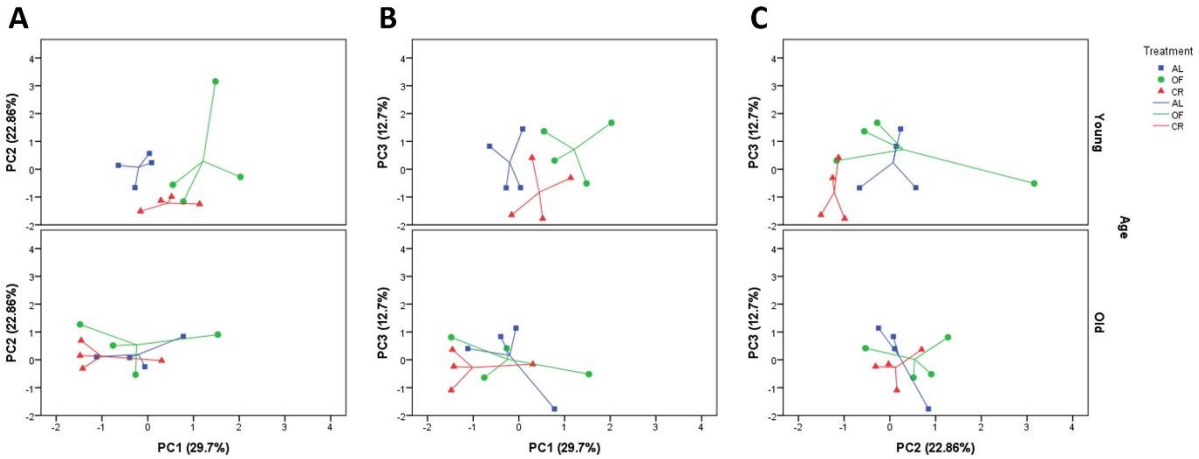

Figure 12 Expression levels of genes of interest cluster in an age- and the treatment-specific manner in the principal component analysis. Data is visualized in 2-dimensions using the principal component 1 (PC1), principal component 2 (PC2), and principal component 3 (PC3). The factor of age arranges data shown in scatterplots on a, b, and c. (A) On the PC1 axis, in which rest, *tfdp1, lcp1, sox2, tp53, myca, tnfa,* and *il1b* are the leading positive contributors, the young OF group clusters higher than young AL group. Young OF and CR groups cluster at higher values of the PC1 axis than the old OF and CR groups, respectively. (B) On the PC3 axis, to which *sox2* contributed positively and *rest* negatively, CR samples cluster at lower values than OF animals. (C) On the PC2 axis, where *il1b* and *e2f5* are the most substantial positive contributors, and *myca* is the negative contributor, the young CR group clusters closer to the lower margin than young OF and

AL groups. The old CR group samples cluster on higher values of the PC2 axis compared to the young CR group animals. Groups are denoted by different colors, as shown from the legends. AL: Ad libitum-feeding, OF: overfeeding, CR: Caloric restriction feeding.

3.3.7. Significant positive correlations were found among mRNA levels of genes having roles in cell proliferation, cell cycle, inflammation, and cytoskeletal regulations in the zebrafish brains

Following the RT-PCR studies, a second correlation matrix was calculated and illustrated in Table 8. Significant positive correlations were detected between the gene expression levels of *tfdp1* and *sox2*, both known for their roles in promoting proliferation. Although there was no significant group difference in *tfdp1* expression levels for diet, while *sox2* expression was decreased with CR treatment, a positive correlation might be reflecting a pattern of similar effect for *tfdp1*. This was also supported by a marginally significant decrease in *tfdp1* levels with CR diet treatment. Together they may negatively regulate proliferation in CR and positively in OF diets. This is in good agreement with the picture of decreasing proliferation with CR (Cavallucci et al. 2016a), an effect possibly especially on stem cells due to the *sox2* marker. Other positive correlations were found between *tfdp1* and *tnfa*, *il1b* and *e2f5*, *sox2* and *tnfa*. Since *tfdp1*, *e2f5* and *sox2* are markers associated with cell proliferation, and *tnfa* and *il1b* are inflammatory-related markers, proliferation (*tfdp1*, *e2f5*, and *sox2*) seems to be related to inflammation (*tnfa*, and *il1b*). Indeed, decreased proliferation might help avoid DNA damage, and subsequently decrease DNA damage response and inflammation. The correlation between *tp53* and *lcp1* (*l-plastin*) might have been detected due to their shared responses in DNA damage control/inflammation. *tp53* is the best-known tumor suppressor, functioning in DNA repair, and where the damage is extensive provides signals for apoptosis (Schafer 1998).

Kyritsis et al. (2012) have used actin-bundling protein lymphocyte cytosolic protein 1 (*lcp1*/l-*plastin*) to mark regions of inflammation in the zebrafish brain. It is implicated in the regulation of the cytoskeleton, an important element in cell migration in health and disease in addition to having roles in immunity and cancer metastasis (Park et al. 1994; Otsuka et al. 2001; Kell et al. 2018; Park et al. 1994; Otsuka et al. 2001; Kell et al. 2018). Therefore, a positive correlation between Tp53 and L-plastin may be due to their common roles in immune system functioning. Also, in the correlation matrix, the positive relationship found between Il1b and Rest, Myca and Rest, as well as between L-plastin (Lcp1) and Rest, may imply that the mechanisms of inflammation might be related to the activation of neuroprotective responses that are controlled by Rest-mediated stress resistance processes. Lastly, the correlation detected between Tp53 and Myca was unexpected since the first induces cell cycle arrest and tumor suppression, and the second is a cell cycle activator. The correlation could result from adjustments of cell cycle dynamics affecting both genes in different pathways that respond to nutrient uptake alterations, perhaps in different cell types.

		Tfdp1	E2f5	Sox2	Alcamb	Il1b	Lcp1	Tnfa	Tp53	Myca	Rest
Tfdp1	Correlation Coefficient	*1.000*									
	Sig. (2-tailed)										
E2f5	Correlation Coefficient	.017	*1.000*								
	Sig. (2-tailed)	.936									
Sox2	Correlation Coefficient	.611**	.208	*1.000*							
	Sig. (2-tailed)	.002	.330								
Alcamb	Correlation Coefficient	.110	.207	.158	*1.000*						
	Sig. (2-tailed)	.610	.332	.460							
Il1b	Correlation Coefficient	.283	.474*	.150	.050	*1.000*					
	Sig. (2-tailed)	.179	.019	.485	.818						
Lcp1	Correlation Coefficient	.257	.014	.221	-.028	.270	*1.000*				
	Sig. (2-tailed)	.226	.949	.300	.897	.203					
Tnfa	Correlation Coefficient	.497*	.240	.418*	-.103	.177	.246	*1.000*			
	Sig. (2-tailed)	.013	.259	.042	.630	.409	.246				
Tp53	Correlation Coefficient	.200	-.235	.149	-.201	-.073	.450*	.202	*1.000*		
	Sig. (2-tailed)	.349	.269	.488	.347	.734	.027	.344			
Myca	Correlation Coefficient	.345	-.218	.185	-.297	.114	.363	.230	.604**	*1.000*	
	Sig. (2-tailed)	.098	.306	.386	.159	.596	.082	.281	.002		
Rest	Correlation Coefficient	.199	.268	.048	.013	.540**	.480*	.190	.295	.531**	*1.000*
	Sig. (2-tailed)	.351	.206	.824	.952	.006	.018	.373	.162	.008	

****. Correlation is significant at the 0.01 level (2-tailed).**

***. Correlation is significant at the 0.05 level (2-tailed).**

Table 8 Spearman correlation matrix of the expression levels of genes of interest in the whole brain samples (n = 24). The significance of correlation coefficients is shown in the gray boxes.

3.4. Conclusion

The third chapter of the thesis aimed to investigate the neurobiological alterations in the aging brain following short-term overfeeding (OF) and caloric restriction (CR) regimens. In this work, young and old groups of fish were given one of the three dietary regimens (AL, OF, or CR) for 12 weeks. The brain protein and mRNA levels of selected genes

having key roles in aging and/or diet were examined. At the end of the treatments with AL, OF, and CR, the CR-treated fish, had significantly lower BMI values than AL and OF-fed animals. Following protein level comparisons, no statistically significant group effects of dietary treatment or age on the selected protein levels were detected. At the transcriptional level, *lcp1* (*l-plastin*), *myca* (*c-MYC* in humans), and *tp53* mRNA levels significantly decreased with age. Interestingly, *sox2* mRNA levels were significantly upregulated in the brains of animals given an OF feeding regimen compared to CR, which supports the notion that the CR dietary regimen maintains the stem cell pool in order to keep the energy reserve for cell survival rather than proliferation. Lastly, multivariate analyses performed on both protein and gene expression datasets suggested that the OF diet positively regulates proliferation- and inflammation-related mechanisms. In contrast, a CR diet negatively drives these pathways, suggesting a crucial mechanism of how CR induces health span and longevity. In summary, our data demonstrate that the negative effect of CR on cellular proliferation likely reinforces the stem cell pool in the brain to maintain quiescence, which is essential for the conservation of the limited energy produced due to the low amount of nutrient uptake. Moreover, CR also helps promote DNA repair and protects the cells in the brain against accumulation of DNA damage. On the other hand, OF induces a higher metabolism demand by promoting cell proliferation and decreasing the time spent for DNA damage control, and the consequence is the exhaustion of the stem cell pool. Such conceptual conclusions from this chapter related to nutrient interventions and effects on metabolism, and at the same time, the results we obtained from a pilot microarray between AL and CR applied animal brains that will be explained in the next chapter, led us to make a connection between CR and the cell cycle regulations. Therefore, in the last fourth chapter, we first aimed to discover the transcriptional alterations with CR

and then try to establish a CR mimicking approach by manipulating the expression of the *tfdp1* gene in a way similar to its CR response.

3.5. Discussion

In the third chapter of the thesis, we applied both a short-term OF and CR regimen to understand the neurobiological underpinnings of how these different diets contribute to brain aging. The 12-week intervention period was chosen considering the previous reports that it takes at least 8 weeks to affect both cognitive and molecular phenotypes (Arslan-Ergul et al. 2016b; Meguro et al. 2019; Celebi-Birand et al. 2020; Karoglu-Eravsar et al. 2021). The results demonstrated that the 12-week CR regimen significantly decreased the BMI compared to AL- and OF-fed animals at both young and old ages. Moreover, aged animals had higher body-mass index (BMI) values than the young groups, which was consistent with previous studies (Arslan-Ergul et al. 2016a; Celebi-Birand et al. 2020). Moreover, the effects of age and diet were tested on proteins and genes of interest that have previously been implicated in the aging process. These include markers of cell proliferation, cell-cycle regulation, inflammation, and cytoskeletal regulation. While many were stable, our results showed that the OF regimen significantly upregulated the expression levels of Sox2, a proliferation marker, compared to the CR diet. Moreover, we observed age-related declines in the levels of the proliferation marker, Myca, the negative proliferation marker, Tp53, and the inflammatory marker, Lcp1, expression levels.

In the current chapter, cell proliferation was tested by measuring the protein levels of Proliferating cell nuclear antigen (Pcna) and the mRNA levels of Sex determining region Y box2 (Sox2). Pcna is a marker of the actively dividing cells (Zhang and Jiao 2015). In our study, no significant changes were observed in Pcna protein levels with respect to age or diet. Another proliferation marker, Sox2, a well-known stem cell marker that is also active

in neural stem cells NSCs) was examined (Mercurio et al. 2019). Its gene encodes a transcription factor known to promote cell proliferation, regulate various physiological processes, and its dysregulation was implicated in cancer research due to gene amplification and protein overexpression (Zhang et al. 2020). In our study, consistent with Pcna measurements, no significant differences were observed in *sox2* expression with age. However, sox2 expression levels were upregulated following OF-feeding as compared to a CR diet. Sox2 is widely regarded as an NSC marker in both embryo and adult tissues (Mercurio et al. 2019). Due to its function in promoting proliferation, *Sox2* dysregulation/overexpression has been closely attributed to cancer incidence in the literature, including brain cancer and stated to be positively correlated with the malignancy grade (Mansouri et al. 2016; Capatina et al. 2019; Zhang et al. 2020). Actually, Sox2 is better known as an NSC maintenance factor promoting the cells self-renewal or pluripotency, than being a proliferation marker like Pcna (Sato et al. 2019). With no effect of our dietary application on Pcna, here we suggest that *sox2* upregulation with OF, may not imply a direct increase in overall proliferation but may infer an increase in stem cell proliferation, leading to a fast depletion of the stem cell reserve. Thus, the significant *sox2* upregulation with OF treatment as compared to CR could be interpreted as an increase in proliferative status of stem cells with an OF diet that could have detrimental effects as compared to CR. Therefore, this may be one mechanism as to how CR promotes health-span in individuals.

Indeed, CR was previously found to inhibit cell proliferation in various tissues including the brain. This is likely due to the mechanisms being energetically expensive, and conversely, excess nutrients were stated to exhaust NSCs accelerating brain aging (Lu et al. 1993; Cavallucci et al. 2016b; Seim et al. 2016; Erbaba et al. 2020a). CR has been shown to push the cells to spend more time regulating genomic stability and suppress cell

cycle progression, which eventually helps decrease the cancer risk (Seim et al. 2016). Mercken et al. (2013) also found a metabolic shift in skeletal muscle cells subjected to CR from proliferation to repair and maintenance. Therefore, our data suggests that the decrease in cell proliferation via CR increases the time that cells spend in the G0/G1 phase of cell cycle. This may form the basis of how CR-mediated protective mechanisms are thought to be exerted at the cellular level. Thus, the damaged cells would have more time for repairing their DNAs before entering S phase (Charnley and Tannenbaum 1985; Lu et al. 1993). On the other hand, increasing cell proliferation, was determined to be associated with decreased time spent for DNA repair adding to the risk for unrepaired DNA synthesis (Charnley and Tannenbaum 1985), eventually increasing DNA damage and driving towards the potential for cancer (Tudek et al. 2010).

This suggests an excellent protective mechanism achieved by CR against both cancer and aging compared to OF diet (Gensler and Bernstein 1981; Warner and Price 1989; Tudek et al. 2010; Nicolai et al. 2015). This proposed mechanism is supported by the PCA presented in the Results section. These are the data showing negative correlations between a CR diet and cell proliferation/cell cycle promotion with PC2 and PC3. To our knowledge, it is the first time that Sox2 is suggested as one of the regulators of diet-mediated improvement of neuroprotection mechanisms in the brain.

After we examined how changes in cell proliferation were regulated by CR and OF, positive regulators of cell cycle were measured. Tfdp1 and its binding partner E2f5 are known for their roles in promoting the cell cycle progression (Vaishnav and Pant 1999; Chan et al. 2002). Together they stimulate E2f-dependent transcription of many genes having roles in cell cycle progression from the G1 to S phase transition by enhancing their binding activity to DNA (Vaishnav and Pant 1999; Chan et al. 2002). Previously no known

significant association has been made between Tfdp1 and CR or age in the brain. For both *tfdp1* and *e2f5* gene expression levels, there were no significant changes with age or diet in the brains, although, Tfdp1 protein levels showed a marginally significant main effect of treatment with numerically decreased values in the CR group compared to AL and OF. We also observed a significant downregulation following short-term CR in aged animal brains in a previous pilot study using microarray analysis (Erbaba et al. 2019). In the protein multivariate analysis as suggested by PC3, which is negatively driven by Tfdp1, CR treated young animal brains clustered around higher values than young AL and OF, suggesting a decrease in cell proliferation with CR. Combining this subtle result with the Pcna and *sox2* expression level differences with respect to the different dietary groups, the effects of OF and CR diet regimens on cell proliferation are likely exerted on the stem cells in the brain rather than the overall proliferation status of all cells.

With aging there is a gradual deterioration in the immune system, also referred to as immunosenescence. This concept is viewed as a possible evolutionary adaptation or a remodeling rather than solely detrimental as such changes are also attributed to the extended lifespan/longevity (Fulop et al. 2018). Myc protein, Myca in zebrafish, is a proto-oncogene, which is known to stimulate proliferation, and Tp53 functions as a tumor suppressor by arresting the cell cycle, or inducing apoptosis. Our data demonstrated statistically significant decreases in myca and *tp53* mRNA levels with advanced age.

The downregulation of *myca* and *tp53* with age could be attributed to immunosenescence and its association with healthy brain aging. This hypothesis is supported by the roles of the genes that were examined. Myc is related to proliferation stimulation and there is an inverse correlation of Myc with longevity (Hofmann et al. 2015). c-Myc was previously reported as having dual functions depending on a phosphorylation switch deciding its path

to proliferation or differentiation. It was shown that tumor malignancy is increased when it is in an unphosphorylated state, while on the other hand, stimulating differentiation and reducing tumorigenesis when it is phosphorylated (Uribesalgo et al. 2012). In this study, the age-dependent decrease in *myca* expression was driven by the CR group such that in aged CR fish *myca* expression levels were significantly lower than those observed in young CR animals ($p = 0.006$) (Figure 11d). This pattern of diet changing within the context of age reflects the complexity of brain aging as an independent contributor to neurobiological alterations in the brain. This age-dependent decrease in *myca* expression that we encountered might be caused by a phosphorylation switch induced by aging as Uribesalgo et al. (2012) suggested.

With respect to the downregulation of *tp53* expression with age, this could be a result of the aging-accumulated byproducts in senescent cells. These cells have been shown to accumulate factors that are known to repress Tp53 functions (Gudkov and Komarova 2016). In this way, the repression of *tp53* in senescent cells of aged brains might further be increasing their survival rates by preventing the Tp53 induced apoptotic events. Our conclusion related to immunosenescence with a concomitant decrease in proliferation induced by the downregulation of *myca* and *tp53* with age, is supported by the gene expression multivariate analysis. In the PC1 driven by *myca*, *tp53*, *tfdp1*, *sox2*, *tnfa* and *il1b*, the young OF group scores were found to be higher compared to the young AL group, suggesting an OF-induced increase in proliferation and inflammation. From this perspective OF is creating an aging brain profile by exhausting the stem cell pool reserve and increasing inflammation.

In order to check neuronal identity, Dcamkl1 and HuC protein levels were investigated. Dcamkl1 regulates microtubule polymerization and has been shown to be involved in the

dynamic rearrangement of the cytoskeletal machinery with roles in neuronal migration, neuronal development, and formation of axonal projections related to axonal wiring (Koizumi et al. 2006; Shimomura et al. 2007; Vreugdenhil et al. 2007). Regarding the Dcamkl1 protein levels in our study, there were no significant alterations with respect to age or diet. Yet, there was a marginally significant effect with regards to the interaction between treatment and age on the Dcamkl1 protein levels. This indicates that any effect of diet on Dcamkl1 levels depends on the age of the subject. For the early-differentiated neuronal marker HuC protein levels, in the current study, we did not detect any clear alterations with respect to age or diet. Thus, neuronal levels were not affected drastically with respect to our dietary manipulations.

Glial cells are responsible mainly for supporting and nurturing neurons for proper functioning. Age-dependent alterations in glial cells have been characterized by a gradual loss of function, which facilitates neurodegenerative processes, in addition to shifting regional gene expression patterns (Soreq et al. 2017; Verkhratsky et al. 2019). Gfap is an intermediate filament protein that has roles in cytoskeletal function, cell communication and functioning of the blood brain barrier, as well as being a widely accepted marker of CNS astrocytes. We detected Gfap protein levels with a GFP signal in the transgenic line, which was utilized in the current study to compare Gfap protein levels among the groups. In this transgenic line the fusion of the Gfap-GFP protein very closely mimics endogenous Gfap (Lam et al. 2009). The use of this line aided us for the Western blotting experiments in the zebrafish brain, as most of the commercial antibodies against Gfap are developed mostly for mice or human and result in many extra nonspecific bands that would jeopardize the reliability of the analysis. Thus, the signals using the GFP antibody (ab6556, Abcam, UK) worked well and gave a clear specific band with zebrafish brain tissues, which was previously used by Lam et al. (2009). In our results, there was no main effect of

age with respect to Gfap protein levels, which is consistent with another study published from our group (Celebi-Birand et al. 2020). However, our findings revealed a marginally significant main effect of diet treatment, in which CR upregulated Gfap protein levels in the fish brains compared to AL and OF-fed animals. The increase that was observed with CR compared to AL and OF diets, might be due to an astroglial response.

Since there is heterogeneity in astrocyte reactivity, the observed upregulation needs to be considered in a context-dependent manner as the response can be either beneficial or detrimental. For example, expression level changes in astrocytes after the induction of reactivity was found to be shifting the cells either towards repair and protective functions, which is common after stroke and/or ischemia, or driving the transcriptome towards increasing the detrimental inflammatory immune responses, such as after LPS induction, a potent injury model (Zamanian et al. 2012). In our study, the inflammatory markers were not triggered with a CR diet as demonstrated from the gene expression data. Therefore, the astroglial response is unlikely to result from the detrimental inflammatory responses. From this perspective, compared to the AL and OF regimens, the CR diet might presumably be inducing a low amount of stress resulting from a process called ‘hormesis’, the term of which is defined as the beneficial effects from a low dose of stress. The occurring hormesis state in the cells then might trigger the astroglial responses in the case of CR, shifting the cells towards repair and protective functions.

Activated leukocyte cell adhesion molecule (Alcamb) is a cell adhesion protein that is associated with leukocyte cell adhesion, engraftment of stem cells, immune cell migration into the CNS, neural development, synaptic transmission modulation, axonal outgrowth, and maintaining blood brain barrier (BBB) integrity, in addition to being associated with neuroinflammation (Swart 2002; Cayrol et al. 2008; Thelen et al. 2012; Jeannet et al. 2013;

Shahaduzzaman et al. 2015; Kim et al. 2017; Lécuyer et al. 2017; Erbaba et al. 2020b). For a*lcamb* expression levels, though the effect of age was not profound, we observed a marginally decreasing trend especially in the CR groups as compared to AL groups. It has been suggested by Swart et al. (2002) that Alcam functions in tumor growth and induction of cell migration, as well as invasiveness contributing to the growth of tumor cells. Thus, from many aspects, Alcam seems to be highly correlated with the inflammatory and cancerous states of the brain by attracting and recruiting leukocytes to the inflammation site. In fact, blockade of Alcam was suggested to alleviate inflammation and disease severity in autoimmune encephalomyelitis, suggesting this is a contributing factor to allergic asthma induced inflammation, and was found to be increased with the inflammatory response against oxygen-glucose deprivation (Shahaduzzaman et al. 2015; Kim et al. 2018; Michel et al. 2019). Its expression is found among many cells including neurons, fibroblasts, epithelial cells, lymphoid and myeloid cells, so *ALCAM* is thought to be upregulated in response to neuroinflammation to attract and recruit leukocytes to the inflammation site. Therefore, the decreasing trend in its expression observed within the CR group as compared to the AL and OF groups may suggest a role for CR exerting anti-inflammatory properties in the brain. Therefore, it is very likely to be a good target for further investigation of its roles in anti-inflammatory behaviors of specific cell types exposed to nutrient restriction. To our knowledge, this is the first time that a role has been proposed for *Alcamb* with respect to nutrient intake.

Multivariate statistical testing revealed significant relationships that were age- and diet-dependent for both the protein and gene expression datasets. Overall, the PCA results for both datasets demonstrated that the CR group data scored higher values for the components with factors related to cytoskeletal/migratory/plasticity regulation (L-plastin, Dcamkl1, HuC), while having lower scores or being negatively associated with factors related to

proliferation/cell cycle promotion (Pcna, Sox2, Tfdp1, E2f5), inflammation (Il1b, Tnfa) and tumor suppression (Tp53). In contrast, the data from the OF group had trends toward higher values in the components with factors related to proliferation/cell cycle promotion (Pcna, Sox2, Tfdp1, Myca, E2f5), and inflammation (Il1b, Tnfa), tumor suppression (Tp53). Such conceptual conclusions from the third chapter, and same time the results we obtained from a pilot microarray between AL and CR applied animal brains that will be explained in the next chapter, led us make a connection between CR and the cell cycle regulations. Therefore, in the last fourth chapter, we first aimed to discover the transcriptional alterations with CR, and then try to establish a CR mimicing approach by manipulating the expression of tfdp1 gene in a way similar to its CR response.

CHAPTER 4

EFFECTS OF TRANSIENT KNOCKDOWN OF TFDP1 ON ZEBRAFISH EMBRYO AND ADULT BRAINS USING MORPHOLINO OLIGOS

4.1. Introduction

4.1.1. Caloric restriction and cell cycle regulations

Calorie restriction (CR) was previously shown to extend lifespan in various studies, from worms to humans. The mechanisms underlying this non-genetic intervention are yet to be understood clearly. CR was shown previously to inhibit cell proliferation on bone marrow, mice thymus, spleen, and kidney tissues (Lu, 1993) as well as being proposed so via analysis of human transcriptome datasets on different tissues due to its being energetically expensive (Seim, 2016). Seim et al. (2016) found that cell cycle maintenance related factors such as CDK regulators were negatively correlated with cell turnover rates according to analysis of 21 somatic cell transcriptome data including the brain indicating a support for CR to suppress cell cycle progression for promoting the cells to spend more

time on genomic stability, which decreases the cancer risk. The gene expression profile of long lived neurons were associated with reduced protein metabolism, which was similar to that observed with calorie restriction mediated profiles (Stout 2013; Mayer, 2006). It is proposed that the decrease in cell proliferation via CR increases the time that cells spend on G0/G1 phase of cell cycle. Thus the damaged cells would have more time for repairing their DNAs before entering S phase (Charnly, 1985; Lu, 1993). Mercken et al. (2013) also mentions a metabolic shift on skeletal muscle cells under CR from proliferation to repair and maintenance. On the other way around, increasing cell proliferation was pointed to be associated with decreased time spent for DNA repair adding to the risk for unrepaired DNA synthesis (Charnly, 1985), eventually increasing DNA damage and driving to cancer (Tudek, 2010). This suggests an excellent protective mechanism achieved by CR against both cancer and aging, acknowledging the relationship between DNA damage build-up and aging (Warner, 1989; Gensler, 1981; Tudek, 2010; Nicolai, 2015). Not only to lifespan, but cell cycle regulation was also found to be associated with neurodegenerative diseases (Ting, 2014; van Leeuwen, 2015; Copani, 2007). Abnormal exits from cell cycle arrest cause differentiated neurons to raise tau phosphorylation leading to apoptosis and progressing Alzheimer's disease (Ueberham, 2005). Along these lines, the gains with CR on life- and health-span seem to be strongly correlated with cell cycle maintenance, therefore research investigating the cell cycle regulators with CR are essential to understand CR mediated lifespan extension along with proposing new therapeutic solutions to neurodegenerative diseases for the ultimate goal of healthy brain aging. In search for new targets, here we attempted to investigate the roles of transcription factor Dimerization Partner 1 (Tfdp1) gene that was implicated with its key roles during cell cycle regulation.

4.1.2. Transcription Factor Dp1 (Tfdp1)

Tfdp1 is a G1 cell cycle related protein that functions as transcription factor. It is implicated in promoting the S phase forming a complex with E2F proteins. Together they stimulate E2F-dependent transcription of many genes having roles in cell cycle progression from G1 to S transition by enhancing their binding activity to DNA (Vaishnav, 1999; Chan, 2002). Previously no association has been made between TFDP1 in aging brain or brain under CR (Erbaba et al., 2020). *TFDP1* was mostly investigated by its roles in cancer shown with its overexpression (Hsu, 2014). It is upregulated in colorectal carcinoma (Pellatt, 2018), and implicated on hepatocellular carcinomas (Yasui, 2002). Other than oncogenic regulations, it was also implicated to be induced in the hippocampus on global cerebral ischemia (Jin, 2001). Though no known study providing a link between TFDP1 and aging, Podolskiy et al. (2016) stated an indirect correlation that has been made between cancer and aging. Another study showed that a senescence-like cell cycle arrest was induced by decreasing E2F/DP activity related reduction in the expression of many E2F target genes (Maehara, 2005).

While Tfdp1 literature resides mostly on cancer research, here in this study we studied Tfdp1 mediated cell cycle regulation with CR and aging on zebrafish brains. Different zebrafish cohorts were used to study the effects of diet and aging, analyzed on both protein and mRNA levels. Conducting our experiments we ultimately aimed to intervene brain aging with non-invasive dietary interventions in search for a reliable therapeutic approach for reversing neurobiological changes during brain aging, besides to be able to propose new drug targets for neurodegenerative diseases.

4.2. Experimental

4.2.1. Animals

In the current study, a total of 62 zebrafish were used in different protocols. We initially performed microarray to investigate changes in the brain transcriptome in response to Caloric Restriction (CR). Using Affymetrix GeneChips, we compared the effects of CR on 3 CR-fed and 3 Ad-libitum-fed (AL: control feeding) wild type (AB) aged male fish brains (27-33-month old). Fish were euthanized and decapitated following a 4-week CR treatment with a weekly feeding regimen adapted from Arslan-Ergul et al. (2016), shown in Table 9.

	MONDAY	*TUESDAY*	*WEDNESDAY*	*THURSDAY*	*FRIDAY*	*SATURDAY*	*SUNDAY*
AL	100mg Dry Food	100mg Dry Food	100mg Dry Food	100mg Dry Food	100mg Dry Food	100mg Dry Food	100mg Dry Food
	100mg Dry Food	100mg Dry Food	100mg Dry Food	100mg Dry Food	100mg Dry Food	100mg Dry Food	100mg Dry Food
	1x Artemia		1x Artemia		1x Artemia		
CR	100mg Dry Food		100mg Dry Food		100mg Dry Food		100mg Dry Food
			1x Artemia				

Table 9 Feeding regimen applied prior to microarray. 3 CR-fed (4-weeks) fish were compared with 3 AL-fed fish.

Following microarray, selected differentially expressed genes with respect to diet were further examined on RT-PCR experiments with 23 wild type (25-33-month) male fish brain RNAs whose fish were fed with different durations of CR regimens in a previous study. Since the samples were primarily utilized in that earlier study, the limited amounts of the left-over RNA samples did not allow us to use them individually to run with 23 selected gene primers in 4 technical repeats. Therefore the RNAs were pooled regarding their CR treatment groups as AL (5 individuals' brain RNAs; ibR), 1-week CR (5 ibR), 2-week CR (5 ibR), 4-week CR (5 ibR), 10-week CR (3 ibR) (Table 10). Then, to examine age-related Tfdp1 protein level differences, 4 young (3-month) and 4 aged adults (21-

month) TgBAC(Gfap-GFP)zf167 line male fish brains were utilized in Western blot experiments.

For the adult fish cerebroventricular microinjection (CVMI) of Tfdp1 Vivo Morpholino (Vivo-MO) oligo for transient knockdown of Tfdp1 on fish brains, we used 9 middle-aged (12-month) (6 male, 3 female) wild-type AB strain fish in RT-PCR experiments, and 16 young (7-month) TgBAC line fish in Western blot experiments. Brain samples were collected after anesthesia, snap-frozen in liquid nitrogen, and stored at -80°C. Embryos used for the MO injection experiments were also collected from wild-type AB strain zebrafish parents. Approximately a total of 3600 zebrafish embryos were used for embryo injection experiments for transient knock-down of Tfdp1. All fish were kept in a controlled system designed by ZebTec Zebrafish Housing System (Tecniplast, Italy) with 14-hour light and 10-hour dark cycles at 28°C system water. All protocols applied to the animals were performed under protocols approved by the Bilkent University Local Animal Ethics Committee (HADYEK).

Table 10 The list of pooled RNA samples used in RT-PCR validation experiments following microarray

AL	**1-week CR**	**2-week CR**	**4-week CR**	**10-week CR**
27mo, Male	*28mo, Male*	*28mo, N/A*	*32mo, N/A*	*Old, N/A*
27mo, Male	*28mo, Male*	*28mo, N/A*	*32mo, N/A*	*Old, Male*
33mo, Male	*28mo, Male*	*28mo N/A*	*33mo, N/A*	*Old, Male*
25mo, N/A	*27mo, Male*	*33mo, Male*	*27mo, N/A*	
25mo, N/A	*33mo, Male*	*27mo, Male*	*27mo, N/A*	

4.2.2. RNA Isolation

All the RNAs were extracted from the individual whole-brain samples for the adult animals. Overall the RT-PCR validation experiments following microarray comprised of a

total of 23 fish brain RNAs pooled in 5 treatment groups of AL, 1week-CR, 2week-CR, 4week-CR, and 10week CR. In the case of embryo RT-PCR experiments, due to their small sizes, RNAs were isolated by pooling around 30-40 injected embryos on their 3-5 days post-injection (dpi). Total RNAs were isolated either by using Qiagen's Rneasy Mini Kit (for microarray experiment) or Thermo Fisher Scientific's TRIzol Reagent (for RT-PCR experiments) according to the manufacturer's instructions. The isolation protocols were followed by Dnase treatment with an Ambion TURBO DNA-free Kit from Thermo Fisher Scientific. The concentrations of the isolated RNA samples were measured via either an Agilent 2100 Bioanalyzer instrument (prior to microarray) or a NanoDrop 2000 (prior to RT-PCR).

4.2.3. Gene Expression Profiling

Microarray was performed for gene expression profiling of 3 aged (27-33-month old) CR-fed male fish whole brains. We obtained the 3 AL-fed aged male fish whole-brain datasets (27-33-month old) from an earlier study published by our lab, treated by the same person (Arslan-Ergul et al., 2014). We used a GeneChip 3' IVT PLUS Reagent Kit for the microarray experiments and prepared targets for GeneChip 3' Expression Arrays manually following the manufacturer's instructions. Samples were first quality checked prior to the procedure. 3' Array Hybridization parts were completed at Prof. Dr. Hilal Özdağ's laboratory at Ankara University Biotechnology Institute. In order to analyze the GeneChip Zebrafish Genome array data, we utilized the R programming language and software environment for statistical computing and to visualize data. We first normalized the data before performing the principal component analysis (PCA). P-value distributions of the probe sets were obtained employing a t-test, and significantly differentially expressed 526 genes were extracted from the data. For further analysis of the microarray data, DAVID

Functional Annotation Tool was utilized to study the most enriched functional categories in these differentially expressed genes and to discover the associated KEGG pathways.

4.2.4. Embryo Injections and Cerebroventricular Microinjection

Morpholino oligos (MO) are specifically designed and synthesized oligo molecules that are used to transiently alter the transcription (splice blocking morpholinos) or translation (translation blocking morpholinos) of a gene of interest. We used translational blocking MO specifically designed and synthesized (Gene Tools) to bind *tfdp1* mRNAs for knockdown experiments. The translational blocking morpholinos, by name, inhibit translation of its target mRNAs. By design, there are two types of morpholino oligos, one is the traditional type used to inject zebrafish embryos, and the other is Vivo morpholino used for in vivo studies. The Vivo morpholinos are traditional morpholinos attached to a delivery moiety to facilitate its entry into the tissues and cells.

In this study, two kinds of injection protocols were applied for transient knockdown of the *tfdp1* gene, one to the fish embryos, the other one to the adult fish heads. For the embryo injections, the injection solution containing a specifically designed morpholino oligo (*tfdp1*-MO) and a tracking dye was delivered to the fish embryos via manual injection to the yolks at the 1 to 4 cell stage of the embryonic development (Figure 13). The injection solution was prepared to contain 1:10 dilution of Phenol Red as the coloring agent and different concentrations of *tfdp1*-MO (2ng, 4ng, or 8ng). Among a total of 3600 zebrafish embryo injections, around 1200 embryos were injected for each concentration group of 2ng, 4ng, and 8ng. Each concentration group was divided into three further subgroups of Tfdp1 MO (*tfdp1*-MO) injection group, Negative Control MO (NC-MO) injection group, and Non-injected group (NI). Finally, for each of these three treatment groups, two different time points were selected to observe, as 3dpi and 5dpi groups. After injections,

embryo RNAs were isolated by pooling around 30-40 embryos due to their small sizes, so five biological replicates were made available for each subgroup (N=5 for each). The experimental scheme for embryo injections is demonstrated in Figure 14. Injected adult brain and embryo samples were collected after anesthesia, snap-frozen with liquid nitrogen, and stored at -80°C to be assayed via RT-PCR to detect changes on 7 Tfdp1 downstream genes.

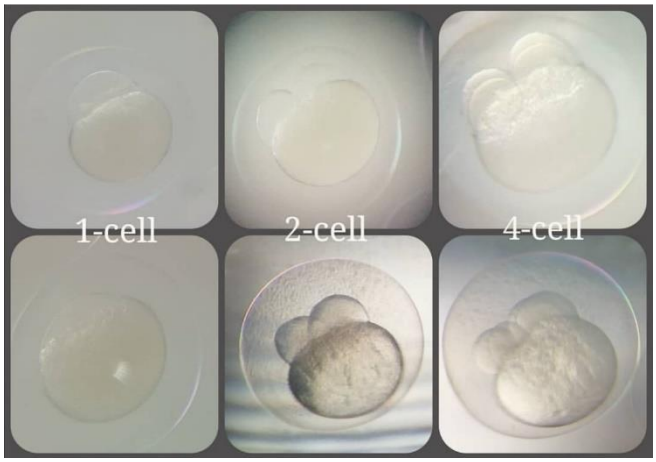

Figure 13 Embryo injections were performed at 1-4 cell stage of embryos as shown

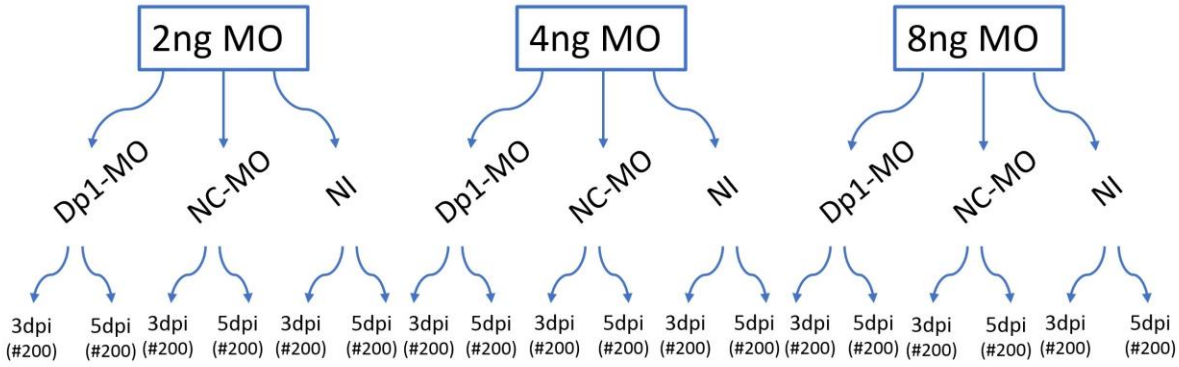

Figure 14 Embryo MO injections comprised of approximately 200 embryos injected per group for each subgroup. NC: Negative Control Morpholino injected group. NI: Non-injected group.

For the second part of injections, the Vivo-MO delivery to the adult animals was employed for in total of 25 fish via an automated microinjector apparatus applying Cerebroventricular Microinjection (CVMI) method developed by Kizil et al. (2011). The procedure involves an injection mixture composed of 9µl of 500 µM MO solution (*tfdp1*-MO, or Negative Control (NC) MO) and 1µl of a fluorescent tracking dye (Invitrogen, CellTracker Red CMTPX) were injected into the cerebroventricular region of the heads' of the anesthetized (0.168 mg/ml Tricaine, Sigma-Aldrich) adult zebrafish after a quick incision into the skull generating a small slit to facilitate the delivery (Figure 15). To assess the Vivo-MO injection efficiency, a time-plot was constructed regarding the Tfdp1 brain protein levels. 16 TgBAC 7mo-old adult fish were used for those experiments, assigning 2 fish per 7 time point and 2 fish for the negative control group. For these western blot experiments, the negative control group (NC) heads were incised, and anesthesia was performed as done for treatment groups; but no injection solution was given and taken one day after the treatment. Time points were as follows 1,5 hours post-injection (hpi) , 4hpi, 12hpi, 1 days post-injection (dpi), 2dpi, 3dpi, and 4dpi. For adult brain, RT-PCR measurements following *tfdp1*-Vivo-MO injection to detect changes in 7 Tfdp1 downstream target genes, after anesthesia 9 AB+,+ wild type line 12-month old adult fish were either Dp1 Vivo MO-injected, or Negative Control (NC) Vivo MO-injected, or saved as Sham-injection control. Among 9 fish, 3 animals were injected with 500uM Dp1-Vivo-MO solution, 3 were injected with NC-Vivo-MO solution, and lastly, 3 were taken as a non-injected control group. For the injected groups, the signals were successfully dispersed till telencephalon from the injection site of the right Optic tectum. So overall, among the successful injections 9 were decapitated, and the whole brains were dissected under the stereomicroscope. Injection success has been determined by eye under the microscope checking whether the fluorescent tracking dye injected with the injection solution has been

diffused in the brain properly. RNA extractions were performed from individual whole brains. Injected embryo and adult brain samples were collected after anesthesia, snap-frozen with liquid nitrogen, and stored at -80oC to be assayed via RT-PCR to detect changes on 7 Tfdp1 downstream genes. Three technical repeats for each biological replicate were included in the analysis for the RT-PCR experiments.

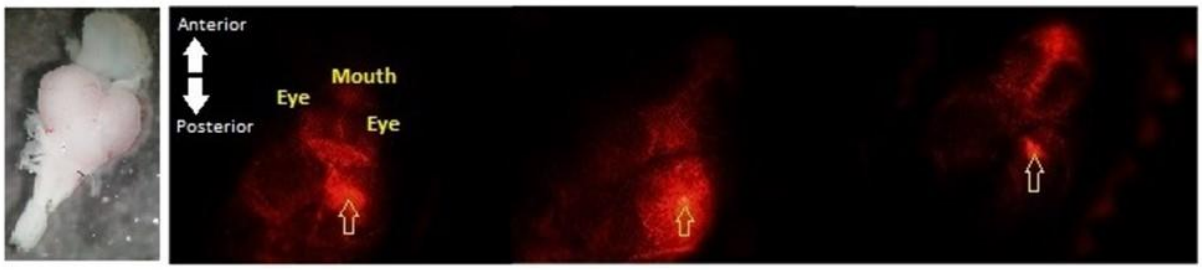

Figure 15 Left image shows a zebrafish brain (right image taken in our fish facility). Right images show fluorescent tracking dye CMTP-X (red) delivered with the morpholino solution given with the injection solution to track its diffusion during CVMI optimized in our facility. Three different zebrafish brains are shown. Images were taken under diluted anesthetic solution 30 minutes after injection. Injection sites are shown with yellow arrows.

4.2.5. Western Blotting

Fish head samples snap-frozen for western blot experiments were dissected, and individual brain proteins were extracted according to a protocol described earlier in Karoglu et al. article (2017). Proteins were first extracted using RIPA lysis buffer, and quantifications were performed via Bradford Assay with respect to known concentrations of BSA on a spectrophotometer. We utilized BioRad's Mini-PROTEAN 4-gel electrophoresis system to cast and run western gels and BioRad's Mini Trans-Blot module system to transfer the proteins to the PVDF membrane. 5% Milk powder in TBS-T is preferred as the blocking agent during procedures. The primary antibody concentrations were decided in an assay-

dependent manner, considering the manufacturer's instructions; for the Anti-Dp1 (45kDa, ab208945) antibody 1:1000, and for the Anti- β-Tubulin (55kDa, CST-2146S) antibody 1:10.000 concentrations were used. As the secondary antibody, 1:5000 Anti-rabbit HRP linked antibody (CST-7074S) was used against both antibodies. 26616 PageRuler Prestained Protein Ladder (10 to 180 kDa) was utilized as the protein ladder. 40ug protein was used for each well per gel. Loading was performed in alternating order to prevent experimental bias on the blot. For the western blot experiments examining the Tfdp1, Pcna, and Lplastin protein levels following 8ng *tfdp1*-MO injections, 3 injected embryo samples (40ug for each well), each pooled for 20 embryos, were used, and 2 technical repeats for each set of samples was performed. For the western blot experiments of TfDp1 protein level time plot following Dp1-Vivo-MO injections, 16 individual brain protein sample (10ug for each well) was used, and 3 technical repeats were performed per biological replicate. For the western blots to examine age-related differences on Tfdp1 protein levels, 4 individual animal brain protein lysates (40ug for each well) were used for two age groups in 3 technical replicates. Lastly, chemiluminescent detections were performed using Thermo Scientific SuperSignal West Femto Maximum Sensitivity Substrate on BioRad's ChemiDoc Imaging System. Band intensities were quantified on ImageJ software, and within gel and tubulin normalizations were performed prior to all analysis.

4.2.6. Real-time Polymerase Chain Reaction

In this study, we used Real-time Polymerase Chain Reaction (RT-PCR) first to validate microarray results for 23 genes selected from 3 main implicated KEGG pathways that were found to be associated with the 526 differentially expressed genes between AL and CR treated samples. Primer sequences of those 23 genes are given in Table 11. Among those 23 differentially expressed genes, we are specifically interested in a less-popular but

crucial cell cycle gene, Tfdp1. Therefore, we utilized RT-PCR secondly to screen alterations with Tfdp1 MO knockdown as a mimic for CR, in Tfdp1 downstream target genes, after both embryo and adult fish head injections. For the first part of RT-PCR validation experiments following microarray, RNAs from a total of 23 wild-type aged (23-33-mo old) fish brains were pooled due to the low RNA sample volumes left from a prior study. We pooled 3 to 5 individual fish brain RNA samples from the same treatment (AL/CR) and age groups (Table 10). Regarding their treatments, 5 groups were gathered as; AL, 1week-CR, 2week-CR, 4week-CR, and 10week CR. The samples were run on RT-PCR in 4 technical replicas. For the second part, the downstream target genes of *TFDP1* transcription factor; *CCNA2, CCNE1, CDK1, MYCA, RRM1, TP53,* and *TYMS,* were acquired from both literature search and by using STRING and TRRUST bioinformatics tools, all of which play roles in the cell cycle. The list of primers used in the study is provided in Table 3. LifeScience's LightCycler® 480 SYBR Green I Master kit, and LightCycler® 480 white 96 Multiwell Plates with LightCycler® 480 Instrument were utilized for the RT-PCR experiments. The protocol was applied using 2µl of cDNA, 2 µl of primer mix, 6µl of nuclease-free water, and 10µl of SYBR Green I dye. Each experiment had 3-4 technical repeats of each PCR plate run. The measurements were performed by normalizing Ct values to the reference genes of *beta-Actin1* and *18s ribosomal RNA* genes (*Rpl13*) controls (delta Ct). Following actin normalizations, $2^{(-\text{delta delta ct})}$ values were calculated for each sample with respect to their control groups (AL or NI).

Table 11 Among 526 preliminary significant differentially expressed genes with CR, 23 genes were chosen from the selected pathways to further proceed with RT-PCR validation, adding additional 3 groups with different durations of CR.

Primer	**Sequence**
ccnb2Left	GACTGTTGCCATTCTTGATCG

ccnb2Right	GACACCCACCAGCTGAAGTT
chek2Left	AACAAACACGACTTTCCATCAAT
chek2Right	ATTTCGATTTCCCGCTCAG
crebbpbLeft	GCCCAAACTGAACTCACCTG
crebbpbRight	TCGAACAAGGACACGAAGTCT
gadd45aaLeft	ACATGCAACATGACTTTTGAAGA
gadd45aaRight	TACATCCCTGCGGTAATGC
gadd45gaLeft	AACACAGCTACTACTGGCGATAGA
gadd45gaRight	GACAGTAAGACAGTCCTGCTTTTTAG
Skp2Left	TCCGGCTGAATTTATGTGG
Skp2Right	ACACGTTCATTTCTTCAATTCG
tfdp1aLeft	CAGGCTTTGACTGTTGGAAAA
tfdp1aRight	GGCCTCTGAGGTGTGCTAAT
Wee2Left	GAGGTTGGATGGTTGCATGT
Wee2Right	TGGGCGTACACTTCCTTCA
ywhaqaLeft	CATTTGCAACGAGGTGTTGA
ywhaqaRight	TGCTCTCAGAGTTTGTCGAGTT
ywhaqbLeft	AATCCGGTGGAGCCAACTAT
ywhaqbRight	GATCAAAGGAGGGGAATGAAC
btg2Left	AGTTTTGTTTGCCGGCTGT
btg2Right	ACCAATGGTGCTGGTAGTGTT
btg3Left	CACGTCGGATTACCACTCTG
btg3Right	CCCTCACACTAACACCGATGA
btg4Left	AAATGCATCCCAACGGTCT
btg4Right	GGTATGTACCCCAGCTTTGC
cnot6aLeft	ACCTCGCTCATGGATACCAC
cnot6aRight	GCACATCACAGAGAAAAGTGCT
hspd1Left	AAAAACTCAAAGCCCGTCAC
hspd1Right	TTGGCAGAAATAGTAGCCACCT
lsm4Left	ACTGAAGACGGCACAGAACC
lsm4Right	CGTTGTATGTCTCGCCATTCT
rqcd1Left	GAACGCTTTTCACATGTAGCC
rqcd1Right	GAGCCGAGGGTTCCTTAGAC
ncbp2Left	GGAAATCTGGTGGTCAGGTC
ncbp2Right	TCCCATAACCCCCTCTGG
nudt21Left	CTGGAGGCGAGTTGAACC
nudt21Right	ATCCTGGCGTCCCAAAAT
papolgLeft	CAGCCTCCACACCTGAAGAC
papolgRight	GGCTGTCCATGAACACAAGA
ppp2r2caLeft	CTCTGCGACAGACACTCCAA
ppp2r2caRight	TCAGAGAAAAAGGAACGATTGC
upf1Left	GCGAAAGCAGACTCTGTGGT
upf1Right	AGACTGCTCTGACTGGCACA
zgc56064Left	GACGACACGCTCAAGTACTCTTT
zgc56064Right	CACAGGAAGTAGTCAGGTGTGC
ccna2Left	AAAGCAGCTAACAACAGGACAGT
ccna2Right	GGTTTACACGCAATTATCTGTGG
ccne1Left	CATGTGCCTTACTTGGAATGG
ccne1Right	AGTGGGAACCGGAGACCT
cdk1Left	TTGGGGTCCCAGTAAGAGTCTA

cdk1Right	GGTGTGGAATAGCGTGAAGC
mycaLeft	AACGGCATTCGTTAAACACA
mycaRight	ATCCTCATCGTCGTTGTCG
rrm1Left	TTAAGGAGAAGATTGCAAAGCA
rrm1Right	TCTGAGCTGTGGAGGCAGT
tp53Left	GAGGTCGGCAAAATCAATTC
tp53Right	TGGGGGCTGAATACTTATCAA
tymsLeft	GGAGCCGAATACAAAGATATGC
tymsRight	TGGGTTTGACTTGATGGTGTC

4.2.7. Statistical Analysis

All the statistical calculations were performed using IBM's SPSS statistical software. Whenever age and treatment variables were tested, we performed factorial ANOVA test followed by Bonferroni post hoc tests applied with Bonferroni adjustment for multiple comparisons. For normality or homogeneity of variance assumption violations tested by Kolmogorov Smirnov test and Levene's test, we performed Kruskal Wallis test followed by Mann Whitney U tests for posthoc tests with Bonferroni corrected p-value (0.0167).

4.3. Results

4.3.1. Microarray suggests that calorie restriction application causes gene expression differences

In order to examine the gene expression differences occurring with CR treatment, we performed microarray using Affymetrix GeneChips. CR-fed aged male fish whole-brain RNAs were used in the expression arrays. We compared the 4-week CR applied aged (27-33-month old) male fish brain transcriptome datasets (N=3) (not published) with AL-fed aged male fish brain transcriptome datasets that were also obtained by our group previously (Arslan-Ergul et al., 2014). Using R programming for analysis, 526 genes were suggested to be differentially expressed ($p < 0.001$) following a 4-week diet applied during their advanced age (unpublished data). Principal component analysis (PCA) was performed

to investigate the pattern of expression level differences with the dietary application. Analysis was performed for the 526 putatively differentially expressed genes regarding their normalized expression values. *P*-value distributions of the normalized microarray data after t-test and visualization of the PCA data in two dimensions are shown in Figure 16. Looking at the most profound functional categories in these 526 significantly differentially expressed genes (DEGs) via DAVID Functional Annotation Tool, we selected 3 KEGG pathways of Cell cycle, RNA degradation, and mRNA surveillance (Figure 17). We narrowed down the DEG list to 23 to examine with RT-PCR. Microarray patterns in these 23 gene expressions are plotted in Figure 18, while RT-PCR validation results regarding the same genes are demonstrated in Figure 19 by including additional durations of CR in the RT-PCR validation experiments; 1-week CR, 2-week CR, 4-week CR, 10-week CR, and AL. Among the RT-PCR results, the genes showing consistent up- or downregulation with CR compared to AL feeding were *tfdp1a*, *wee2*, *ywhaqa*, *lsm4*, *ncbp2*, and *zgc56064*. However, the ones consistent with their expression patterns in microarray results were only *tfdp1a* and *wee2*, both of which were related to cell cycle pathway regulations. Finally, due to missing data points for the other gene (*wee2*) and considering its central roles in cell cycle progression, we further proceeded our experiments around the regulation of the *tfdp1* gene, which downregulated with CR in both microarray and RT-PCR experiments.

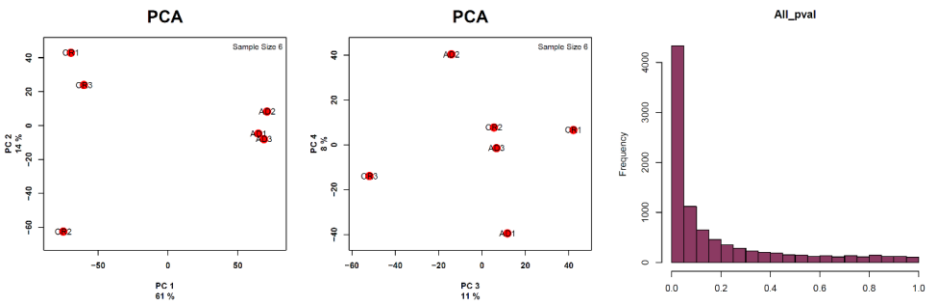

Figure 16 A histogram of the p-value distribution of the probe sets obtained from the t-test was plotted. Probe sets accumulate around $p < 0.001$.

	Selected Pathways	Selected Genes
1	*Cell cycle pathway*	ccnb2
2		chek2
3		crebbpb
4		gadd45aa
5		gadd45ga
6		Skp2
7		tfdp1a
8		Wee2
9		ywhaqa
10		ywhaqb
11	*RNA degradation pathway*	btg2
12		btg3
13		btg4
14		cnot6a
15		hspd1
16		lsm4
17		rqcd1
18	*mRNA surveillance pathway*	ncbp2
19		nudt21
20		papolg
21		ppp2r2ca
22		upf1
23		zgc56064

Figure 17 Looking at the most profound functional categories among 526 differentially expressed genes on the microarray, three KEGG pathways were extracted via DAVID Functional Annotation Tool. The figure shows the DEGs associated with these pathways.

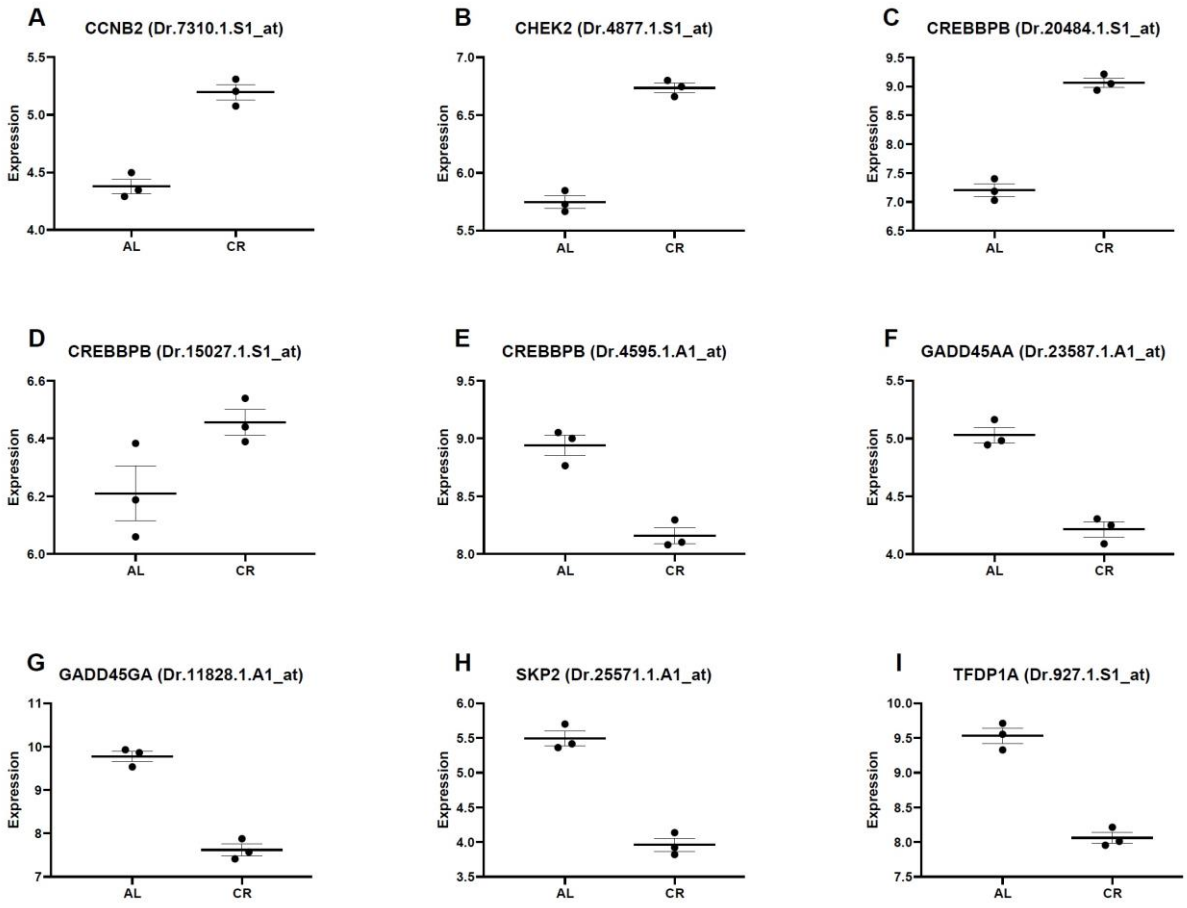
A
CCNB2 (Dr.7310.1.S1_at)
B
CHEK2 (Dr.4877.1.S1_at)
C
CREBBPB (Dr.20484.1.S1_at)
D
CREBBPB (Dr.15027.1.S1_at)
E
CREBBPB (Dr.4595.1.A1_at)
F
GADD45AA (Dr.23587.1.A1_at)
G
GADD45GA (Dr.11828.1.A1_at)
H
SKP2 (Dr.25571.1.A1_at)
I
TFDP1A (Dr.927.1.S1_at)
Expression
AL
CR

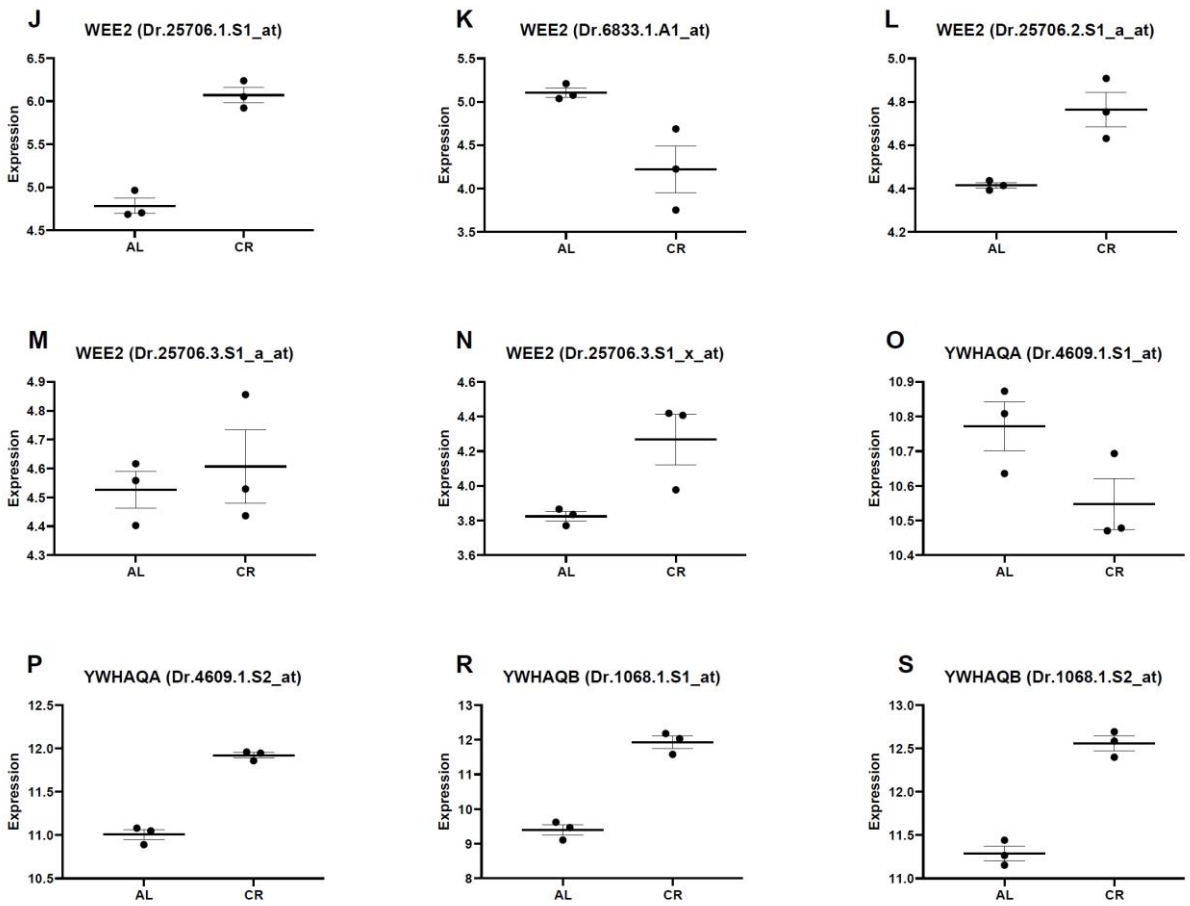
J
WEE2 (Dr.25706.1.S1_at)
Expression
6.5
6.0
5.5
5.0
4.5
AL
CR
K
WEE2 (Dr.6833.1.A1_at)
Expression
5.5
5.0
4.5
4.0
3.5
AL
CR
L
WEE2 (Dr.25706.2.S1_a_at)
Expression
5.0
4.8
4.6
4.4
4.2
AL
CR
M
WEE2 (Dr.25706.3.S1_a_at)
Expression
4.9
4.8
4.7
4.6
4.5
4.4
4.3
AL
CR
N
WEE2 (Dr.25706.3.S1_x_at)
Expression
4.6
4.4
4.2
4.0
3.8
3.6
AL
CR
O
YWHAQA (Dr.4609.1.S1_at)
Expression
10.9
10.8
10.7
10.6
10.5
10.4
AL
CR
P
YWHAQA (Dr.4609.1.S2_at)
Expression
12.5
12.0
11.5
11.0
10.5
AL
CR
R
YWHAQB (Dr.1068.1.S1_at)
Expression
13
12
11
10
9
8
AL
CR
S
YWHAQB (Dr.1068.1.S2_at)
Expression
13.0
12.5
12.0
11.5
11.0
AL
CR

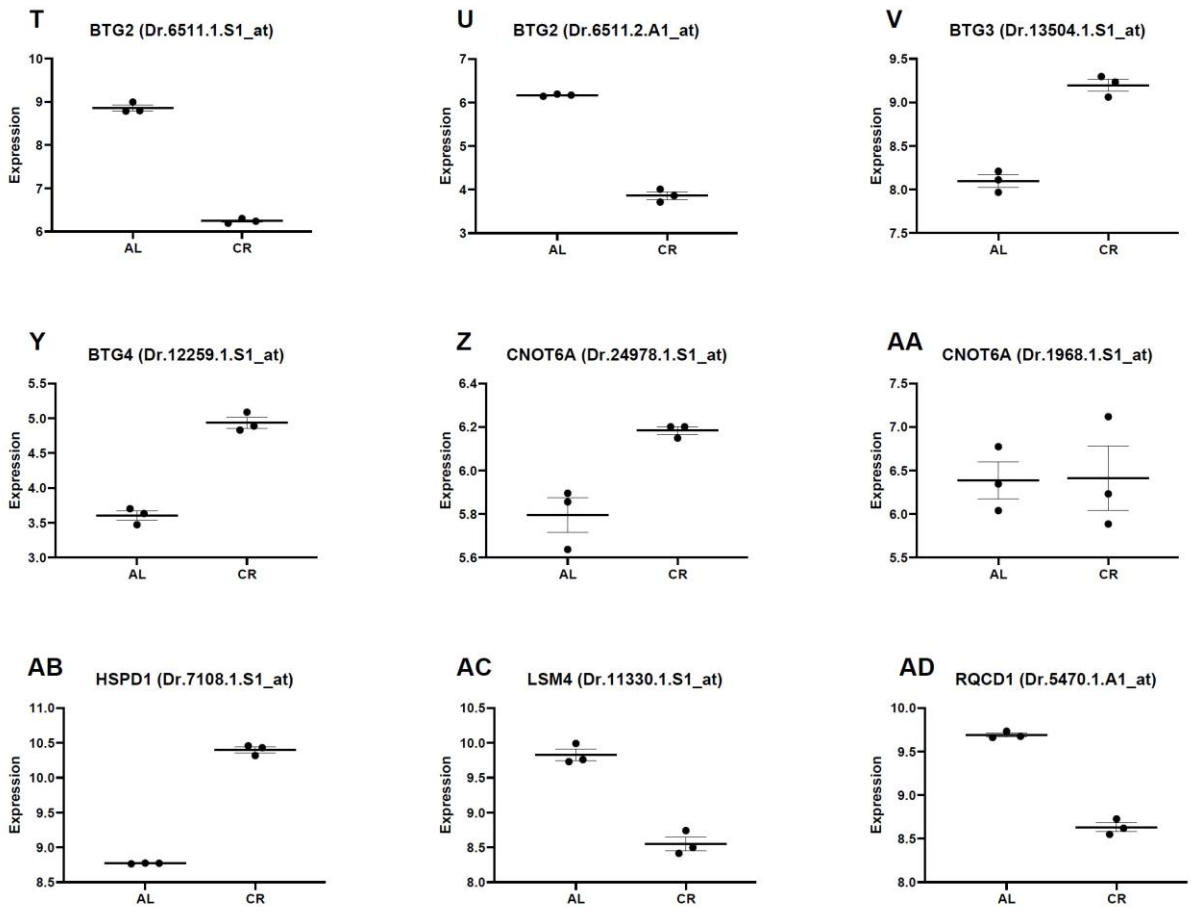
T
BTG2 (Dr.6511.1.S1_at)
U
BTG2 (Dr.6511.2.A1_at)
V
BTG3 (Dr.13504.1.S1_at)
Y
BTG4 (Dr.12259.1.S1_at)
Z
CNOT6A (Dr.24978.1.S1_at)
AA
CNOT6A (Dr.1968.1.S1_at)
AB
HSPD1 (Dr.7108.1.S1_at)
AC
LSM4 (Dr.11330.1.S1_at)
AD
RQCD1 (Dr.5470.1.A1_at)
Expression
AL
CR

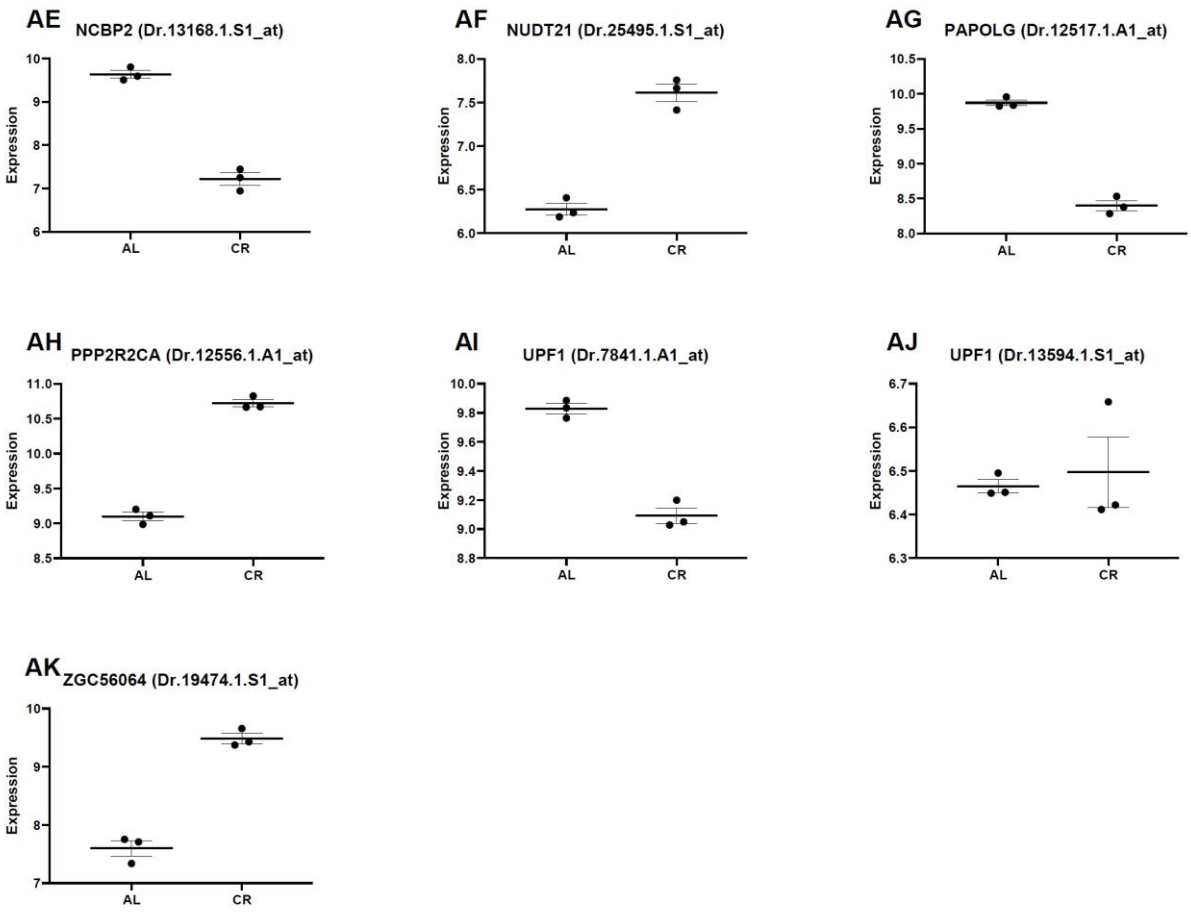

Figure 18 Microarray results for selected 23 DEGs are shown. Each plot shows a different probe set measuring mRNA levels of each gene indicated in the title. Plots were obtained using Graphpad software.

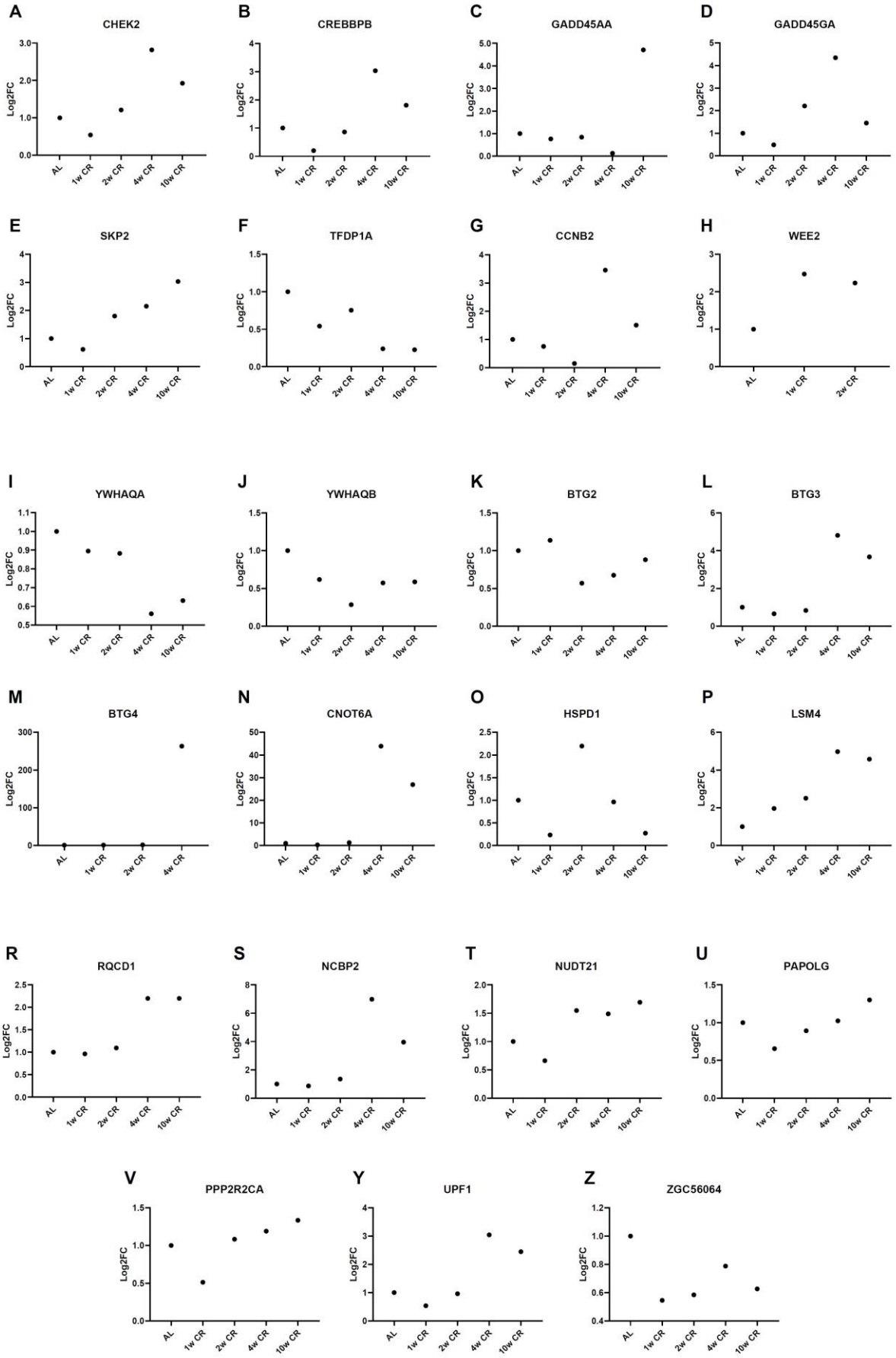
A
CHEK2
B
CREBBPB
C
GADD45AA
D
GADD45GA
E
SKP2
F
TFDP1A
G
CCNB2
H
WEE2
I
YWHAQA
J
YWHAQB
K
BTG2
L
BTG3
M
BTG4
N
CNOT6A
O
HSPD1
P
LSM4
R
RQCD1
S
NCBP2
T
NUDT21
U
PAPOLG
V
PPP2R2CA
Y
UPF1
Z
ZGC56064
Log2FC
AL
1w CR
2w CR
4w CR
10w CR

Figure 19 RT-PCR results for selected 23 DEGs with additional durations of CR are shown. Plots were obtained using Graphpad software.

4.3.2. Tfdp1 protein levels significantly increased by age

Following the detection of the decreasing effect of diet on *tfdp1* expression, next age-related protein level differences of the gene were further validated on 4 young (3mo) and 4 old adults (21mo) male zebrafish individual brains. Results show that aging significantly increases Tfdp1 protein levels on the brain (Figure 20) ($t(6) = -10.031$, $p < 0.001$, two-tailed).

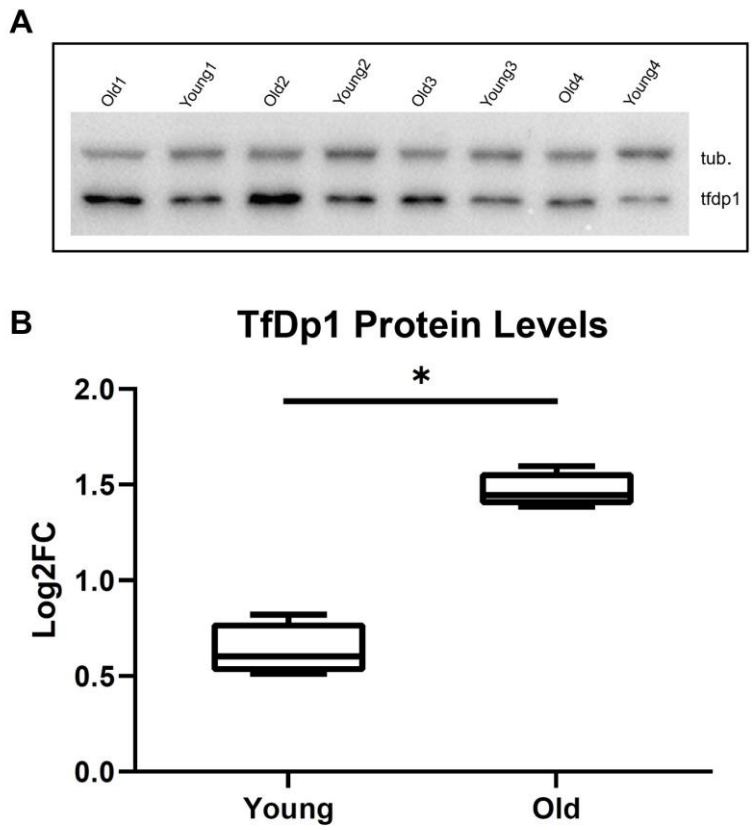

Figure 20 A) Representative western blot image of zebrafish whole-brain Tfdp1 protein levels comparing young and old adult fish. **B)** Tfdp1 protein level differences with respect to age. Tfdp1 protein levels in old fish brains are significantly higher than in young fish brains ($p < 0.001$). Whole-brain lysates from four animals per age group were used for

Western blot experiments. Band intensities were quantified on ImageJ software. For each well, firstly within gel normalization, then tubulin normalization was performed.

4.3.3. *tfdp1*-MO Embryo Injections

Translational blocking morpholino oligos designed for Tfdp1 were used to knock down *tfdp1* gene. The experimental plan was divided into two to work on Embryo and Adult animals for the morpholino treatments. The embryo injections were performed in three different doses of *tfdp1*-MO (2ng, 4ng, 8ng) and on two time points (3dpi and 5dpi) (Figure 14). After injections, Western Blot and RT-PCR protocols were applied. By Western blot, we measured the Tfdp1 protein levels as well as Pcna and Lplastin for MO treatments on the embryo. Via RT-PCR we measured the effects of *tfdp1* knockdown on the relative expression differences of its 7 target genes; *ccna2, ccne1, cdk1, myca (c-myc), rrm1, tp53,* and *tyms*, all of which play roles in cell cycle. Pooling around 30 embryos performed per group, 5 biological replicates were made available for RT-PCR experiment for both time points (3-day post injection (dpi) / 5dpi) of *tfdp1*-MO-injected, NC-MO injected, and NI groups.

4.3.3.1. Embryo Tfdp1, Pcna or Lplastin protein levels did not alter following *tfdp1*-MO injections

We measured the effect of *tfdp1*-MO knockdown on zebrafish embryos on Tfdp1, Pcna (proliferation marker) and Lplastin (inflammation indicator cytoskeletal protein) protein levels by performing Western blot (Figure 21). No significant changes were observed at the embryo protein levels of neither Tfdp1 ($F(2,5) = 0.112$, $p = 0.896$), nor Pcna ($F(2,5) = 1.854$, $p = 0.25$), or Lplastin ($F(2,5) = 0.105$, $p = 0.902$) following 8ng *tfdp1*-MO injection (3dpi).

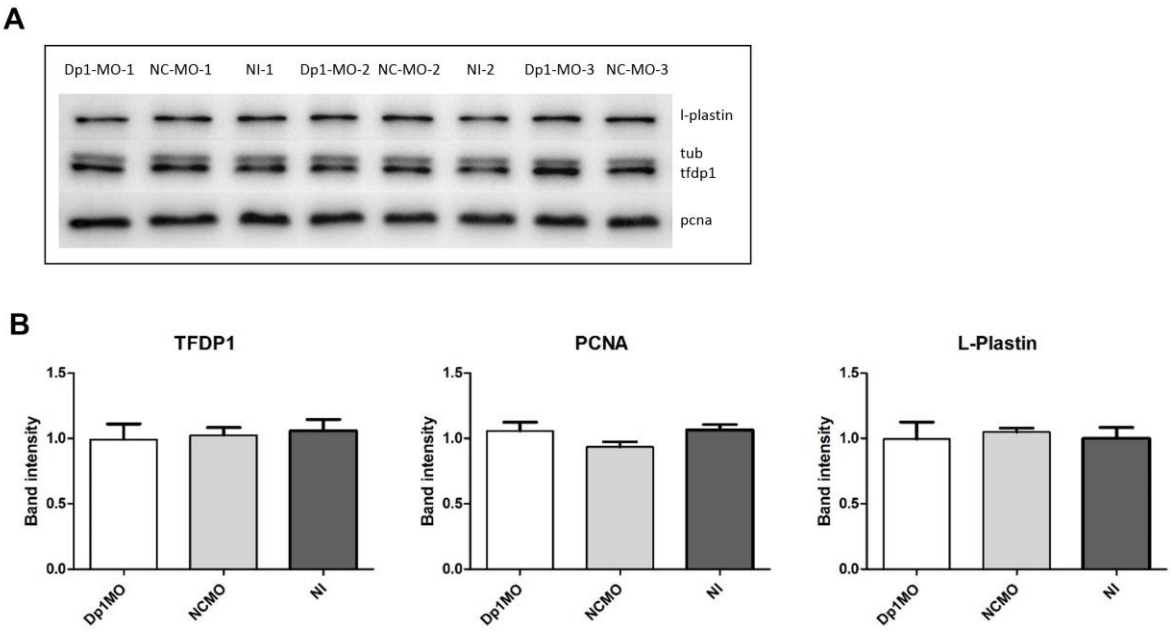

Figure 21 A) Representative western blot membrane bands of a set of 8ng embryo injections (3dpi) are shown measuring Lplastin, Tubulin, Tfdp1, and Pcna protein levels. *tfdp1*-MO: 8ng Dp1 morpholino injected ~20 pooled embryos; NC-MO: 8ng Negative Control morpholino injected ~20 pooled embryos; NI: non-injected ~20 pooled embryos. **B)** No significant change was observed at the embryo protein levels of Tfdp1, Pcna, or Lplastin following 8ng *tfdp1*-MO injection (3dpi).

4.3.3.2. *tfdp1*-MO injections in zebrafish embryos increased *tp53* and *myca* gene expression levels

For 2ng injections, there were no significant effect of MO treatments (*tfdp1*-MO/NC-MO/NI) on Tfdp1 downstream gene expressions of *ccna2* ($H(2) = 3.541$, $p = 0.17$), *ccne1* ($H(2) = 2.781$, $p = 0.249$), *cdk1* ($H(2) = 1.556$, $p = 0.459$), *myca* ($F(2, 24) = 0.489$, $p = 0.619$), *rrm1* ($F(2, 24) = 0.853$, $p = 0.439$), *tp53* ($F(2, 24) = 1.911$, $p = 0.170$), or *tyms* ($F(2, 24) = 0.664$, $p = 0.524$) (Figure 22). In terms of the effect of duration (3dpi/5dpi) on gene expressions after MO treatments, there was a significant main effect in *ccna2* expression

(U = 58, z = -2.261, p = 0.024), and a marginally significant effect in *ccne1* expression (U = 66, z = -1.929, p = 0.054) where 3dpi groups ranked higher for expression levels than 5dpi groups for both genes. There was statistically no difference in duration for *cdk1* (U = 106, z = -0.270, p = 0.787), *myca* (F(1, 24) = 0.092, p = 0.764), *rrm1* (F(1, 24) = 0.980, p = 0.332), *tp53* (F(1, 24) = 0.899, p = 0.352), *tyms* (F(1, 24) = 1.874, p = 0.184).

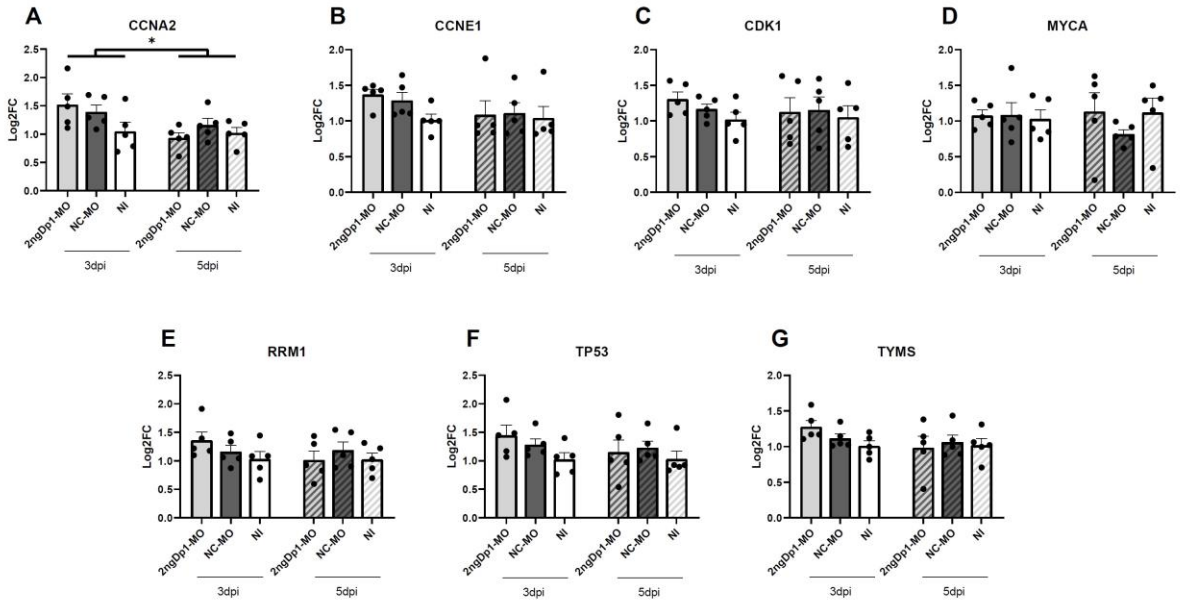

Figure 22 Tfdp1 downstream gene expression levels following 2ng MO injections on embryos. No significant effect of treatment was observed. In terms of duration after injections, there was a significant main effect on *ccna2* expression levels (*p* = 0.024). (N=5 for each group, N=30 in total).

For 4ng injections, there were no significant effect of MO treatments on Tfdp1 downstream gene expressions of *ccna2* (F(2, 24) = 0.737, p = 0.489), *ccne1* (H(2) = 1.727, p = 0.422), *cdk1* (F(2, 24) = 1.043, p = 0.368), *myca* (H(2) = 3.474, p = 0.176), *rrm1* (F(2, 24) = 0.366, p = 0.698), *tp53* (F(2, 24) = 0.274, p = 0.763), or *tyms* (H(2) = 3.672, p = 0.159) (Figure 23). In terms of the effect of duration on gene expressions after MO treatments, there was a significant main effect in *ccne1* (U = 27, z = -3.547, p < 0.001),

cdk1 (F(1, 24) = 5.604, p = 0.026), *rrm1* (F(1, 24) = 5.471, p = 0.028), and *tp53* (F(1, 24) = 5.251, p = 0.031) expressions; and a marginally significant effect in *ccna2* expression (F(1, 24) = 3.576, p = 0.071) where 3dpi groups showed higher expression levels than 5dpi groups for all. There was statistically no difference in duration for *myca* (U = 78, z = -1.431, p = 0.152), or *tyms* (U = 33, z = -3.298, p = 0.001).

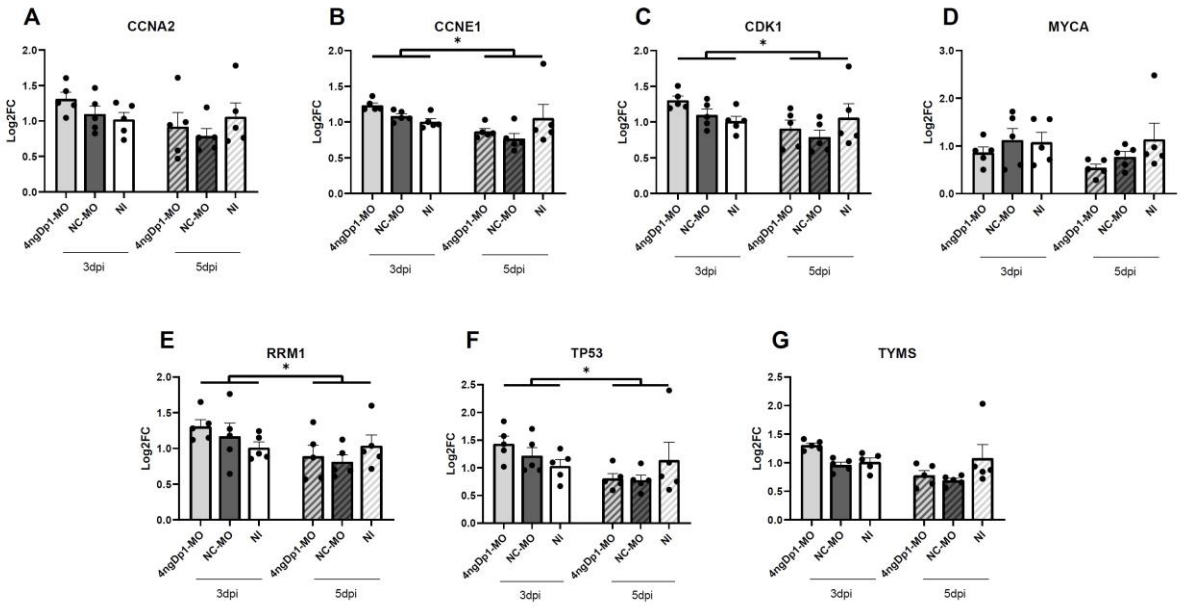

Figure 23 Tfdp1 downstream gene expression levels following 4ng MO injections on embryos. No significant effect of treatment was observed. In terms of duration after injections, there was a significant main effect of duration on *ccne1* (p < 0.001), *cdk1* (p = 0.026), *rrm1* (p=0.028), and *tp53* (p = 0.031) expression levels. (N=5 for each group, N=30 in total).

For 8ng injections on a different set of embryos than used for western blot experiments, there were a significant main effect of MO treatments on Tfdp1 downstream gene expressions of *myca* (H(2) = 7.076, p = 0.029), and *tp53* (F(2, 23) = 5.601, p = 0.01) (Figure 24). For the effect seen in *myca* expressions, performing Mann Whitney U post hoc tests following this finding (where the significance level becomes 0.0167 with Bonferroni

correction), the expression level differences were found significant between 8ng *tfdp1*-MO and 8ng NC-MO injected groups (p = 0.016), marginally significant between 8ng *tfdp1*-MO and NI groups (p = 0.041), and not significant between 8ng NC-MO and NI groups (p = 0.568). For the effect detected in *tp53* levels, the post hoc tests revealed a significant difference between 8ng *tfdp1*-MO and NI groups (p = 0.011), and a marginally significant effect between 8ng *tfdp1*-MO and 8ng NC-MO groups (p = 0.098). There were no statistical difference regarding the treatments in expression levels of *ccna2* (F(2, 23) = 2.164, p = 0.138), *ccne1* (H(2) = 3.379, p = 0.185), *cdk1* (H(2) = 3.865, p = 0.145), *rrm1* (F(2, 23) = 1.452, p = 0.255), or *tyms* (F(2, 23) = 2.287, p = 0.295). In terms of the effect of duration on gene expressions after MO treatments, there was no significant difference between 3dpi and 5dpi groups for *ccna2* (F(1, 23) = 1.492, p = 0.234), *ccne1* (U = 72, z = -1.440, p = 0.150), *cdk1* (U = 86, z = -0.829, p = 0.407), *myca* (U = 96, z = -0.393, p = 0.694), *rrm1* (F(1, 23) = 0.669, p = 0.422), *tp53* (F(1, 23) = 0.301, p = 0.588), *tyms* (F(1, 23) = 0.938, p = 0.177).

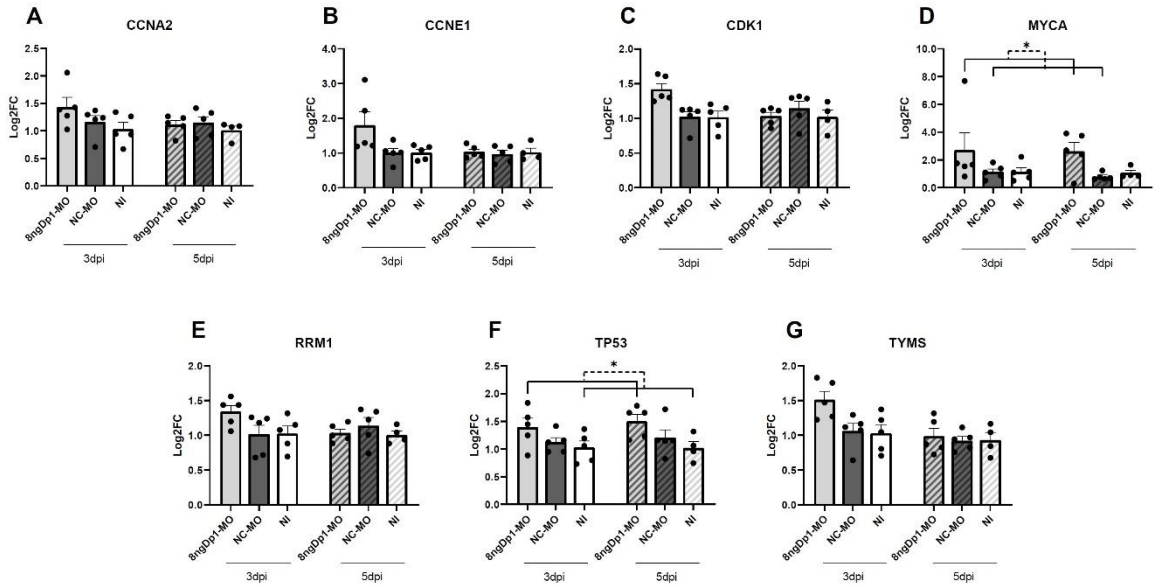

Figure 24 Tfdp1 downstream gene expression levels following 8ng MO injections on a different set of embryos than used for western blot experiments. A significant main effect

of treatment was observed for *myca* expression levels (p=0.029) between *tfdp1*-MO and NC-MO injected groups (p = 0.016) and for *tp53* expression levels (p=0.01) between *tfdp1*-MO and NI groups (0.011). In terms of duration after injections, there was no significant difference between 3dpi and 5dpi groups on the Tfdp1 downstream gene expression levels. (N=5 for each group, N=30 in total).

4.3.4. Transient Knockdown of Tfdp1 on Zebrafish Adults

The Vivo injections for adult fish heads were performed using an automated microinjector system utilizing a predefined method called Cerebroventricular Microinjection (CVMI) (Kizil, 2011; Kizil, 2013). The method allows delivery of an injection solution above the optic tectum region of the fish brain to the telencephalon region, which encompasses a structure called lateral pallium that is regarded as the fish equivalent of the hippocampus. The Vivo delivery procedure comprised a fixed and approximate dose of 500uM MO.

4.3.4.1. Adult brain Tfdp1 protein levels did not significantly differ between time points following Dp1-Vivo-MO injections

A plot was constructed using western blot analyses of adult injected fish to assess the efficiency of the *tfdp1* Vivo MO on Tfdp1 protein levels. Representative western blot bands are shown in Figure 25A, and the plot is in Figure 25B. The plot shows Tfdp1 brain protein levels regarding NC fish and *tfdp1*-VivoMO-injected fish at time points of 1,5-hour post-injection (hpi), 4hpi, 12hpi, 1-day post injection (dpi), 2dpi, 3dpi, 4dpi. The plot shows that *tfdp1* Vivo MO injections to adult zebrafish brain cerebroventricular regions (N=16) successfully lower Tfdp1 protein levels numerically compared to NC fish. However, there was no statistical difference between time points ($H(7) = 8.162$, $p = 0.319$).

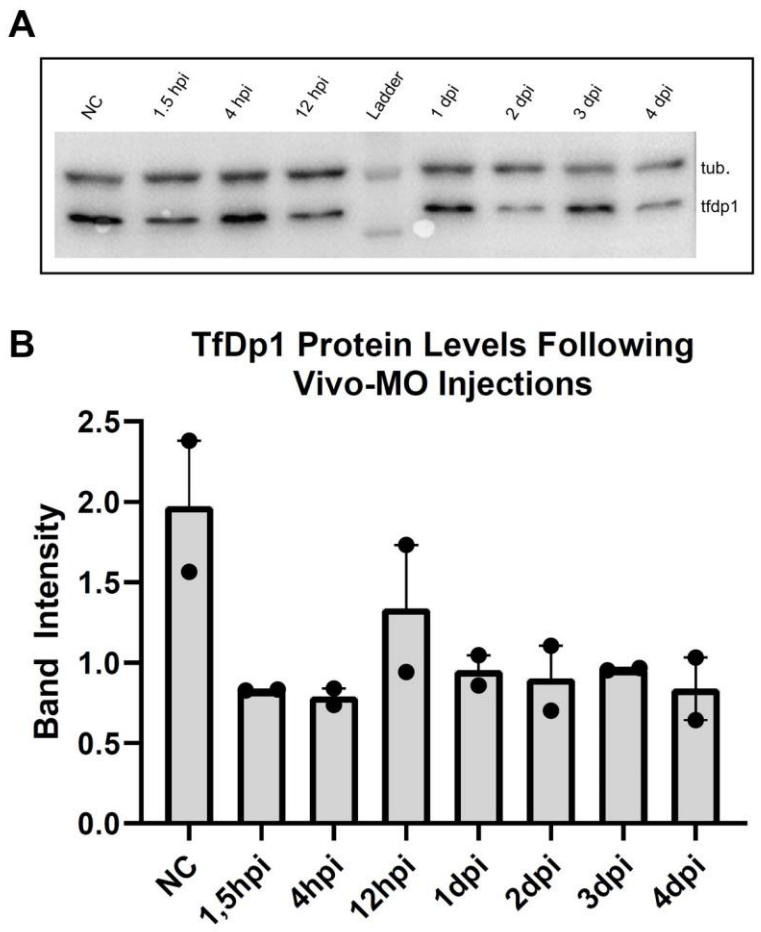

Figure 25 A) A representative western blot is shown for Dp1 protein levels after Dp1 Vivo-MO injection. Blotting was performed against Tfdp1 and tubulin antibodies. NC stands for the negative control group; heads were incised and anesthesia was performed for treatment groups, but no injection solution was given. **B)** Dp1 Vivo-MO Time curve. No statistical difference was found on Tfdp1 protein levels between NC or any time point after Dp1-Vivo-MO injection. N=16 (N=2 for each group).

4.3.4.2. *tfdp1*-Vivo-MO injections did not significantly alter Tfdp1 downstream gene expressions in the adult zebrafish brains

To be able to see the downstream effects of *tfdp1* Vivo MO injection on adult animal brains, we performed RT-PCR experiments to examine alterations in Tfdp1 target gene

expression levels (Figure 26). Results showed no statistical difference among the treatment groups (*tfdp1*-Vivo-MO, NC-vivo-MO, NI) on expression levels of *ccna2* (H(2) = 5.067, p = 0.079), *ccne1* (F(2, 6) = 1.706, p = 0.259), *cdk1* (H(2) = 3.822, p = 0.148), *myca* (H(2) = 2.400, p = 0.301), *rrm1* (H(2) = 2.489, p = 0.288), or *tyms* (F(2, 6) = 1.295, p = 0.341). *tp53* showed marginally significant effect of treatment (F(2, 6) = 4.692, p = 0.059), however this was between NI and NC-vivo-MO groups as can be seen from Figure 26F.

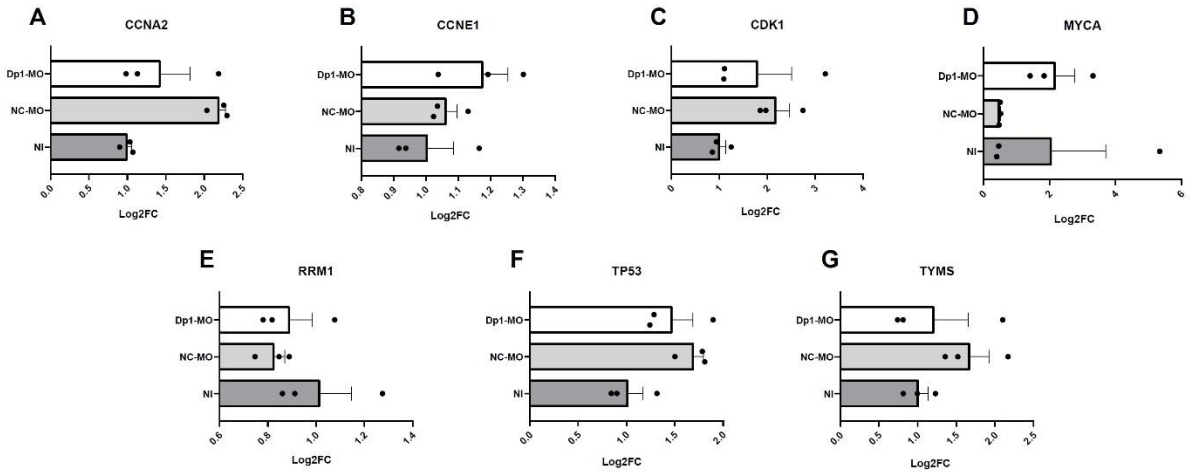

Figure 26 Tfdp1 downstream gene expression levels on adult fish brains following Vivo MO injections. No significant change was detected. *tfdp1*-MO: 500uM Tfdp1 Vivo MO-injected adult fish brains' gene expression levels, NC-Vivo-MO: 500 uM NC-Vivo-MO injected brains, NI: Non Injected brains. N=9.

4. 4. Conclusion

Lastly, in this fourth chapter of the thesis, microarray between AL and CR fed aged animal brains and RT-PCR experiments suggested that cell cycle regulator tfdp1 transcription factor was downregulated with CR. Then to investigate whether tfdp1 was changing with age, young and old zebrafish brain Tfdp1 protein levels were compared and found that Tfdp1 protein was significantly upregulated with advancing age. This outcome increased our interest to investigate Tfdp1 further since it was both significantly downregulated with

CR and clearly upregulated with age. So we further continued trials on mimicking CR-related downregulation behavior of tfdp1 on fish brains by injection of Morpholino oligos (MO) designed to knock down Tfdp1 translation. Adult injections yielded a statistical outcome on neither protein nor mRNA levels of tfdp1 protein and its downstream target genes, respectively. The downstream targets of *the tfdp1* gene were selected as c*cna2, ccne1, cdk1, myca, rrm1, tp53,* and *tyms.* All of them have been implicated with their roles in cell cycle regulation. Trials of knocking down *tfdp1* on embryos did not result in a significant main effect of injection treatments on neither Tfdp1 protein levels nor Tfdp1 downstream target gene expression levels following 2ng or 4ng injection experiments. However, the 8ng MO injection experiments on embryos yielded a significant upregulation in *myca* and *tp53* gene expressions following *tfdp1*-MO injections compared to NC-MO injected and NI groups, respectively.

4.5. Discussion

In the fourth chapter, we started our journey by comparing 4-week CR and AL fed zebrafish brain transcriptome data on microarray. Reviewing significantly altered functional pathways of cell cycle regulation pathway, RNA degredation pathway and mRNA survaillance pathway; we selected 23 genes to further validate on RT-PCR including alternative durations of CR compared to AL (1-week, 2-week, 4-week, 10-week). Among the 23, *transcription factor Dp1* (*Tfdp1*) was selected as the gene of interest to proceed further due to its consistent expression patterns between microarray and RT-PCR experiments. Tfdp1 gene expressions showed downregulation in the brains with CR compared to AL-fed animal brains. We measured the age related effects on Tfdp1 protein levels and found that this time its translation was significantly increased with age on fish brains as in the case of CR application. This inverse pattern intrigued our attention since

the CR could be reversing the age related increase at the Tfdp1 protein levels. Since it is mainly involved in stimulating cell cycle progression, our hypothesis was that CR mediated protection mechanisms could be related to cell cycle regulations centering this transcription factor.

Next, we tried to mimick the effect of CR on cell cycle regulations by manipulating Tfdp1 levels on zebrafish embryo and adults. We used specifically designed translational blocking morpholino oligos (MO) targeting tfdp1 mRNA to transiently knockdown tfdp1. Two kinds of MO were designed and used in this chapter. Dp1-MO (traditional type) was utilized for the embryo injections, and Dp1-Vivo-MO was used to inject adult fish via CVMI method. For the knockdown efficiencies, western blot experiments were conducted both after embryo and adult injections, and no significant changes were observed in Tfdp1 protein levels for both cases. We still checked the downstream gene expressions of *tfdp1* targets for its role of cell cycle promotion from G1/Sphase transition. The target genes were obtained from literature search as well as using STRING database (Functional Protein Association Network) and TRRUST tool (Transcriptional Regulatory Relationships Unraveled by Sentence-based Text mining); that are *ccna2*, *ccne1*, *cdk1*, *myca*, *rrm1*, *tp53*, and *tyms*. These target genes were also cell cycle regulators, and their expected changes with *tfdp1* knockdown were downregulation for *ccna2*, *ccne1*, *cdk1*, *rrm1*, and *tyms* for their roles in promoting cell cycle; whereas upregulation for *myca* and *tp53*. In the transient *tfdp1* knockdown trials via Vivo-MO injections to adult fish, there were no statistically significant effect of injections on neither protein nor gene expression levels.

The knockdown trials on embryos were conducted in 3 different doses (2ng, 4ng, 8ng) and measured after 2 different durations (3dpi, 5dpi). Significant increases in *myca* and *tp53* expression levels were observed following 8ng Dp1-MO injection compared to 8ng NC-

MO injected and NI groups, respectively, as in the expected direction. However, these significant myca and tp53 expression changes following 8ng Dp1-MO injection compared to 8ng NC-MO and NI groups, respectively, seem to be contradicting with the results obtained for the embryo Tfdp1 protein levels following 8ng Dp1-MO injections, where no statistical difference was observed between injection groups. A reason for that might be possible differences at the amounts of the protein or mRNA levels. Thus, this might actually be a question of whether the levels of a protein and its mRNA change similarly with respect to a manipulation. Probably further experiments are needed to be conducted increasing the sample sizes for both experimental schemes to find the right answer to the question.

Though, we could not create a true transient knockdown of *tfdp1* to mimick the effect of CR on cell cycle regulations via *tfdp1* MO injections, the gene still needs attention by further investigations around the aging and nutrient manipulation pathways. This is since as mentioned earlier, it shows significant upregulation with aging and downregulation with CR leading us to a vital question of whether CR mediated extended life span could be as a result of cellular adaptations in the brain. Such adaptations could be preservatively slowing down the cellular metabolism, providing a nice slowing control on cell cycle progression under the control of increased tumor suppressors and decreased Tfdp1 like cell cycle inducers, that are cumulatively leading to a senescence-like quiescent state, however providing a healthy and longer lifespan. By this way, brain cells might be adapting to the new nutrient availability conditions to increase their survival chance. Those adaptations could be by decreasing cell proliferation, promoting cell cycle arrest, and increasing the maintenance of the existing cells. and at the end protecting against tumor development. By means of such regulations, cells would prevent energy waste on excess proliferation, and decrease the risk of mutation with each cell divisions. Our hypothesis on CR induced

lowered proliferation and inflammation along with increased neuronal protection hypothesis was supported partially by the Chapter 2 feeding group experiments, mostly for the young group animals' data, with the following outcomes. There we found that CR was associated with significantly lowered expression levels of *sox2*, marginally significantly decreased expression levels of tfdp1 and alcamb, lastly numerically ($p > 0.05$) increased levels of *myca* and *tp53* expression levels compared to overfeeding (OF) and Ad-libitum (AL) groups. Sox2 is widely regarded as an NSC marker, and known as a NSC maintenance factor promoting the cells self-renewal or pluripotency, than being a proliferation marker like Pcna (Mercurio et al. 2019; Sato et al. 2019). With no effect of our dietary application on Pcna, here suggested in the previous chapter that *sox2* downregulation with CR compared to OF, may not imply a direct decrease in overall proliferation but may infer to a decrease in stem cell proliferation, promoting the maintenance of the stem cell reserve. ALCAM has previously been associated with reduced neuroinflammation and reduced migration, adhesion and engraftment of stem cells (Erbaba, 2020; Cayrol, 2008; Kim, 2017). *myca* is a proto-oncogene known to stimulate proliferation, however was reported previously that it has dual functions depending on a phosphorilation switch deciding its path to proliferation or differentiation (Uribesalgo et al. 2012). Tp53 is a very well known tumor suppressor and an inducer of the cell cycle arrest. The expression levels of *myca* and *tp53* were both increased with age in the previous chapter. Both of the genes were previously stated to be inversely correlated with *tfdp1* expression (Chen, 2002; O'Connor, 1995; TRRUST database results), therefore with *tfdp1* knockdown their expressions were expected to be increased as in the case of the 8ng *tfdp1*-MO injected embryo results given in the results section (Figure 24). Around the *tfdp1-myca-tp53* regulations, here one might make a connection between the stories as in the following lines. If the following statements are true; *myca* and *tp53* expression levels are

actually higher in aged brains (referring to the Chapter 2 results, $p < 0.05$), TfDp1 is actually inversely correlated with *myca* and *tp53* (Chen, 2002; O'Connor, 1995; TRRUST database results), *myca* and *tp53* expression expressions were increased following *tfdp1*-MO injections with resepect to control groups (referring to the results of this chapter, $p < 0.05$); then, there might be an exciting link between the three concepts of *tfdp1-myca-tp53* triangle, aging, and dietary manipulations.

A concern in this chapter that might worth mentioning is the design of the microarray experiment, for which the AL-fed and CR-fed group brain RNA samples were profiled in different times. However the treatment of the animals and tissues, as well as the RNA extraction procedures were conducted in the same laboratory and with the same protocols. Although we accept that this is not an ideal design, we followed this way since the AL samples that were treated similarly and same time with CR samples could not pass the quality check due to experimental difficulties. Acknowledging that, we tried to validate the results with RT-PCR experiment afterwards.

To sum up, as gain of function Tfdp1 mutation was previously and numerously reported to be increased in cell proliferation, migration, and invasion of cancer cells (Chen, 2014), as the opposite case, here we report a decreased Tfdp1 via CR could be one of the mechanisms that CR shows its effects on lifespan. We believe that our study suggests new and hopefully efficient drug targets designed to be targeting cell cycle mechanism as in the state of CR, in purpose of treating neurodegenerative diseases and possibly slowing down the detrimental effects of aging besides providing a healthy and extended lifespan. It is hoped that our results would help create new routes for studies on aging, nutrition and neurodegenerative diseases. We believe that before trying to understand the diseased states

of mind, it might be better and crucial first to first understand the molecular operations and connections taking place on the healthy aging brains.

CHAPTER 5

OVERALL DISCUSSION

In this thesis, the first chapter provided an introduction to the concepts studied. The second chapter investigated the age-related gene expression level differences in the brain, leading us to reach a group of cell adhesion molecules, the most promising ones being the *alcamb* and *cx47*. Among the two, we found alcamb more intriguing to follow further since its reduction has been associated with reduced neuroinflammation. According to Cayrol et al. (2008), blocking ALCAM reduces neuroinflammation, and increased *ALCAM* expression levels appear to be associated with cancerous and inflammatory phenotypes in some cell types by promoting leukocyte recruitment into the central nervous system (Soto, 2014). Therefore, in the next chapter, we wanted to see *alcamb* expression behavior following nutrient interventions and the behavior of several other genes of interest to understand the nutrient-mediated anti-aging strategies better. Then, in the third chapter of the thesis, in order to be able to intervene/overcome these aging-related transcriptomic alterations, or at least slow down the aging process and to counteract the degenerative changes in the aging brain, we applied non-genetic nutrient interventions of two, as CR and overfeeding (OF),

on aging zebrafish. Along with other markers for different concepts to better understand alterations in the aging brain following nutrient interventions, we checked *alcamb* expression levels for diet and age. Results showed that *alcamb* and *tfdp1* followed a marginally significant reduction with CR diet, a significant reduction in *sox2* expression levels, and lastly numerically ($p > 0.05$) increased levels of *myca*, *tp53* expression levels with CR treatment compared to overfeeding (OF) and Ad-libitum (AL) groups. *sox2* is widely regarded as an NSC marker and known as an NSC maintenance factor promoting the cells' self-renewal or pluripotency than being a proliferation marker like Pcna (Mercurio et al. 2019; Sato et al. 2019). With no effect of our dietary application on Pcna, here suggested in the previous chapter that *sox2* downregulation with CR compared to OF may not imply a direct decrease in overall proliferation but may reflect a decrease in stem cell proliferation, promoting the maintenance of the stem cell reserve. ALCAM was previously associated with reduced neuroinflammation, migration, adhesion, and engraftment of stem cells (Erbaba et al., 2020b; Cayrol et al., 2008; Kim et al., 2017).

Therefore, CR treatment may be possibly lowering inflammation (*alcamb*), reducing stem cell proliferation (*sox2*, *tfdp1*), and strengthening cell cycle control against DNA damage (*tp53*), although the effects here observed are weak and require further data collection and analysis. Additionally, multivariate analysis on the protein and gene expression data led us to infer some conceptual results regarding the two different nutrient regimens. The regulation mechanisms mediated via CR might likely be showing their effects on lifespan by decreasing cell proliferation, inducing neural stem cell quiescence, protecting the stem cell reserve, decreasing overall inflammation, and protecting the brain by decreasing cancer incidence. The OF diet, in contrast, could be increasing the proliferation and inflammation status of the cells, which supports the hypothesis of Cavallucci et al. (2016). In fact, CR could be exerting an outcome resembling senescence in the case of cell

proliferation, thereby inhibiting cell cycle progression and providing a protective barrier against cancerous development. Therefore, decreasing proliferation can be viewed preferably as an adaptive response rather than a detrimental one (Erbaba et al. 2020a). Unlike CR, OF might consume the stem cell reserve by forcing it to proliferation, thereby leading to excessive production of metabolic by-products and accumulation of DNA damage, which are the drivers of inflammation. Such adaptations could help preserving the soma by slowing down the cellular metabolism, providing an excellent slowing control on cell cycle progression under the control of increased tumor suppressors and decreased Tfdp1 like cell cycle inducers that are cumulatively leading to a senescence-like quiescent state, however providing a healthy and longer lifespan. In this way, brain cells might be adapting to the new nutrient availability conditions to increase their survival chance.

Myca is a proto-oncogene known to stimulate proliferation. However, it was reported previously that it has dual functions depending on a phosphorylation switch deciding its path to proliferation or differentiation (Uribesalgo et al., 2012). Tp53 is a well-known tumor suppressor and an inducer of cell cycle arrest. The expression levels of *myca* and *tp53* both increased with age in the previous chapter. Both of the genes were previously stated to be inversely correlated with *tfdp1* expression (Chen, 2002; O'Connor, 1995; TRRUST database results), therefore with *tfdp1* knockdown in the fourth chapter, their expressions were expected to be increased as in the case of the 8ng *tfdp1*-MO-injected embryo results given in the results section. Around the *tfdp1-myca-tp53* regulations, one might connect the stories as in the following lines. If the following statements are factual; *myca* and *tp53* expression levels are actually higher in aged brains (referring to the Chapter 2 results, $p < 0.05$), *tfdp1* is actually inversely correlated with *myca* and *tp53* (Chen, 2002; O'Connor, 1995; TRRUST database results), *myca* and *tp53* expression expressions were increased following *tfdp1*-MO injections compared to the control groups (referring to the

results of this chapter, $p < 0.05$); then, there might indeed be an exciting link between the three concepts of the *tfdp1-myca-tp53* axis, aging, and dietary manipulations.

As a gain of function *tfdp1* mutation was previously and numerously reported to be increased in cell proliferation, migration, and invasion of cancer cells (Chen, 2014); increased *ALCAM* expression levels appear to be associated with cancerous and inflammatory phenotypes; as *TP53* knockouts and upregulations in *SOX2* expression were associated with cancer incidences; and as CR therapies can reverse these mechanisms, we might be tracking the right way to slow down brain aging process. These could be related to the protective mechanisms that CR shows its effects on lifespan. We believe that our study suggests new and, hopefully, efficient drug targets designed to target cell cycle mechanisms as in the state of CR to treat neurodegenerative diseases and possibly slow down the detrimental effects of aging besides providing a healthy and extended lifespan. It is hoped that our results would help create new routes for studies on aging, nutrition, and neurodegenerative diseases. We believe that, before trying to understand the diseased states of mind, it might be better and crucial first to understand the molecular operations and connections taking place on healthy aging brains.

6. FUTURE DIRECTIONS

Next experiments following the studies mentioned in this thesis, could be 1) testing a longer duration of or lifelong OF diet on the fish brains in order to create a BMI difference between the OF and AL fed fish, 2) if/when available commercially, comparing human Alzheimers brain sample transcriptome to healthy aged human brain transcriptome and at the same time to zebrafish Alzheimers model brain transcriptome, 3) To investigate different paralogs of Tfdp1 (*tfdp1a*/*tfpd1b*) testing their responses to nutrient interventions and aging separately, and to be able to see whether there occurs any compensation mechanisms with respect to these concepts, 4) to examine Tfdp1 on different zebrafish aging models, such as *mtor* and *tsc2* mutants, lastly 5) instead of MO, using other and more reliable methods to manipulate *tfdp1* gene expression in the zebrafish brains, such as creating conditional knockout and overexpression models.

During the above-mentioned Ph.D. work in chapters, I was also involved in mutant fish characterization experiments for another project. Creating mutants is another way to determine the causal consequences of the genes that are studied. Two nutrient pathway-related fish lines are maintained in our fish facility: *mtor* and *tsc2* mutant lines. Our predictions on these mutants are that the *mtor* mutant line is the decelerated aging model with a repressed Mtor function, and the *tsc2* mutant line is the accelerated aging model with an overactive Mtor. The experiments that I was involved in were related to the

characterization of the *tsc2* mutant fish model. Our lab obtained the mutant *tsc2*$^{vu242/+}$ fish line from the University of Cambridge, UK, for a TUBİTAK project (214S236). For the *tsc2*^{vu242} nonsense mutation, the allele encodes a truncated Tuberin protein. The mutation is predicted to remove the GTPase-activating protein (GAP) domain leaving intact the Hamartin-binding domain of TSC2 protein. GAP domain is the domain responsible for inhibition of G-protein Rheb. Therefore, by logic, removing the GAP domain in mutant animals would cause Rheb activation and mTORC1 activation in the end.

tsc2$^{vu242/vu242}$ homozygous mutant fish were found to be lethal at early larval stages of development (by 11dpf), manifesting increased cell size (approximately 1.5-times larger neuronal cell bodies in the brain), and morphological organ defects started to occur between stages of 5dpf and 7dpf which are deflated swim bladders and enlarged livers (Figure 3). Immunochemical staining of trunk sections using an antibody against phospho-S6, a downstream effector of mTORC1, shows that 24h rapamycin treatment of homozygous 3.5 dpf embryos seems to fix/diminish the increased levels of *tsc2*^{vu242} mutation related mTORC1 activation phenotype and increased hepatocyte cell size in a dose-dependent manner.

Swim bladders are gas-filled sacs considered as vertebrate lung equivalent of teleost fish. They are contributing to the swimming ability of the fish, helping them to control their buoyancy in water (Winata, 2009). The lethality seen by 11 dpf of the mutant larval stage is thought by low nutrient intake due to swimming inabilities with defective swim bladder (Kim, 2011). A swim bladder morphogenesis study mentions about three stages of development that are budding (2dpf), growth (3dpf), and inflation phases (5dpf for posterior sac– 21 dpf for anterior sac inflation) (Winata, 2009). Thus, in summary, in our lab, *tsc2*$^{vu242/+}$ mutants are predicted to be a possible accelerated aging model, and their

characterizations were essential to proceed with further experiments with them. Therefore, below, I will explain my trials regarding the characterization process of these *tsc2*$^{vu242/+}$ embryos.

6.1. Characterization trials according to swim bladder morphology

Homozygous *tsc2* mutants show embryonic lethality at the earlier stages of development (11dpf) due to underdeveloped/deflated swim bladder. Fish fries typically start swimming and feeding approximately on day five after fertilization. A partial or non-developed swim bladder cause inability to swim, therefore, the inability to feed. For the characterization trials, we randomly selected a male and a female fish for each breeding tank of *tsc2* mutants and wild-type controls (8 breeding tanks can be organized on the same day) and collected embryos on the following day. Examining the embryos on each day, we noticed that on the 5th to 7th days after fertilization, most of the mutant derived embryos and wild-type controls had visually detectable-sized swim bladders. However, some of the embryos of tsc2 mutants (around 1:4) were lack of them (Figure 27). This was consistent with the Kim et al. article (Kim et al., 2011). Isolating these embryos with deflated swim bladders into a new plate, we tracked their development and compared their viability to the mutant fish embryos with visible swim bladders and wild-type embryos. As expected from the Kim et al. (2011) article findings, we again observed lethality around 11dpf.

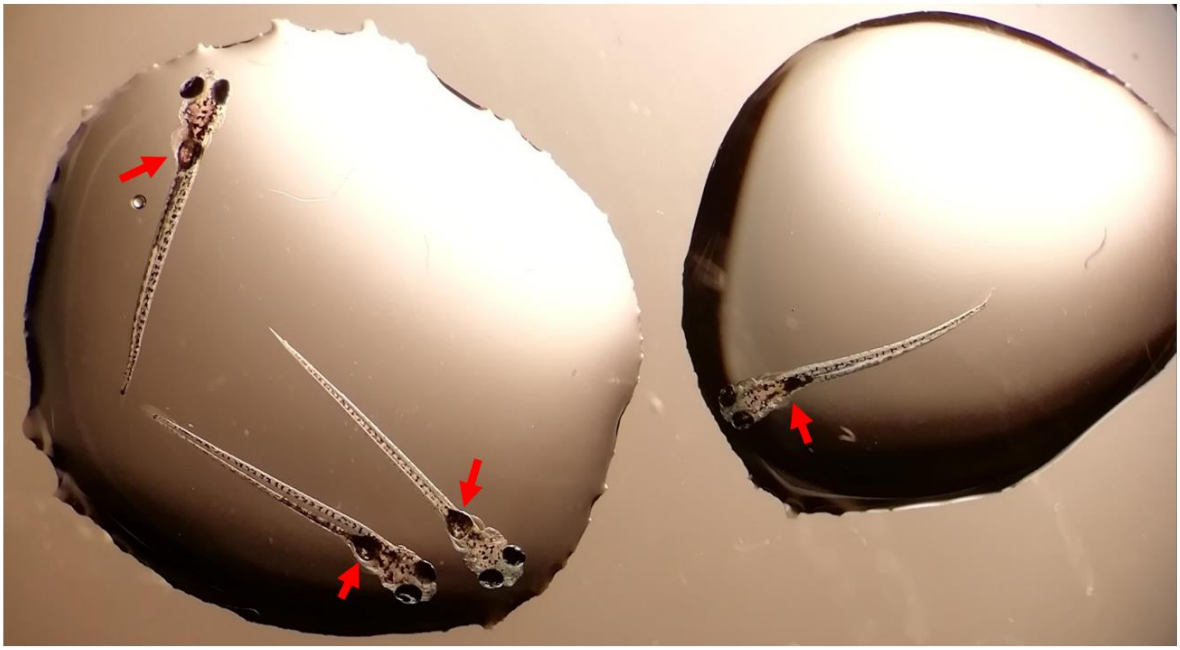

Figure 27 Zebrafish embryos 5dpf are shown. The left three embryos are with normal swim bladders (thought to be heterozygous or wild type), while the left is with a deflated swim bladder (thought to be homozygous). Red arrows show regions where swim bladders are found. The image was taken in Bilkent University Zebrafish Facility.

6.2. Characterization trials according to the absence of HpyCh4IV restriction enzyme recognition site

Consulting to Nicola Goodwin and Antonio Pagan from the Cambridge University, whose aquatics facility we obtained the embryos of *tsc2* mutants from, for the genetic screening of the mutants HpyCh4IV restriction enzyme digestion was stated to be preferred in their lab to confirm the absence of restriction enzyme recognition site in mutant fish. Thus for this purpose, we next ordered the restriction enzyme. Upon arrival, we planned to confirm the results and breed the adult mutants for the F2 generation.

The *tsc2* mutant fish genotyping method was described briefly in Kim et al. (2011). The mutation introduces a C3087 to A transversion in the sequence on which a restriction

enzyme (RE) called HpyCh4IV has a recognition site. Thus, since the homozygous mutant fish are expected to have a HpyCh4IV restriction enzyme (RE) cut site that is not recognizable by the enzyme due to mutation, they are expected to produce unsuccessful RE cutting, unlike the wild type (WT) fish. WTs are expected to yield efficient RE cut results.

The un-cut PCR product samples are expected to yield 151bp products. WT RE-cut samples are expected to give 120 and 30bp bands, while homozygous mutant RE-cut samples are expected to give un-cut products at 151 bp. The heterozygous case will probably give all three bands but very faint in all.

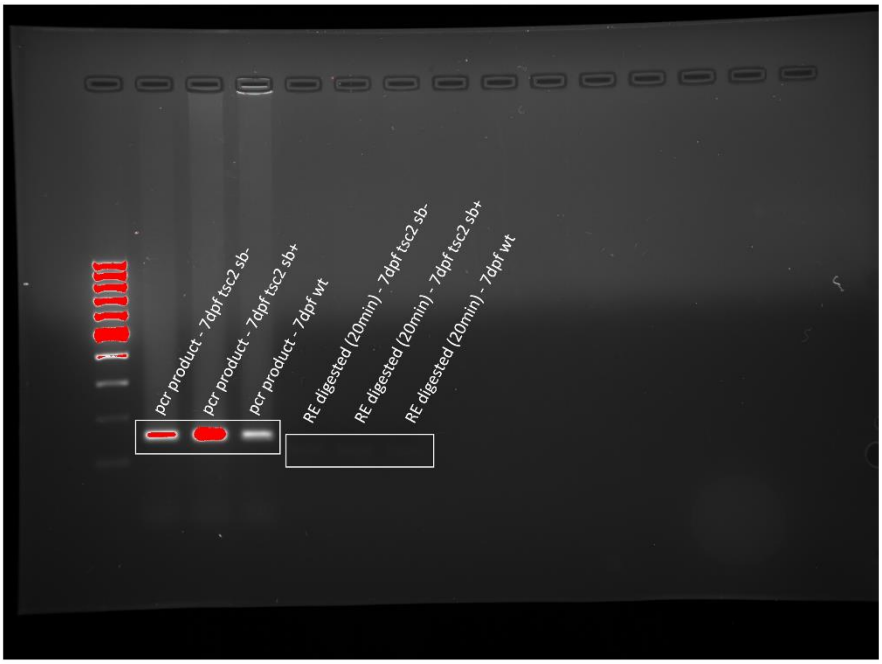

Figure 28 Agarose gel image after PCR and RE digestion with pooled samples (10-30 embryos per sample) first trial. All samples were cut. PCR reaction was set using 250ng DNA. RE digestion was performed using 1ug PCR product for 20min on 37°C. 2% agarose, 25ul PCR product, 48ul RE digested sample used.

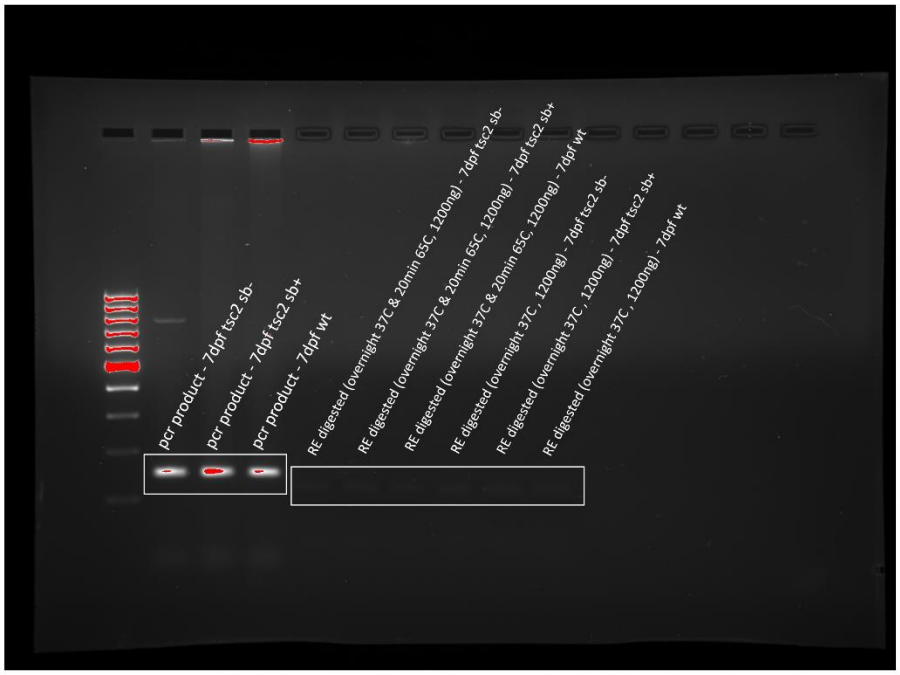

Figure 29 Agarose gel image after PCR and RE digestion with pooled samples (10-30 embryos per sample) second trial. All samples were cut. PCR reaction was set using 250ng DNA. RE digestion was performed using a 1,2ug PCR product at 37°C overnight. 2% agarose, 10ul PCR product, and 45ul RE digested samples used

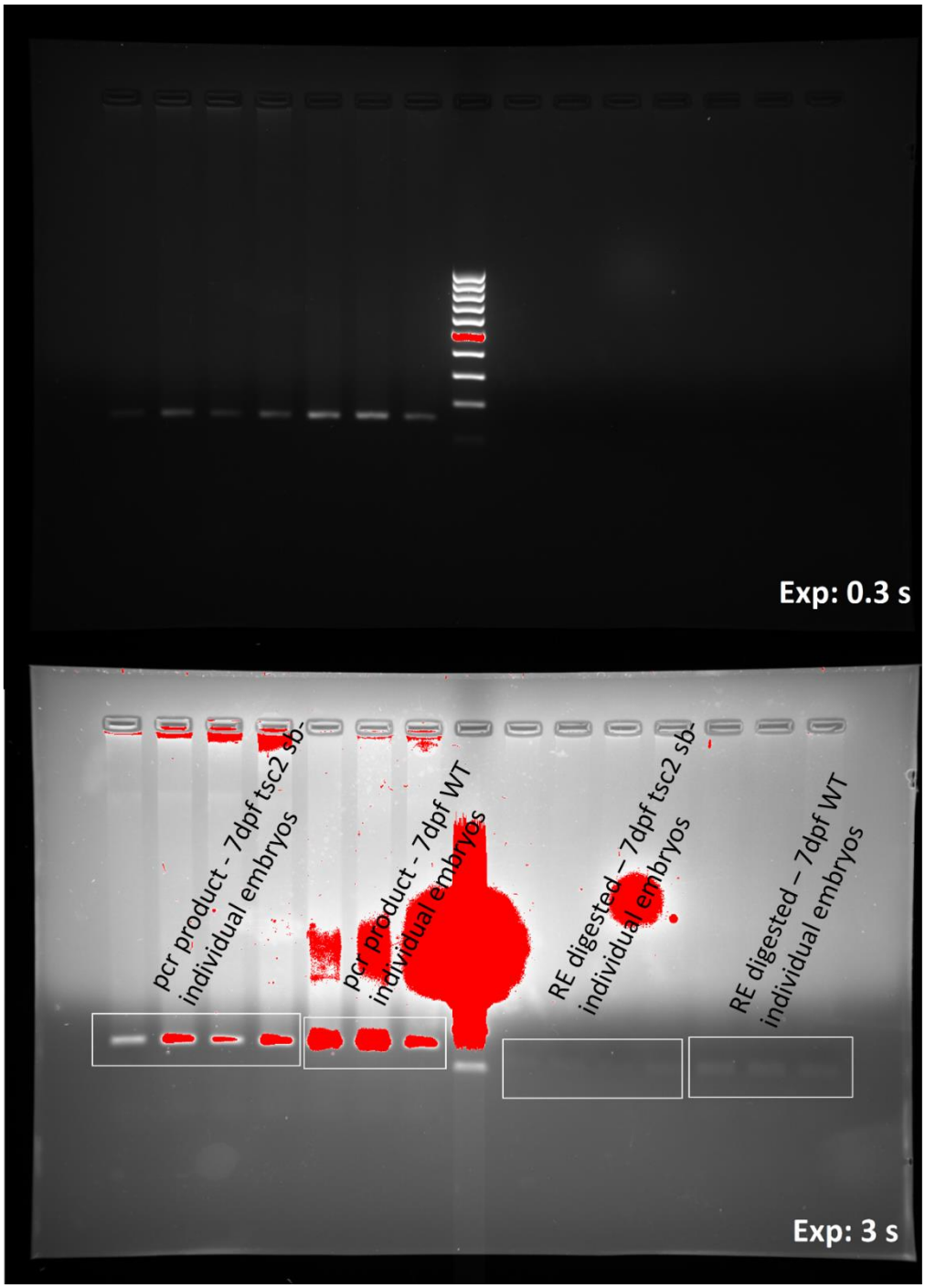

Figure 30 Agarose gel image after PCR and RE digestion with individual samples, first trial. All WT samples were cut; mutant samples seem also cut but with more faint bands, providing a probability of being heterozygous embryos than WT. PCR reaction was set using 250ng DNA. RE digestion was performed using 3ug PCR product for 30min on 37°C. 2% agarose, 40ul sample used

Initial trials showed cut fragment bands after RE digestions though very low yield. Agarose gel images are shown in Figures 28-30, which theoretically and unexpectedly indicate no homozygous detection. RE digestion-based screening protocols were then continued afterward with the trials of different troubleshooting precautions by Beyza Özen, one of the MSc students in our lab. Once settled, these *mtor* and *tsc2* mutant lines are prospective on studying accelerating and decelerating brain aging models. Future experiments are planned to be performed and compared with the CR and OF therapy outcomes, respectively.

7. BIBLIOGRAPHY

Abrams, C.K., 2019. Diseases of connexins expressed in myelinating glia. Neurosci. Lett. 695, 91e99.

Adusumalli, S., Ngian, Z.K., Lin, W.Q., Benoukraf, T., Ong, C.T., 2019. Increased intron retention is a post-transcriptional signature associated with progressive aging and Alzheimer's disease. Aging Cell 18, e12928.

Al-Regaiey, K. A. (2016). The effects of calorie restriction on aging: a brief review. Eur Rev Med Pharmacol Sci, 20(11), 2468-2473.

Al-Yahyaee, S.A., Al-Kindi, M., Jonghe, P.D., Al-Asmi, A., Al-Futaisi, A., Vriendt, E.D., Deconinck, T., Chand, P., 2013. Pelizaeus-Merzbacher-like disease in a family with variable phenotype and a novel splicing GJC2 mutation. J. Child Neurol. 28, 1467e1473.

Apple, D. M., Solano-Fonseca, R., & Kokovay, E. (2017). Neurogenesis in the aging brain. Biochemical pharmacology, 141, 77-85.

Arslan-Ergul, A., & Adams, M. M. (2014). Gene expression changes in aging zebrafish (*Danio rerio*) brains are sexually dimorphic. *BMC neuroscience*, *15*(1), 29.

Arslan-Ergul, A., Erbaba, B., Karoglu, E. T., Halim, D. O., & Adams, M. M. (2016). Short-term dietary restriction in old zebrafish changes cell senescence mechanisms. Neuroscience, 334, 64-75.

Arslan-Ergul, A., Ozdemir, A. T., & Adams, M. M. (2013). Aging, neurogenesis, and caloric restriction in different model organisms. Aging and disease, 4(4), 221.

Ashburner, M., Ball, C.A., Blake, J.A., Botstein, D., Butler, H., Cherry, J.M., Davis, A.P., Dolinski, K., Dwight, S.S., Eppig, J.T., Harris, M.A., Hill, D.P., Issel-Tarver, L., Kasarskis, A., Lewis, S., Matese, J.C., Richardson, J.E., Ringwald, M., Rubin, G.M., Sherlock, G., 2000. Gene ontology: tool for the unification of biology. The Gene Ontology Consortium. Nat. Genet. 25, 25e29.

Bae, S.H., Kim, H.W., Shin, S., Kim, J., Jeong, Y.H., Moon, J., 2018. Decipher reliable biomarkers of brain aging by integrating literature-based evidence with interactome data. Exp. Mol. Med. 50, 28.

Bao, X., Liu, G., Jiang, Y., Jiang, Q., Liao, M., Feng, R., Zhang, L., Ma, G., Zhang, S., Chen, Z., Zhao, B., Wang, R., Li, K., Liu, G., 2015. Cell adhesion molecule pathway genes are regulated by cis-regulatory SNPs and show significantly altered expression in Alzheimer's disease brains. Neurobiol. Aging 36, 2904.e1e2904.e7.

Barrientos, R. M., Kitt, M. M., Watkins, L. R., & Maier, S. F. (2015). Neuroinflammation in the normal aging hippocampus. Neuroscience, 309, 84-99.

Bartsch, U., 1996. Myelination and axonal regeneration in the central nervous system of mice deficient in the myelin-associated glycoprotein. J. Neurocytol. 25, 303e313.

Berchtold, N. C., Coleman, P. D., Cribbs, D. H., Rogers, J., Gillen, D. L., & Cotman, C. W. (2013). Synaptic genes are extensively downregulated across multiple brain regions in normal human aging and Alzheimer's disease. Neurobiology of aging, 34(6), 1653-1661.

Bergmann, O., Spalding, K. L., & Frisén, J. (2015). Adult neurogenesis in humans. Cold Spring Harbor perspectives in biology, 7(7), a018994.

Bowen, M.A., Bajorath, J., D'Egidio, M., Whitney, G.S., Palmer, D., Kobarg, J., Starling, G.C., Siadak, A.W., Aruffo, A., 1997. Characterization of mouse ALCAM (CD166): the CD6-binding domain is conserved in different homologs and mediates cross-species binding. Eur. J. Immunol. 27, 1469e1478.

Bowen, M.A., Patel, D.D., Li, X., Modrell, B., Malacko, A.R.,Wang,W.C., Marquardt, H., Neubauer, M., Pesando, J.M., Francke, U., Haynes, B.F., Aruffo, A., 1995. Cloning, mapping, and characterization of activated leukocyte-cell adhesion molecule (ALCAM), a CD6 ligand. J. Exp. Med. 181, 2213e2220.

Burgett, M.E., Lathia, J.D., Roth, P., Nowacki, A.S., Galileo, D.S., Pugacheva, E., Huang, P., Vasanji, A., Li, M., Byzova, T., Mikkelsen, T., Bao, S., Rich, J.N., Weller, M., Gladson, C.L., 2016. Direct contact with perivascular tumor cells enhances integrin avb3 signaling and migration of endothelial cells. Oncotarget 7, 43852e43867.

Caracciolo, B., Xu, W., Collins, S., & Fratiglioni, L. (2014). Cognitive decline, dietary factors and gut–brain interactions. Mechanisms of ageing and development, 136, 59-69.

Cavallucci, V., Fidaleo, M., & Pani, G. (2016). Neural stem cells and nutrients: poised between quiescence and exhaustion. Trends in Endocrinology & Metabolism, 27(11), 756-769.

Cayrol, R., Wosik, K., Berard, J.L., Dodelet-Devillers, A., Ifergan, I., Kebir, H.,

Cerletti, M., Jang, Y. C., Finley, L. W., Haigis, M. C., & Wagers, A. J. (2012). Short-term calorie restriction enhances skeletal muscle stem cell function. Cell stem cell, 10(5), 515-519.

Chan, J. A., Olvera, M., Lai, R., Naing, W., Rezk, S. A., & Brynes, R. K. (2002). Immunohistochemical expression of the transcription factor DP-1 and its heterodimeric partner E2F-1 in non-Hodgkin lymphoma. Applied Immunohistochemistry & Molecular Morphology, 10(4), 322-326.

Chandler, H., & Peters, G. (2013). Stressing the cell cycle in senescence and aging. *Current opinion in cell biology*, 25(6), 765-771.

Chen, C. R., Kang, Y., Siegel, P. M., & Massagué, J. (2002). E2F4/5 and p107 as Smad cofactors linking the TGFβ receptor to c-myc repression. Cell, 110(1), 19-32.

Cherif, A., Roelands, B., Meeusen, R., & Chamari, K. (2016). Effects of intermittent fasting, caloric restriction, and Ramadan intermittent fasting on cognitive performance at rest and during exercise in adults. Sports Medicine, 46(1), 35-47.

Chicas, A., Wang, X., Zhang, C., McCurrach, M., Zhao, Z., Mert, O., ... & Lowe, S. W. (2010). Dissecting the unique role of the retinoblastoma tumor suppressor during cellular senescence. Cancer cell, 17(4), 376-387.

Copani, A., Caraci, F., Hoozemans, J. J., Calafiore, M., Sortino, M. A., & Nicoletti, F. (2007). The nature of the cell cycle in neurons: focus on a “non-canonical” pathway of DNA replication causally related to death. Biochimica et Biophysica Acta (BBA)-Molecular Basis of Disease, 1772(4), 409-412.

Csiszar, A., Labinskyy, N., Jimenez, R., Pinto, J. T., Ballabh, P., Losonczy, G., ... & Ungvari, Z. (2009). Anti-oxidative and anti-inflammatory vasoprotective effects of caloric

restriction in aging: role of circulating factors and SIRT1. Mechanisms of ageing and development, 130(8), 518-527.

Curis, C., Percher, F., Jeannin, P., Montange, T., Chevalier, S.A., Seilhean, D., Cartier, L., Couraud, P.O., Gout, O., Gessain, A., Ceccaldi, P.E., Afonso, P.V., 2016. Human Tlymphotropic virus type 1-induced overexpression of activated leukocyte cell adhesion molecule (ALCAM) facilitates trafficking of infected lymphocytes through the blood-brain barrier. J. Virol. 90, 7303e7312.

de Git, K. C. G., & Adan, R. A. H. (2015). Leptin resistance in diet-induced obesity: the role of hypothalamic inflammation. Obesity reviews, 16(3), 207-224.

Delmont, E., Manso, C., Querol, L., Cortese, A., Berardinelli, A., Lozza, A., Belghazi, M.,

Devaux, J.J., Miura, Y., Fukami, Y., Inoue, T., Manso, C., Belghazi, M., Sekiguchi, K., Kokubun, N., Ichikawa, H., Wong, A.H., Yuki, N., 2016. Neurofascin-155 IgG4 in chronic inflammatory demyelinating polyneuropathy. Neurology 86, 800e807.

Dönertas¸ , H.M., _Izgi, H., Kamacıo glu, A., He, Z., Khaitovich, P., Somel, M., 2017. Gene expression reversal toward pre-adult levels in the aging human brain and agerelated loss of cellular identity. Sci. Rep. 7, 5894.

Dorfman, M. D., & Thaler, J. P. (2015). Hypothalamic inflammation and gliosis in obesity. Current opinion in endocrinology, diabetes, and obesity, 22(5), 325.

Ebel, J., Beuter, S., Wuchter, J., Kriebel, M., Volkmer, H., 2014. Organisation and control of neuronal connectivity and myelination by cell adhesion molecule neurofascin. Adv. Neurobiol. 8, 231e247.

Ellis, A., Crowe, K., & Lawrence, J. (2013). Obesity-related inflammation: implications for older adults. Journal of nutrition in gerontology and geriatrics, 32(4), 263-290.

Encinas, J. M., Michurina, T. V., Peunova, N., Park, J. H., Tordo, J., Peterson, D. A., ... & Enikolopov, G. (2011). Division-coupled astrocytic differentiation and age-related depletion of neural stem cells in the adult hippocampus. Cell stem cell, 8(5), 566-579.

Erbaba, B., Arslan-Ergul, A., & Adams, M. M. (2020a). Effects of Caloric Restriction on the Antagonistic and Integrative Hallmarks of Aging. *Ageing Research Reviews,* 101228.

Erbaba, B., Burhan, Ö. P., Şerifoğlu, N., Muratoğlu, B., Kahveci, F., Adams, M. M., & Arslan-Ergül, A. (2020b). Zebrafish brain RNA sequencing reveals that cell adhesion molecules are critical in brain aging. *Neurobiology of Aging*, 94, 164-175.

Eriksson, P. S., Perfilieva, E., Björk-Eriksson, T., Alborn, A. M., Nordborg, C., Peterson, D. A., & Gage, F. H. (1998). Neurogenesis in the adult human hippocampus. Nature medicine, 4(11), 1313.

Feldman, E. B. (Ed.). (2013). Nutrition in the middle and later years. Butterworth-Heinemann.

Foster, T. C., Kyritsopoulos, C., & Kumar, A. (2017). Central role for NMDA receptors in redox mediated impairment of synaptic function during aging and Alzheimer's disease. Behavioural brain research, 322, 223-232.

Frahm, C., Srivastava, A., Schmidt, S., Mueller, J., Groth, M., Guenther, M., Ji, Y., Priebe, S., Platzer, M., Witte, O.W., 2017. Transcriptional profiling reveals protective mechanisms in brains of long-lived mice. Neurobiol. Aging 52, 23e31.

Garratt, M., Nakagawa, S., & Simons, M. J. (2016). Comparative idiosyncrasies in life extension by reduced mTOR signalling and its distinctiveness from dietary restriction. Aging Cell, 15(4), 737-743.

Georgiou, E., Sidiropoulou, K., Richter, J., Papaneophytou, C., Sargiannidou, I., Kagiava, A., von Jonquieres, G., Christodoulou, C., Klugmann, M., Kleopa, K.A., 2017. Gene therapy targeting oligodendrocytes provides therapeutic benefit in a leukodystrophy model. Brain 140, 599e616.

Gerhard, G. S. (2007). Small laboratory fish as models for aging research. Ageing research reviews, 6(1), 64-72.

Giménez-Mascarell, P., Schirrmacher, C.E., Martínez-Cruz, L.A., Müller, D., 2018. Novel aspects of renal magnesium homeostasis. Front. Pediatr. 6, 77. Howe, K., Clark, M.D., Torroja, C.F., Torrance, J., Berthelot, C., Muffato, M.,

Grandel, H., Kaslin, J., Ganz, J., Wenzel, I., & Brand, M. (2006). Neural stem cells and neurogenesis in the adult zebrafish brain: origin, proliferation dynamics, migration and cell fate. Developmental biology, 295(1), 263-277.

Guillemot-Legris, O., & Muccioli, G. G. (2017). Obesity-induced neuroinflammation: beyond the hypothalamus. Trends in neurosciences, 40(4), 237-253.

Hadem, I. K. H., Majaw, T., Kharbuli, B., & Sharma, R. (2017). Beneficial effects of dietary restriction in aging brain. Journal of chemical neuroanatomy.

Han, S. N., Adolfsson, O., Lee, C. K., Prolla, T. A., Ordovas, J., & Meydani, S. N. (2006). Age and vitamin E-induced changes in gene expression profiles of T cells. The Journal of Immunology, 177(9), 6052-6061.

Hao, S., Dey, A., Yu, X., & Stranahan, A. M. (2016). Dietary obesity reversibly induces synaptic stripping by microglia and impairs hippocampal plasticity. Brain, behavior, and immunity, 51, 230-239.

Haqqani, A.S., Kreymborg, K., Krug, S., Moumdjian, R., Bouthillier, A., Becher, B., Arbour, N., David, S., Stanimirovic, D., Prat, A., 2008. Activated leukocyte cell adhesion molecule promotes leukocyte trafficking into the central nervous system. Nat. Immunol. 9, 137e145.

Hernandez-Segura, A., Rubingh, R., & Demaria, M. (2019). Identification of stable senescence-associated reference genes. *Aging cell*, *18*(2), e12911.

Hickman, S., Izzy, S., Sen, P., Morsett, L., & El Khoury, J. (2018). Microglia in neurodegeneration. Nature neuroscience, 21(10), 1359.

Hornsby, A. K., Redhead, Y. T., Rees, D. J., Ratcliff, M. S., Reichenbach, A., Wells, T., ... & Davies, J. S. (2016). Short-term calorie restriction enhances adult hippocampal neurogenesis and remote fear memory in a Ghsr-dependent manner. Psychoneuroendocrinology, 63, 198-207.

Howe, K., Clark, M. D., Torroja, C. F., Torrance, J., Berthelot, C., Muffato, M., ... & McLaren, S. (2013). The zebrafish reference genome sequence and its relationship to the human genome. Nature, 496(7446), 498.

Hsu, H. P., Li, C. F., Lee, S. W., Wu, W. R., Chen, T. J., Chang, K. Y., ... & Shiue, Y. L. (2014). Overexpression of stathmin 1 confers an independent prognostic indicator in nasopharyngeal carcinoma. Tumor Biology, 35(3), 2619-2629.

Huang, da W., Sherman, B.T., Lempicki, R.A., 2009a. Bioinformatics enrichment tools: paths toward the comprehensive functional analysis of large gene lists. Nucleic Acids Res. 37, 1e13.

Huang, da W., Sherman, B.T., Lempicki, R.A., 2009b. Systematic and integrative analysis of large gene lists using DAVID bioinformatics resources. Nat. Protoc. 4, 44e57.

Ianov, L., De Both, M., Chawla, M.K., Rani, A., Kennedy, A.J., Piras, I., Day, J.J., Siniard, A., Kumar, A., Sweatt, J.D., Barnes, C.A., Huentelman, M.J., Foster, T.C., 2017. Hippocampal transcriptomic profiles: subfield vulnerability to age and cognitive impairment. Front. Aging Neurosci. 9, 383.

Ishaq, A., Hanson, P.S., Morris, C.M., Saretzki, G., 2016. Telomerase activity is downregulated early during human brain development. Genes (Basel) 7. https://doi.org/10.3390/genes7060027.

Jeannet, R., Cai, Q., Liu, H., Vu, H., Kuo, Y.H., 2013. Alcam regulates long-term hematopoietic stem cell engraftment and self-renewal. Stem Cells 31, 560e571.

Jia, J. M., Zhao, J., Hu, Z., Lindberg, D., & Li, Z. (2013). Age-dependent regulation of synaptic connections by dopamine D2 receptors. Nature neuroscience, 16(11), 1627.

Jin, K., Mao, X. O., Eshoo, M. W., Nagayama, T., Minami, M., Simon, R. P., & Greenberg, D. A. (2001). Microarray analysis of hippocampal gene expression in global cerebral ischemia. Annals of Neurology: Official Journal of the American Neurological Association and the Child Neurology Society, 50(1), 93-103.

Jones, O. R., Scheuerlein, A., Salguero-Gómez, R., Camarda, C. G., Schaible, R., Casper, B. B., ... & Quintana-Ascencio, P. F. (2014). Diversity of ageing across the tree of life. Nature, 505(7482), 169.

Kamil, K., Yazid, M.D., Idrus, R.B.H., Das, S., Kumar, J., 2019. Peripheral demyelinating diseases: from biology to translational medicine. Front. Neurol. 10, 87.

Kang, Y. J., Lu, M. K., & Guan, K. L. (2011). The TSC1 and TSC2 tumor suppressors are required for proper ER stress response and protect cells from ER stress-induced apoptosis. Cell death and differentiation, 18(1), 133.

Karoglu, E. T., Halim, D. O., Erkaya, B., Altaytas, F., Arslan-Ergul, A., Konu, O., & Adams, M. M. (2017). Aging alters the molecular dynamics of synapses in a sexually dimorphic pattern in zebrafish (*Danio rerio*). *Neurobiology of aging*, *54*, 10-21.

Kedlian, V.R., Donertas, H.M., Thornton, J.M., 2019. The widespread increase in interindividual variability of gene expression in the human brain with age. Aging (Albany NY) 11, 2253e2280. https://doi.org/10.18632/aging.101912.

Kempermann, G. (2015). Activity dependency and aging in the regulation of adult neurogenesis. Cold Spring Harbor perspectives in biology, 7(11), a018929.

Kennerdell, J.R., Liu, N., Bonini, N.M., 2018. MiR-34 inhibits polycomb repressive complex 2 to modulate chaperone expression and promote healthy brain aging. Nat. Commun. 9, 4188.

Kiefel, H., Bondong, S., Hazin, J., Ridinger, J., Schirmer, U., Riedle, S., Altevogt, P., 2012. L1CAM: a major driver for tumor cell invasion and motility. Cell Adh Migr 6, 374e384.

Kim, M.S., Gloor, G.B., Bai, D., 2013. The distribution and functional properties of Pelizaeus-Merzbacher-like disease-linked Cx47 mutations on Cx47/Cx47 homotypic and Cx47/Cx43 heterotypic gap junctions. Biochem. J. 452, 249e258.

Kim, R., Park, S.I., Lee, C.Y., Lee, J., Kim, P., Oh, S., Lee, H., Lee, M.Y., Kim, J., Chung, Y.A., Hwang, K.C., Maeng, L.S., Chang, W., 2017. Alternative new mesenchymal stem cell source exerts tumor tropism through ALCAM and N-cadherin via regulation of microRNA-192 and -218. Mol. Cell Biochem. 427, 177e185.

Kim, S. H., Speirs, C. K., Solnica-Krezel, L., & Ess, K. C. (2011). Zebrafish model of tuberous sclerosis complex reveals cell-autonomous and non-cell-autonomous functions of mutant tuberin. *Disease models & mechanisms*, 4(2), 255-267.

Kishi, S. (2004). Functional aging and gradual senescence in zebrafish. Annals of the New York Academy of Sciences, 1019(1), 521-526.

Kishi, S., 2014. Using zebrafish models to explore genetic and epigenetic impacts on evolutionary developmental origins of aging. Transl. Res. 163, 123e135.

Kishi, S., Slack, B. E., Uchiyama, J., & Zhdanova, I. V. (2009). Zebrafish as a genetic model in biological and behavioral gerontology: where development meets aging in vertebrates–a mini-review. Gerontology, 55(4), 430-441.

Kishi, S., Uchiyama, J., Baughman, A. M., Goto, T., Lin, M. C., & Tsai, S. B. (2003). The zebrafish as a vertebrate model of functional aging and very gradual senescence. Experimental gerontology, 38(7), 777-786.

Kitada, M., & Koya, D. (2013). The use of calorie restriction mimetics to study aging. In Biological Aging (pp. 95-107). Humana Press, Totowa, NJ.

Kizil, C., & Brand, M. (2011). Cerebroventricular microinjection (CVMI) into adult zebrafish brain is an efficient misexpression method for forebrain ventricular cells. *PLoS One*, *6*(11), e27395.

Kizil, C., 2018. Mechanisms of pathology-induced neural stem cell plasticity and neural regeneration in adult zebrafish brain. Curr. Pathobiol. Rep. 6, 71e77.

Knoth, R., Singec, I., Ditter, M., Pantazis, G., Capetian, P., Meyer, R. P., ... & Kempermann, G. (2010). Murine features of neurogenesis in the human hippocampus across the lifespan from 0 to 100 years. PloS one, 5(1), e8809.

Kuhn, H. G., Dickinson-Anson, H., & Gage, F. H. (1996). Neurogenesis in the dentate gyrus of the adult rat: age-related decrease of neuronal progenitor proliferation. Journal of Neuroscience, 16(6), 2027-2033.

Lécuyer, M.A., Saint-Laurent, O., Bourbonnière, L., Larouche, S., Larochelle, C., Michel, L., Charabati, M., Abadier, M., Zandee, S., Haghayegh Jahromi, N., Gowing, E., Pittet, C., Lyck, R., Engelhardt, B., Prat, A., 2017. Dual role of ALCAM in neuroinflammation and blood-brain barrier homeostasis. Proc. Natl. Acad. Sci. U. S A. 114, E524eE533.

Lee, J., Duan, W., & Mattson, M. P. (2002). Evidence that brain-derived neurotrophic factor is required for basal neurogenesis and mediates, in part, the enhancement of neurogenesis by dietary restriction in the hippocampus of adult mice. Journal of neurochemistry, 82(6), 1367-1375.

Lee, J., Duan, W., Long, J. M., Ingram, D. K., & Mattson, M. P. (2000). Dietary restriction increases the number of newly generated neural cells, and induces BDNF expression, in the dentate gyrus of rats. Journal of Molecular Neuroscience, 15(2), 99-108.

Lei, C. Y., Wang, W., Zhu, Y. T., Fang, W. Y., & Tan, W. L. (2016, May). The decrease of cyclin B2 expression inhibits invasion and metastasis of bladder cancer. In Urologic Oncology: Seminars and Original Investigations (Vol. 34, No. 5, pp. 237-e1). Elsevier.

Li, Z., Bammann, H., Li, M., Liang, H., Yan, Z., Phoebe Chen, Y.P., Zhao, M., Khaitovich, P., 2013. Evolutionary and ontogenetic changes in RNA editing in human, chimpanzee, and macaque brains. RNA 19, 1693e1702.

Lieschke, G. J., & Currie, P. D. (2007). Animal models of human disease: zebrafish swim into view. Nature Reviews Genetics, 8(5), 353.

Linneberg, C., Toft, C.L.F., Kjaer-Sorensen, K., Laursen, L.S., 2019. L1cam-mediated developmental processes of the nervous system are differentially regulated by proteolytic processing. Sci. Rep. 9, 3716.

Liu, C. C., Tsai, C. W., Deak, F., Rogers, J., Penuliar, M., Sung, Y. M., ... & Estus, S. (2014). Deficiency in LRP6-mediated Wnt signaling contributes to synaptic abnormalities and amyloid pathology in Alzheimer's disease. *Neuron*, 84(1), 63-77.

Liu, G., Jiang, Y., Wang, P., Feng, R., Jiang, N., Chen, X., Song, H., Chen, Z., 2012. Cell adhesion molecules contribute to Alzheimer's disease: multiple pathway analyses of two genome-wide association studies. J. Neurochem. 120, 190e198.

López-Otín, C., Blasco, M. A., Partridge, L., Serrano, M., & Kroemer, G. (2013). The hallmarks of aging. *Cell*, 153(6), 1194-1217.

Lossos, A., Elazar, N., Lerer, I., Schueler-Furman, O., Fellig, Y., Glick, B., Zimmerman, B.E., Azulay, H., Dotan, S., Goldberg, S., Gomori, J.M., Ponger, P., Newman, J.P., Marreed, H., Steck, A.J., Schaeren-Wiemers, N., Mor, N., Harel, M., Geiger, T., Eshed-Eisenbach, Y., Meiner, V., Peles, E., 2015. Myelin-associated glycoprotein gene mutation causes Pelizaeus-Merzbacher disease-like disorder. Brain 138 (Pt 9), 2521e2536.

Lugert, S., Basak, O., Knuckles, P., Haussler, U., Fabel, K., Götz, M., ... & Giachino, C. (2010). Quiescent and active hippocampal neural stem cells with distinct morphologies respond selectively to physiological and pathological stimuli and aging. Cell stem cell, 6(5), 445-456.

Luo, J., Daniels, S. B., Lennington, J. B., Notti, R. Q., & Conover, J. C. (2006). The aging neurogenic subventricular zone. Aging cell, 5(2), 139-152.

Maehara, K., Yamakoshi, K., Ohtani, N., Kubo, Y., Takahashi, A., Arase, S., ... & Hara, E. (2005). Reduction of total E2F/DP activity induces senescence-like cell cycle arrest in cancer cells lacking functional pRB and p53. *The Journal of cell biology*, 168(4), 553-560.

Mahler, J., Driever,W., 2007. Expression of the zebrafish intermediate neurofilament Nestin in the developing nervous system and in neural proliferation zones at postembryonic stages. BMC Dev. Biol. 7, 89.

Malissart, P., Labauge, P., Taieb, G., Yuki, N., Illa, I., Attarian, S., Devaux, J.J., 2017. Autoantibodies to nodal isoforms of neurofascin in chronic inflammatory

März, M., Chapouton, P., Diotel, N., Vaillant, C., Hesl, B., Takamiya, M., Lam, C.S., Kah, O., Bally-Cuif, L., Strähle, U., 2010. Heterogeneity in progenitor cell subtypes in the ventricular zone of the zebrafish adult telencephalon. Glia 58, 870e888.

Maslov, A. Y., Barone, T. A., Plunkett, R. J., & Pruitt, S. C. (2004). Neural stem cell detection, characterization, and age-related changes in the subventricular zone of mice. Journal of Neuroscience, 24(7), 1726-1733.

Mazin, P., Xiong, J., Liu, X., Yan, Z., Zhang, X., Li, M., He, L., Somel, M., Yuan, Y., Phoebe Chen, Y.P., Li, N., Hu, Y., Fu, N., Ning, Z., Zeng, R., Yang, H., Chen, W., Gelfand, M., Khaitovich, P., 2013. Widespread splicing changes in human brain development and aging. Mol. Syst. Biol. 9, 633.

McCurley, A. T., & Callard, G. V. (2008). Characterization of housekeeping genes in zebrafish: male-female differences and effects of tissue type, developmental stage and chemical treatment. *BMC molecular biology*, *9*(1), 102.

Meynet, O., & Ricci, J. E. (2014). Caloric restriction and cancer: molecular mechanisms and clinical implications. Trends in molecular medicine, 20(8), 419-427.

Miller, A. A., & Spencer, S. J. (2014). Obesity and neuroinflammation: a pathway to cognitive impairment. Brain, behavior, and immunity, 42, 10-21.

Ming, G. L., & Song, H. (2011). Adult neurogenesis in the mammalian brain: significant answers and significant questions. Neuron, 70(4), 687-702.

Mo, M. L., Chen, Z., Li, J., Li, H. L., Sheng, Q., Ma, H. Y., ... & Xu, M. L. (2010). Use of serum circulating CCNB2 in cancer surveillance.

Mohammadi, M., Ghaznavi, R., Keyhanmanesh, R., Sadeghipour, H. R., Naderi, R., & Mohammadi, H. (2014). Caloric restriction prevents lead-induced oxidative stress and inflammation in rat liver. The Scientific World Journal, 2014.

Mrazkova, B., Dzijak, R., Imrichova, T., Kyjacova, L., Barath, P., Dzubak, P., Holub, D., Hajduch, M., Nahacka, Z., Andera, L., Holicek, P., Vasicova, P., Sapega, O., Bartek, J., Hodny, Z., 2018. Induction, regulation and roles of neural adhesion molecule L1CAM in cellular senescence. Aging (Albany NY) 10, 434e462.

Murphy, T., Dias, G. P., & Thuret, S. (2014). Effects of diet on brain plasticity in animal and human studies: mind the gap. Neural plasticity, 2014.

Nieberler, M., Reuning, U., Reichart, F., Notni, J., Wester, H.J., Schwaiger, M., Weinmüller, M., Räder, A., Steiger, K., Kessler, H., 2017. Exploring the role of RGD-recognizing integrins in cancer. Cancers 9, 116.

Notturno, F., Di Febo, T., Yuki, N., Fernandez Rodriguez, B.M., Corti, D., Nobile- Orazio, E., Carpo, M., De Lauretis, A., Uncini, A., 2014. Autoantibodies to neurofascin-186 and gliomedin in multifocal motor neuropathy. J. Neuroimmunol. 276, 207e212.

O'Connor, D. J., Lam, E. W., Griffin, S., Zhong, S., Leighton, L. C., Burbidge, S. A., & Lu, X. (1995). Physical and functional interactions between p53 and cell cycle co-operating transcription factors, E2F1 and DP1. The EMBO journal, 14(24), 6184-6192.

Ouyang, J., Carcea, I., Schiavo, J. K., Jones, K. T., Rabinowitsch, A., Kolaric, R., ... & Carr, K. D. (2017). Food restriction induces synaptic incorporation of calcium-permeable AMPA receptors in nucleus accumbens. European Journal of Neuroscience, 45(6), 826-836.

Pani, G. (2015, April). Neuroprotective effects of dietary restriction: evidence and mechanisms. In Seminars in cell & developmental biology (Vol. 40, pp. 106-114). Academic Press.

Papadimitriou, C., Celikkaya, H., Cosacak, M.I., Mashkaryan, V., Bray, L., Bhattarai, P., Brandt, K., Hollak, H., Chen, X., He, S., Antos, C.L., 2018. 3D culture method for Alzheimer's disease modeling reveals interleukin-4 rescues Ab42-induced loss of human neural stem cell plasticity. Dev. Cel. 46, 85e101.

Park, E.S., Jeon, S.M., Weon, H., Cho, H.J., Youn, D.H., 2017. Activated leukocyte cell adhesion molecule is involved in excitatory synaptic transmission and plasticity in the rat spinal dorsal horn. Neurosci. Lett. 656, 9e14.

Park, J. H., Glass, Z., Sayed, K., Michurina, T. V., Lazutkin, A., Mineyeva, O., ... & Enikolopov, G. (2013). Calorie restriction alleviates the age-related decrease in neural progenitor cell division in the aging brain. European Journal of Neuroscience, 37(12), 1987-1993.

Pellatt, A. J., Mullany, L. E., Herrick, J. S., Sakoda, L. C., Wolff, R. K., Samowitz, W. S., & Slattery, M. L. (2018). The TGFβ-signaling pathway and colorectal cancer: associations between dysregulated genes and miRNAs. Journal of translational medicine, 16(1), 191.

Pellicelli, M., Picard, C., Wang, D., Lavigne, P., & Moreau, A. (2016). E2F1 and TFDP1 regulate PITX1 expression in normal and osteoarthritic articular chondrocytes. PloS one, 11(11), e0165951.

Perdomo-Ramirez, A., Aguirre, M., Davitaia, T., Ariceta, G., Ramos-Trujillo, E., RenalTube Group, Claverie-Martin, F., 2019. Characterization of two novel mutations in the claudin-16 and claudin-19 genes that cause familial hypomagnesemia with hypercalciuria and nephrocalcinosis. Gene 689, 227e234.

Pereira, A.C., Gray, J.D., Kogan, J.F., Davidson, R.L., Rubin, T.G., Okamoto, M., Morrison, J.H., McEwen, B.S., 2017. Age and Alzheimer's disease gene expression profiles reversed by the glutamate modulator riluzole. Mol. Psychiatry 22, 296e305.

Phiel, C., & Kuret J. (2009, July). Amyloid Plaque Formation in Alzheimer's Disease Signaling Interactive Pathway. Retrieved from https://www.cellsignal.com/contents/science-cst-pathways-neuroscience/amyloid-plaque-formation-in-alzheimer-s-disease-signaling-interactive-pathway/pathways-alz

Podolskiy, D. I., Lobanov, A. V., Kryukov, G. V., & Gladyshev, V. N. (2016). Analysis of cancer genomes reveals basic features of human aging and its role in cancer development. Nature communications, 7, 12157.

Pronker, M.F., Lemstra, S., Snijder, J., Heck, A.J., Thies-Weesie, D.M., Pasterkamp, R.J., Janssen, B.J., 2016. Structural basis of myelin-associated glycoprotein adhesion and signalling. Nat. Commun. 7, 13584.

Qian, X., Song, X., He, Y., Yang, Z., Sun, T., Wang, J., ... & You, C. (2015). CCNB2 overexpression is a poor prognostic biomarker in Chinese NSCLC patients. Biomedicine & Pharmacotherapy, 74, 222-227.

Qiu, G., Liu, S., & So, K. F. (2010). Dietary restriction and brain health. Neuroscience bulletin, 26(1), 55-65.

Quarles, R.H., 2007. Myelin-associated glycoprotein (MAG): past, present and beyond. J. Neurochem. 100, 1431e1448.

Raj, T., Li, Y.I., Wong, G., Humphrey, J., Wang, M., Ramdhani, S., Wang, Y.C., Ng, B., Gupta, I., Haroutunian, V., Schadt, E.E., Young-Pearse, T., Mostafavi, S., Zhang, B., Sklar, P., Bennett, D.A., De Jager, P.L., 2018. Integrative transcriptome analyses of the aging brain implicate altered splicing in Alzheimer's disease susceptibility. Nat. Genet. 50, 1584e1592.

Rao, M. S., Hattiangady, B., & Shetty, A. K. (2006). The window and mechanisms of major age-related decline in the production of new neurons within the dentate gyrus of the hippocampus. Aging cell, 5(6), 545-558.

Sanai, N., Nguyen, T., Ihrie, R. A., Mirzadeh, Z., Tsai, H. H., Wong, M., ... & Rowitch, D. H. (2011). Corridors of migrating neurons in the human brain and their decline during infancy. Nature, 478(7369), 382.

Sanfilippo, C., Castrogiovanni, P., Imbesi, R., Tibullo, D., Li Volti, G., Barbagallo, I., Vicario, N., Musumeci, G., Di Rosa, M., 2019. Middle-aged healthy women and Alzheimer’s disease patients present an overlapping of brain cell transcriptional profile. Neuroscience 406, 333e344.

Santos, C. L., Bobermin, L. D., Souza, D. O., & Quincozes-Santos, A. (2018). Leptin stimulates the release of pro-inflammatory cytokines in hypothalamic astrocyte cultures from adult and aged rats. Metabolic brain disease, 1-5.

Satoh, J., Kino, Y., Asahina, N., Takitani, M., Miyoshi, J., Ishida, T., Saito, Y., 2016. TMEM119 marks a subset of microglia in the human brain. Neuropathology 36, 39e49.

Shahaduzzaman, M.D., Mehta, V., Golden, J.E., Rowe, D.D., Green, S., Tadinada, R., Foran, E.A., Sanberg, P.R., Pennypacker, K.R., Willing, A.E., 2015. Human umbilical cord blood cells induce neuroprotective change in gene expression profile in neurons after ischemia through activation of Akt pathway. Cell Transplant. 24, 721e735.

Shannon, P., Markiel, A., Ozier, O., Baliga, N.S., Wang, J.T., Ramage, D., Amin, N., Schwikowski, B., Ideker, T., 2003. Cytoscape: a software environment for integrated models of biomolecular interaction networks. Genome Res. 13, 2498e2504.

Shi, M., Kovac, A., Korff, A., Cook, T.J., Ginghina, C., Bullock, K.M., Yang, L., Stewart, T., Zheng, D., Aro, P., Atik, A., Kerr, K.F., Zabetian, C.P., Peskind, E.R., Hu, S.C., Quinn, J.F., Galasko, D.R., Montine, T.J., Banks, W.A., Zhang, J., 2016. CNS tau efflux via exosomes is likely increased in Parkinson's disease but not in Alzheimer's disease. Alzheimers Dement 12, 1125e1131.

Shiotani, H., Maruo, T., Sakakibara, S., Miyata, M., Mandai, K., Mochizuki, H., & Takai, Y. (2017). Aging-dependent expression of synapse-related proteins in the mouse brain. Genes to Cells, 22(5), 472-484.

Shubbar, E., Kovács, A., Hajizadeh, S., Parris, T. Z., Nemes, S., Gunnarsdóttir, K., ... & Helou, K. (2013). Elevated cyclin B2 expression in invasive breast carcinoma is associated with unfavorable clinical outcome. BMC cancer, 13(1), 1.

Si, H., & Liu, D. (2014). Dietary antiaging phytochemicals and mechanisms associated with prolonged survival. The Journal of nutritional biochemistry, 25(6), 581-591.

Singh, R., Lakhanpal, D., Kumar, S., Sharma, S., Kataria, H., Kaur, M., & Kaur, G. (2012). Late-onset intermittent fasting dietary restriction as a potential intervention to retard age-associated brain function impairments in male rats. Age, 34(4), 917-933.

Singh, R., Manchanda, S., Kaur, T., Kumar, S., Lakhanpal, D., Lakhman, S. S., & Kaur, G. (2015). Middle age onset short-term intermittent fasting dietary restriction prevents brain function impairments in male Wistar rats. Biogerontology, 16(6), 775-788.

Somel, M., Khaitovich, P., Bahn, S., Pääbo, S., & Lachmann, M. (2006). Gene expression becomes heterogeneous with age. *Current Biology*, 16(10), R359-R360.

Sørensen, T. S., Girling, R., Lee, C. W., Gannon, J., Bandara, L. R., & La Thangue, N. B. (1996). Functional interaction between DP-1 and p53. Molecular and cellular biology, 16(10), 5888-5895.

Soto, M.S., Serres, S., Anthony, D.C., Sibson, N.R., 2014. Functional role of endothelial adhesion molecules in the early stages of brain metastasis. Neuro Oncol. 16, 540e551.

Speakman, J. R., & Mitchell, S. E. (2011). Caloric restriction. Molecular aspects of medicine, 32(3), 159-221.

Spilsbury, A., Miwa, S., Attems, J., Saretzki, G., 2015. The role of telomerase protein TERT in Alzheimer's disease and in tau-related pathology in vitro. J. Neurosci. 35, 1659e1674.

Stemple, D.L., 2013. The zebrafish reference genome sequence and its relationship to the human genome. Nature 496, 498e503.

Takashima, S., Saito, H., Takahashi, N., Imai, K., Kudo, S., Atari, M., ... & Minamiya, Y. (2014). Strong expression of cyclin B2 mRNA correlates with a poor prognosis in patients with non-small cell lung cancer. Tumor Biology, 35(5), 4257-4265.

Tang, R., Dodd, A., Lai, D., McNabb, W. C., & Love, D. R. (2007). Validation of zebrafish (*Danio rerio*) reference genes for quantitative real-time RT-PCR normalization. *Acta biochimica et biophysica Sinica*, *39*(5), 384-390.

Taupin, P. (2006). Adult neural stem cells, neurogenic niches, and cellular therapy. Stem Cell Reviews, 2(3), 213-219.

Taylor, A.M., Saifetiarova, J., Bhat, M.A., 2017. Postnatal loss of neuronal and glial neurofascins differentially affects node of Ranvier maintenance and myelinated axon function. Front. Cell Neurosci. 11, 11.

Testa, G., Biasi, F., Poli, G., & Chiarpotto, E. (2014). Calorie restriction and dietary restriction mimetics: a strategy for improving healthy aging and longevity. Current pharmaceutical design, 20(18), 2950-2977.

Thinakaran, G., & Koo, E. H. (2008). Amyloid precursor protein trafficking, processing, and function. *Journal of Biological Chemistry*, 283(44), 29615-29619.

Timchenko, N. A. (2009). Aging and liver regeneration. *Trends in Endocrinology & Metabolism*, 20(4), 171-176.

Ting, J. H., Marks, D. R., Schleidt, S. S., Wu, J. N., Zyskind, J. W., Lindl, K. A., ... & Jordan-Sciutto, K. L. (2014). Targeted gene mutation of E2F1 evokes age-dependent synaptic disruption and behavioral deficits. Journal of neurochemistry, 129(5), 850-863.

Tucsek, Z., Toth, P., Sosnowska, D., Gautam, T., Mitschelen, M., Koller, A., ... & Csiszar, A. (2013). Obesity in aging exacerbates blood–brain barrier disruption,

neuroinflammation, and oxidative stress in the mouse hippocampus: effects on expression of genes involved in beta-amyloid generation and Alzheimer's disease. Journals of Gerontology Series A: Biomedical Sciences and Medical Sciences, 69(10), 1212-1226.

Ueberham, U., & Arendt, T. (2005). The expression of cell cycle proteins in neurons and its relevance for Alzheimer's disease. Current Drug Targets-CNS & Neurological Disorders, 4(3), 293-306.

Vaishnav, Y. N., & Pant, V. (1999). Differential regulation of E2F transcription factors by p53 tumor suppressor protein. DNA and cell biology, 18(12), 911-922.

Vall-Palomar, M., Arévalo, J., Ariceta, G., Meseguer, A., 2018. Establishment of urinary exosome-like vesicles isolation protocol for FHHNC patients and evaluation of different exosomal RNA extraction methods. J. Transl. Med. 16, 278.

Van Houcke, J., Bollaerts, I., Geeraerts, E., Davis, B., Beckers, A., Van Hove, I., Lemmens, K., De Groef, L., Moons, L., 2017. Successful optic nerve regeneration in the senescent zebrafish despite age-related decline of cell intrinsic and extrinsic response processes. Neurobiol. Aging 60, 1e10.

van Leeuwen, L. A., & Hoozemans, J. J. (2015). Physiological and pathophysiological functions of cell cycle proteins in post-mitotic neurons: implications for Alzheimer's disease. Acta neuropathologica, 129(4), 511-525.

Van Praag, H., Fleshner, M., Schwartz, M. W., & Mattson, M. P. (2014). Exercise, energy intake, glucose homeostasis, and the brain. Journal of Neuroscience, 34(46), 15139-15149.

Van Praag, H., Kempermann, G., & Gage, F. H. (1999). Running increases cell proliferation and neurogenesis in the adult mouse dentate gyrus. Nature neuroscience, 2(3), 266.

Vivo-Morpholinos enter cells in adult animals and cultures. Retrieved April 21, 2019, from https://www.gene-tools.com/vivomorpholinos

Volkmer, H., Leuschner, R., Zacharias, U., Rathjen, F.G., 1996. Neurofascin induces neurites by heterophilic interactions with axonal NrCAM while NrCAM requires F11 on the axonal surface to extend neurites. J. Cell Biol. 135, 1059e1069.

Wang, S.B., Xu, T., Peng, S., Singh, D., Ghiassi-Nejad, M., Adelman, R.A., Rizzolo, L.J., 2019. Disease-associated mutations of claudin-19 disrupt retinal neurogenesis and visual function. Commun. Biol. 2, 113.

Ward, R. J., Dexter, D. T., & Crichton, R. R. (2015). Ageing, neuroinflammation and neurodegeneration. Front Biosci (Schol Ed), 7, 189-204.

Weithoff, G. (2007). Dietary restriction in two rotifer species: the effect of the length of food deprivation on life span and reproduction. Oecologia, 153(2), 303-308.

Winata, C. L., Korzh, S., Kondrychyn, I., Zheng, W., Korzh, V., & Gong, Z. (2009). Development of zebrafish swimbladder: The requirement of Hedgehog signaling in specification and organization of the three tissue layers. Developmental biology, 331(2), 222-236.

Won, M., Lee, S., Choi, S., Ro, H., Kim, K.J., Kim, J.H., Kim, K.E., Kim, K.K., 2016. Identification and characterization of the RNA-binding protein Rbfox3 in zebrafish embryo. Biochem. Biophys. Res. Commun. 472, 373e378.

Wu, C. L., Zukerberg, L. R., Ngwu, C., Harlow, E., & Lees, J. A. (1995). In vivo association of E2F and DP family proteins. Molecular and cellular biology, 15(5), 2536-2546.

Xie, Q., Peng, S., Tao, L., Ruan, H., Yang, Y., Li, T. M., ... & Yuan, Z. (2014). E2F transcription factor 1 regulates cellular and organismal senescence by inhibiting Forkhead box O transcription factors. *Journal of Biological Chemistry*, jbc-M114.

Yang, F., Chu, X., Yin, M., Liu, X., Yuan, H., Niu, Y., & Fu, L. (2014). mTOR and autophagy in normal brain aging and caloric restriction ameliorating age-related cognition deficits. Behavioural brain research, 264, 82-90.

Yano, H., Motoshima, T., Ma, C., Pan, C., Yamada, S., Nakayama, T., Kitada, S., Fujimoto, N., Kamba, T., Takeya, M., Komohara, Y., 2017. The significance of TIMD4 expression in clear cell renal cell carcinoma. Med. Mol. Morphol. 50, 220e226.

Yasen, M., Fei, Q., Hutton,W.C., Zhang, J., Dong, J., Jiang, X., Zhang, F., 2013. Changes of number of cells expressing proliferation and progenitor cell markers with age in rabbit intervertebral discs. Acta Biochim. Biophys. Sin. (Shanghai) 45, 368e376.

Yasui, K., Arii, S., Zhao, C., Imoto, I., Ueda, M., Nagai, H., ... & Inazawa, J. (2002). TFDP1, CUL4A, and CDC16 identified as targets for amplification at 13q34 in hepatocellular carcinomas. Hepatology, 35(6), 1476-1484.

Young, M.D., Wakefield, M.J., Smyth, G.K., Oshlack, A., 2010. Gene ontology analysis for RNA-seq: accounting for selection bias. Genome Biol. 11, R14.

Yu, L., Tucci, V., Kishi, S., & Zhdanova, I. V. (2006). Cognitive aging in zebrafish. PloS one, 1(1), e14.

Zech, R., Kiontke, S., Mueller, U., Oeckinghaus, A., & Kümmel, D. (2016). Structure of the Tuberous Sclerosis Complex 2 (TSC2) N-terminus Provides Insight into Complex Assembly and Tuberous Sclerosis Pathogenesis. Journal of Biological Chemistry, jbc-M116.

Zhang, A., Desmazieres, A., Zonta, B., Melrose, S., Campbell, G., Mahad, D., Li, Q., Sherman, D.L., Reynolds, R., Brophy, P.J., 2015. Neurofascin 140 is an embryonic neuronal neurofascin isoform that promotes the assembly of the node of Ranvier. J. Neurosci. 35, 2246e2254.

Zhou, Y., Zhou, B., Pache, L., Chang, M., Khodabakhshi, A.H., Tanaseichuk, O., Benner, C., Chanda, S.K., 2019. Metascape provides a biologist-oriented resource for the analysis of systems-level datasets. Nat. Commun. 10, 1523.

Zupanc, G. K., Hinsch, K., & Gage, F. H. (2005). Proliferation, migration, neuronal differentiation, and long-term survival of new cells in the adult zebrafish brain. Journal of Comparative Neurology, 488(3), 290-319.

8. SUPPLEMENTARY DATA

Supplementary Table 1 Chapter 2 primer list for human samples

Organism	Gene name		Sequence (5'-3')
Human	CLDN19	F	AGTTGGCATGAAGTGTACGC
Human	CLDN19	R	ATGTGCAGCAGAGGAAGGAG
Human	MPZ	F	GCTGTGCTGCTCTTCTCTTC
Human	MPZ	R	GCCAGGTGAAGGAGATGTCA
Human	NFASC	F	GGTTTATTCCCGGGACAACG
Human	NFASC	R	CCGCTTGGTTGTTGGTGTAA
Human	DLG1	F	ACAGATTGCACAGCTTTACCC
Human	DLG1	R	GCTTGTTCTTCTGTTAGACGCT
Human	L1CAM	F	GCCTGACACTGACTACGAGA
Human	L1CAM	R	GCACTCACAAAGCCGATGAA
Human	MAG	F	ATTACCCAGACACGCAGGAA
Human	MAG	R	CTCGTACTTCTCTGGTGCCC
Human	ALCAM	F	TTGTTGGTCTCCTCCTTGCT
Human	ALCAM	R	CCGAGGTCCTTGTTTACATGT
Human	TERT	F	TGTCAAGGTGGATGTGACGG
Human	TERT	R	GAGGAGCTCTGCTCGATGAC
Human	TR	F	CCCTAACTGAGAAGGGCGTA
Human	TR	R	AGAATGAACGGTGGAAGGCG
Human	RPL13a	F	AGCCTACAAGAAAGTTTGCCTAT
Human	RPL13a	R	TCTTCTTCCGGTAGTGGATCTTGGC
Human	DNMT1	F	TGGAAAGAGACAGCTTAACAGAA
Human	DNMT1	R	CGTAATTTGGTTTCCAAGTCACATA
Human	DNMT3a	F	ACCGGCCATACGGTGGA
Human	DNMT3a	R	GTGTTGAGCCCTCTGGTGAA
Human	GAPDH	F	CGGGAAGGAAATGAATGGGC
Human	GAPDH	R	GCCCAATACGACCAAATCAGAGAAT
Human	OCT4	F	GCTCGAGAAGGATGTGGTCC
Human	OCT4	R	CGTTGTGCATAGTCGCTGCT
Human	TUJ1	F	GGCCAAGGGTCACTACACG
Human	TUJ1	R	GCAGTCGCAGTTTTCACACTC
Human	NANOG	F	AGGTTCCCAGTCGGGTTCA
Human	NANOG	R	GCAGAAGGCCTCAGCACCTA
Human	GJC2	F	ATCCACAACCACTCCACCTT
Human	GJC2	R	CGTCCGAGTAGATGGCCTC
Human	SMURF	F	CATGGCATGATCCAAGAGTG
Human	SMURF	R	ACTCTGCCTGTTGCCGTATT
Human	TIMD4	F	CTGGCTGGTTCAACGATGTA
Human	TIMD4	R	CGACTGTTGTTGGAAGTGCA

Supplementary Table 2 Chapter 2 primer list for zebrafish samples

Organism	Gene name		Sequence (5'-3')
Zebrafish	actin	F	GCCTGACGGACAGGTCAT
Zebrafish	actin	R	ACCGCAAGATTCCATACCC
Zebrafish	cx47	F	TGAGAACATCCCCACTGACC
Zebrafish	cx47	R	CTCCTGAGCCATGTTGATGC
Zebrafish	timd4	F	GGACAGATGGACTTGGGGAT
Zebrafish	timd4	R	TTTGGAGCCACAGTTGTTGG
Zebrafish	tmem119b	F	CGTGGATGAGCAAGACAAGG
Zebrafish	tmem119b	R	CCTTCCACGGACTCTTGAGT
Zebrafish	nestin	F	GAGAAAGACTGTCTGGGGCA
Zebrafish	nestin	R	TGTTTGGTGTTGGTCTGTCG
Zebrafish	sox2	F	GACCATTCATCGACGAAGCC
Zebrafish	sox2	R	CCTCCGGGGTCTGTATTTGT
Zebrafish	gfap	F	CGTGCAGCTAGAGAGGAAGA
Zebrafish	gfap	R	CCTGCATGTTAGAGTTGGCC
Zebrafish	blbp	F	TCCAAGTTCAGAGGTGGGAC
Zebrafish	blbp	R	CCTTCTCGTATGTGCGCAC
Zebrafish	neun	F	ACAGATATGCCCAACCAGCC
Zebrafish	neun	R	TGGTGATAAGGGTCTGCTGT
Zebrafish	s100b	F	GACTTAGAGAACTGCCTGGGA
Zebrafish	s100b	R	GAAATCACACTCCGAGTCGC
Zebrafish	p53	F	GGCAATCCGAAAGTCGATAA
Zebrafish	p53	R	CTGTCGTTTTGCGCCATT
Zebrafish	pcna	F	TCTCACAGACCAGCAACGTC
Zebrafish	pcna	R	GCACTGGCTCATTCATCTCA
Zebrafish	p27	F	TGAGTCCGACACCCACATAA
Zebrafish	p27	R	ATCGAAGCGACGACAATGA
Zebrafish	serpine1	F	GAGCAGAATGGGTCTTGGAG
Zebrafish	serpine1	R	TTGGATACACATAAAGGTTCCTCA
Zebrafish	Tert	F	CGGTATGACGGCCTATCACT
Zebrafish	Tert	R	TAAACGGCCTCCACAGAGTT
Zebrafish	Tp53bp2	F	GCCGAGCTGGACAGACTCTA
Zebrafish	Tp53bp2	R	TCTGCTCCACGTTCAGGTT

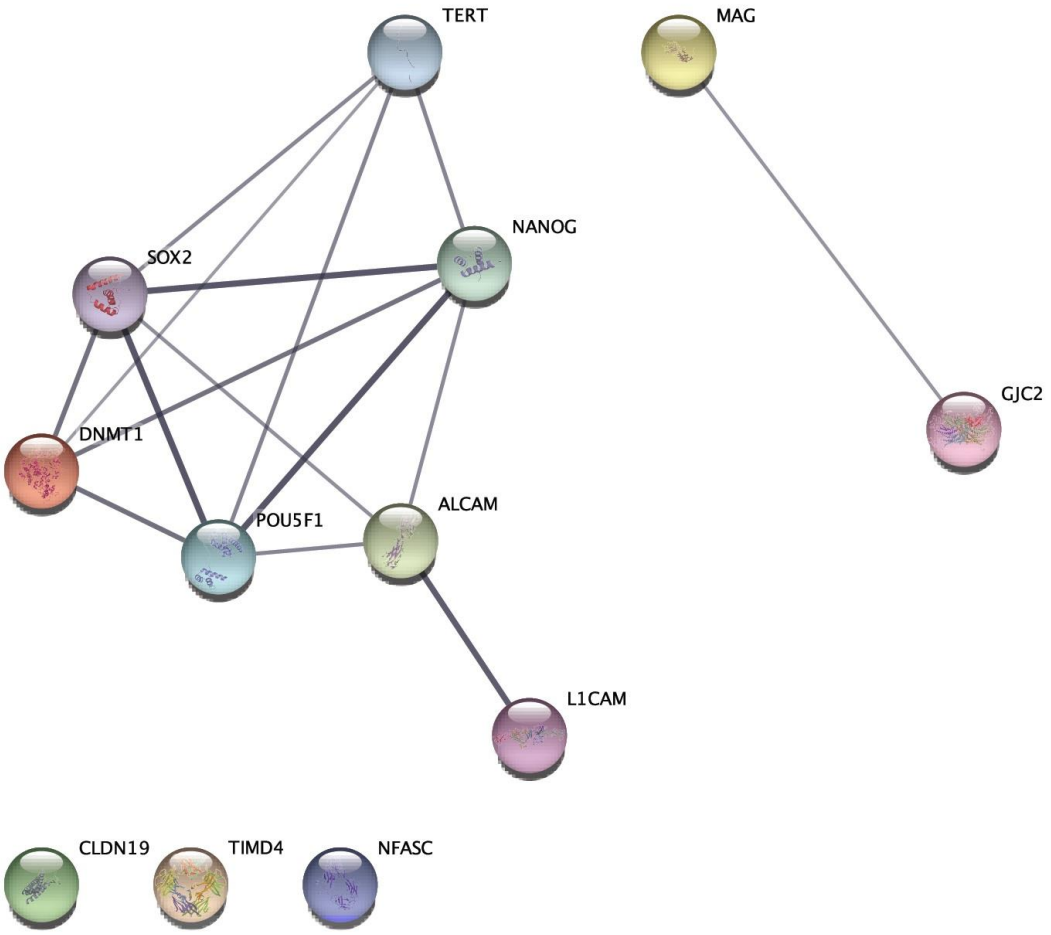

Supplementary Figure 1 The interaction of the proteins of interest with each other and with some age-related proteins in Chapter 2. We used the Cytoscape software. (Reprinted from Erbaba et al., 2020b)